The Thesis Committee for Yaning Wang
Certifies that this is the approved version of the following thesis:

Dynamic Properties of Fine Liquefiable Sand and Calcareous Sand from Resonant Column Testing

APPROVED BY
SUPERVISING COMMITTEE:

Supervisor:

Kenneth H. Stokoe II, Supervisor

Brady R. Cox

Dynamic Properties of Fine Liquefiable Sand and Calcareous Sand from Resonant Column Testing

by

Yaning Wang, B.E.

THESIS

Presented to the Faculty of the Graduate School of

The University of Texas at Austin

in Partial Fulfillment

of the Requirements

for the Degree of

MASTER OF SCIENCE IN ENGINEERING

The University of Texas at Austin

May, 2015

Acknowledgements

First, I would like to thank my supervising professor Dr. Kenneth H. Stokoe, II for his support, guidance and encouragement during my study and research. I feel so lucky being in his research group and I am always inspired by his passion and enthusiasm in the area of Soil Dynamics.

Thanks are also extended to the other faculties in the Geotechnical Engineering at University of Texas at Austin. It is the Soil Dynamic course given by Dr. Brady R. Cox that introduced this area to me and I benefited a great deal from it. I would also like to thank Dr. Gibert, Dr. Zornberg, Dr. Rathge, and Dr. El Mohtar for their excellent lectures and presentations that broadened my knowledge. It is really my honor to study and work in one of the best Geotechnical Engineering departments in the world.

I would like to thank to my colleagues in the Soil and Rock Dynamics Laboratory at University of Texas at Austin – Boonam Shin, Andrew Keene and Bohyoung Lee – from whom I have learned most about the laboratory tests. They helped me with patience and kindness when I first entered the research group and they are more like friends to me. I would also like to extend my appreciations to other graduate students or former graduate students Yubing Wang, Yin Lai, Xiaoyue Wang, Xin Peng, Julia Roberts, and Sungmoon Hwang for their kind assistance and help in both my study and my life here in Austin.

Finally, I would like to thank my parents for their selfless love and care, and all my friends for their friendship. Most of all, I would like to thank the most important one to me – my wife, Run Li – who is willing to marry me when I have nothing. Thank you for your trust and love.

Abstract

Dynamic Properties of Fine Liquefiable Sand and Calcareous Sand from Resonant Column Testing

Yaning Wang, M.S.E.

The University of Texas at Austin, 2015

Supervisor: Kenneth H. Stokoe II

The study of the dynamic properties of two specific kinds of granular soils is performed using torsional resonant column testing. The sandy soils are: (1) liquefiable sand from Christchurch, New Zealand, and (2) calcareous sand from Puerto Rico. The effects of isotropic effective confining pressure (σ_0'), shear strain (γ) amplitude, void ratio (e), and total unit weight (γ_t) on the small-strain and nonlinear dynamic properties of both types of sand are presented and discussed. Empirical models from previous studies are examined to determine how well the models fit the test results.

Void ratio (e) has an influence on the small-strain dynamic properties of both liquefiable sand and calcareous sand in the general way that denser soil granular arrangements of particles form stiffer soil skeletons. The denser specimens with smaller values of e always have higher values of small-strain shear wave velocity (V_S) and small-strain shear modulus (G_{max}) than looser specimens. The denser specimens also

have lower values of material damping ratio (D_{min}) than the looser specimens that have larger values of e at the same σ_0' level. Compared with looser specimens, denser specimens of the same sand have slightly smaller values of n_S, which represent the slope of $\log V_S - \log \sigma_0'$ relationship. The void ratio function $\sqrt{F(e)}$, (where $F(e) = 1/(0.3 + 0.7e^2)$), was found to be an important factor in evaluating the value of V_S at σ_0' equal to one atmosphere.

Void ratio (e) and isotropic effective confining pressure (σ_0') are shown to have an influence on the nonlinear dynamic properties of both liquefiable sand and calcareous sand. The variation of nonlinear shear modulus with shear strain can be described by: the elastic threshold strain (γ_t^e), the reference shear strain (γ_r) at which $G/G_{max} = 0.5$ and the curvature coefficient (a). The modified hyperbolic model ($G/G_{max} = 1/(1 + (\gamma/\gamma_r)^a)$) is affected by void ratio (e) because denser specimens always have smaller values of γ_t^e, γ_r and a than looser specimens for both liquefiable sand and calcareous sand. It is also found that γ_t^e, γ_r and a are all affected by σ_0' since specimens at higher confining pressure levels always have larger values of γ_t^e and γ_r and smaller values of a than specimens at lower confining pressures. For the variations of nonlinear material damping ratio, the reference shear strain ($\gamma_{r,D}$) at which $D/D_{min} = 0.5$ in the modified hyperbolic model ($D/D_{max} = 1 + (\gamma/\gamma_r)^b$) is found to be affected by void ratio (e) since denser specimens always have smaller values of $\gamma_{r,D}$ than looser specimens for the same kind of sand. It is also found that $\gamma_{r,D}$ is affected by σ_0' since

specimens at higher confining pressure levels always have larger values of $\gamma_{r,D}$ than specimens at lower confining pressures.

For the liquefiable sand, Menq's (2003) predictions are somewhat unconservative in calculating the small-strain shear modulus (G_{max}) and small-strain material damping ratio (D_{min}). However, Menq's equations give quite good results for predicting nonlinear shear modulus behavior. On the other hand, for the calcareous sand, Menq's equation for small-strain shear modulus is not applicable. The possible reason may be the unusual angular shaped particles of calcareous sand, which can lead to unusually large values of void ratio. Differences between the RC tests results and Menq's (2003) prediction of nonlinear shear modulus of calcareous sand make the prediction unconservative.

Table of Contents

List of Tables

List of Figures

CHAPTER ONE

INTRODUCTION

1.1 BACKGROUND

One of the key properties that generally impacts the geotechnical engineering design under dynamic loadings is the behavior of soil and rock materials due to shearing motions. To investigate the dynamic behavior under shearing loads of the soil and rock materials, the shear modulus (G) and material damping ratio in shear (D) are most frequently measured. These properties are measured in the linear and nonlinear strain ranges. The shear modulus is a parameter that describes the stiffness of geotechnical materials and is directly related to the deformation under shearing loadings. The material damping ratio in shear describes how much energy is lost during each cycle of shearing motions. These two properties are generally measured in the laboratory with dynamic testing methods. The laboratory measurements are well-suited for parametric studies such as the effects of stress state and strain amplitude. In the field, seismic testing is used to evaluate the shear wave velocity at small strains through which the small strain shear modulus (G_{max}) is calculated.

From previous studies, the dynamic shearing behavior of geotechnical materials can be divided into two parts according to the range of shear strain: the small-strain range and the nonlinear range. In the small-strain range, the shear modulus and material damping ratio are constant; hence, the values do not change with shear strain. Beyond the

small-strain range, the shear modulus decreases and the material damping increases with increasing shear strain in the nonlinear range. Many previous researchers have studied the factors affecting the dynamic behavior of the geotechnical materials in shear in both the small-strain and nonlinear range (i.e. Hardin and Drnevich, 1972; Kokusho, 1980; Seed et al, 1986; Song, 1986; Darendeli, 2001; and Menq, 2003). Many empirical models have been developed to describe the dynamic behavior of soil and rock materials during shearing. Important engineering parameters such as confining pressure, plasticity, void ratio, median grain size and uniformity coefficient have been studied.

The purpose of this study is to investigate the dynamic shearing properties of two specific kinds of sandy soil and to determine their dynamic shearing behavior and to see how well this behavior can be described by previous empirical models. The two specific kinds of sandy soil have very special characteristics; one is a liquefiable sand from Christchurch, New Zealand that can lose nearly all the stiffness and strength under earthquake shakings and the second one is a calcareous sand from Puerto Rico that has very sharp and fragile particle shapes and extremely high void ratio. The unusual features of these two sands are being studied to determine how their dynamic properties compare with common sandy soils.

1.2 OBJECTIVES

The objectives of this study are as follows.

1. Reconstitute uniform specimens from the liquefiable sand and calcareous sand samples and perform resonant column (RC) tests to obtain the linear and nonlinear dynamic properties of both sands.
2. Evaluate the influence of parameters such as isotropic effective confining pressure (σ_0'), void ratio (e) and medium grain size (D_{50}) on shear modulus and material damping ratio of both the sands in small-strain range. Examine if empirical models such as Menq's (2003) model can fit the test results.
3. Evaluate the influence of parameters such as shear strain (γ), isotropic effective confining pressure (σ_0'), void ratio (e) and medium grain size (D_{50}) on shear modulus and material damping ratio of both sands in nonlinear strain range. Examine if the empirical models such as Menq's (2003) model fit the test results.
4. Give recommendations on the application of empirical models to the estimation of dynamic soil properties of these two specific kinds of sandy soils.

1.3 ORGANIZATION

This thesis consists of seven Chapters. Chapter One is a brief introduction to the topic and background information is given. In Chapter Two, an overall review of literatures associated with the dynamic properties of sandy soils is presented. The wave propagation theory in soil dynamics is presented and empirical models used to describe the dynamic behavior of these general soils are discussed.

The resonant column (RC) device in the Soil and Rock Dynamics Laboratory at University of Texas at Austin (UT) is introduced in Chapter Three. In this chapter, the principles of resonant column testing and the methodology of data analysis are discussed. In Chapter Four, the sandy soil materials used in this study are described based on physical properties and sieve analysis results. The testing programs for both sands are also presented.

The dynamic properties of the liquefiable sand from Christchurch that were determined by RC testing are discussed in Chapter Five. These results are also compared to predictions from empirical models in Chapter Five. The dynamic properties of the calcareous sand from RC tests are discussed and compared to the predictions from empirical models in Chapter Six. Finally, conclusions about the dynamic properties of the liquefiable sand and calcareous sand are presented in Chapter Seven. Recommendations for future studies with these materials are also given.

CHAPTER TWO

LITERATURE REVIEW

2.1 INTRODUCTION

In this chapter, an overview of some basic theories in soil dynamics is presented. The theory of wave propagation in soils is presented in Section 2.2. Previous studies on the dynamic properties of sandy soil in both the small-strain and nonlinear-strain ranges are discussed in Section 2.3. Finally, background information on the two specific kinds of sandy soils involved in this study is presented in Section 2.4.

2.2 WAVE PROPAGATION IN SOILS

The propagation of stress waves in soil is affected by the stiffness and damping properties of the soil. A stress wave propagates faster in soil with higher stiffness and it attenuates more slowly in soil with lower damping. These principles have been applied in various ways to obtain the dynamic properties of soil. In addition, there are different kinds of stress waves, and they are governed by different dynamic properties of the soil.

Based on the characteristics and shape of the medium in which stress waves are propagating, the stress waves that propagate in soil systems are generally divided into two main types: body waves and surface waves. Body waves propagate along the surface, and in the interior of soil systems while surface waves propagate only along the

boundaries, generally at the interface where the soil and air or soil and water meet. According to the relation between the direction of particle movement and direction of wave propagation, body waves are subdivided into compression waves (P waves) and shear waves (S waves). If the direction of particle movement is parallel to the direction of wave propagation, these stress waves are called compression waves, constrained compression waves or P waves. If the direction of particle movement is perpendicular to the direction of wave propagation, these stress waves are called shear waves or S waves. When body waves interact with boundaries in the soil, surface waves will be generated that will travel along the soil boundaries (Kramer, 1996). For instance, the interaction of

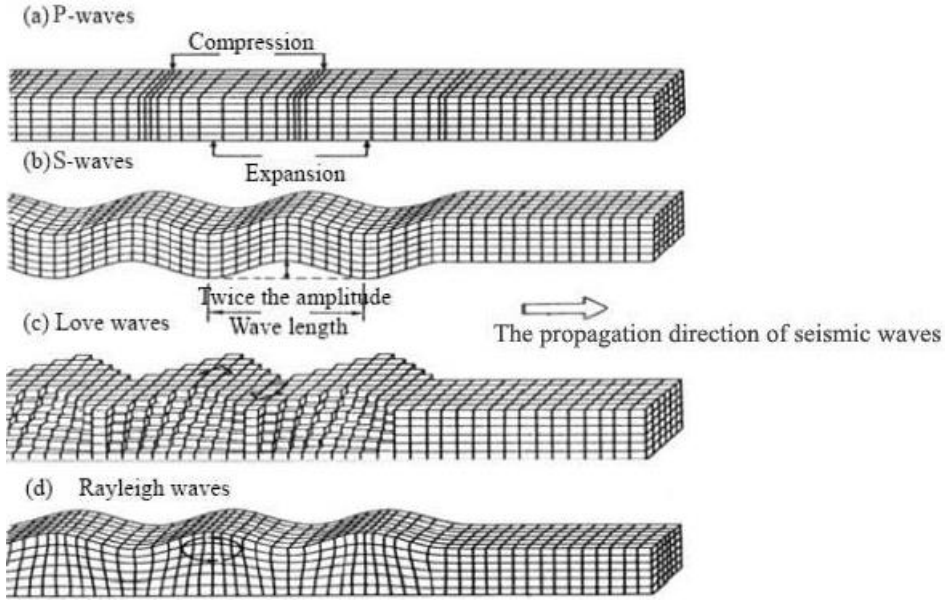

Figure 2.1 Propagation of Body Waves and Surface Waves within and along the Surface of a Uniform, Half Space: (a) Compression Waves, (b) Shear Waves, (c) Love Waves, and (d) Rayleigh Waves (from Bolt, 1993)

P waves or SV waves (SV waves are simply S waves with particle motion in the vertical plane) with the air-solid boundary at the top of the system, these body waves can produce Rayleigh waves. The interaction of SH waves, which are S waves with particle motion in a horizontal plane, with boundaries of soil can generate Love waves. A simplified schematic of the propagation and particle motion direction of body waves and surface waves is presented in Figure 2.1.

As mentioned above, the velocities of different stress waves are related to different stiffness properties of the soil. According to the principles of wave propagation, P waves within the soil mass compress the soil in constrained compression during propagation while S waves distort the soil in shear. Therefore, P-wave velocity is related to the constrained modulus, M, and S-wave velocity is related to the shear modulus, G. If the volumetric mass density of the soil, ρ, the constrained compression wave velocity, V_P, and the shear wave velocity, V_S, are known, M and G of soil can be calculated with the following equations:

$$M = \rho \cdot {V_P}^2 \tag{2.1}$$

$$G = \rho \cdot {V_S}^2 \tag{2.2}$$

Once M and G are determined, Poisson's ratio (v), Young's modulus (E) and the unconstrained compression wave velocity (V_C) can be calculated, assuming the soil is homogeneous and isotropic as follows:

$$v = \frac{M - 2G}{2M - 2G} \tag{2.3}$$

$$E = 2G(1 + v) \tag{2.4}$$

$$V_C = \sqrt{E/\rho} \tag{2.5}$$

In most cases, the shear modulus of the soil is the most important modulus in geotechnical engineering design and G is the focus in this study.

2.3 DYNAMIC PROPERTIES OF SANDY SOIL

2.3.1 General Information

Dynamic properties of soil describe how soil behaves under dynamic loading and also under static loading at small to moderate strains (Kacar, 2014). Normally, the most important dynamic properties in engineering design are the shear modulus (G) and the material damping ratio in shear (D). In general, most studies of the dynamic properties of soil in shear cover two, three of four generalized strain ranges. The three strain ranges most often investigated by dynamic (not cyclic) testing in the laboratory are: (1) the small-strain linear range, (2) the nonlinear "elastic" range and (3) the moderately nonlinear range. These strain ranges are illustrated in Figure 2.2. The small-strain linear range is represented by shear strains at or below the elastic threshold strain, γ_t^e, as shown in Figure 2.2. In small-strain range, G and D are independent of shear strain and are called the maximum shear modulus (G_{max}) and minimum material damping ratio (D_{min}),

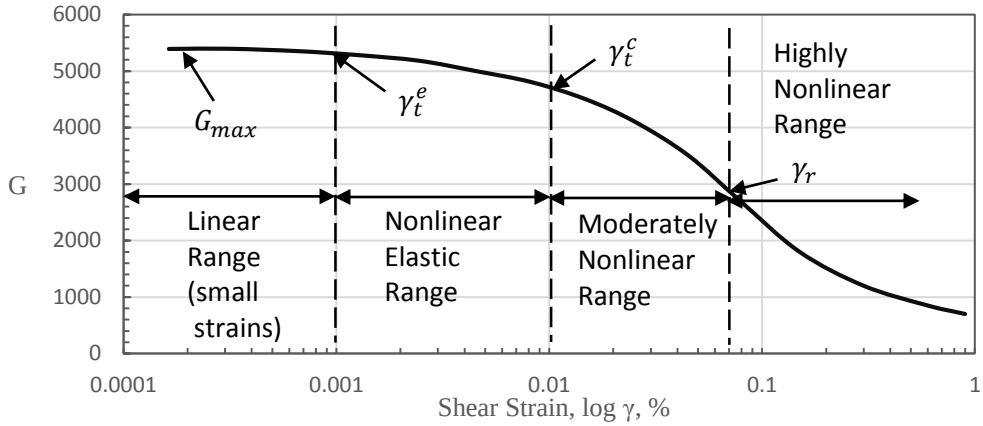

(a) Shear Modulus – Log Shear Strain Curve

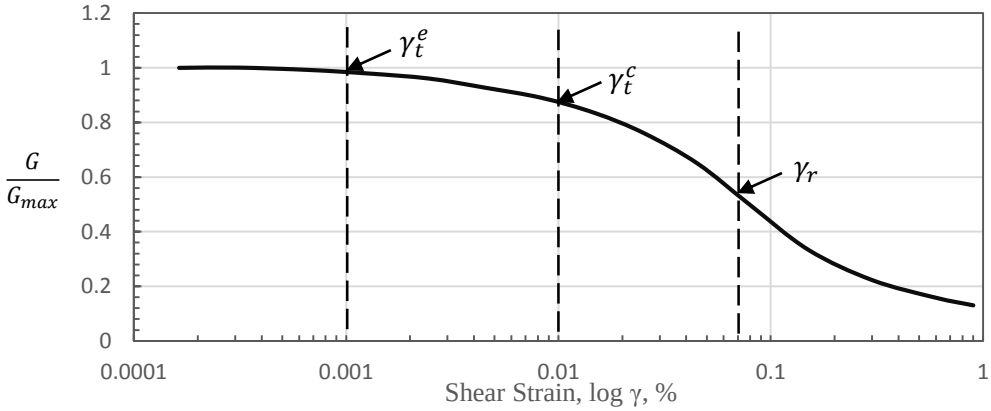

(b) Normalized Shear Modulus – Log Shear Strain Curve

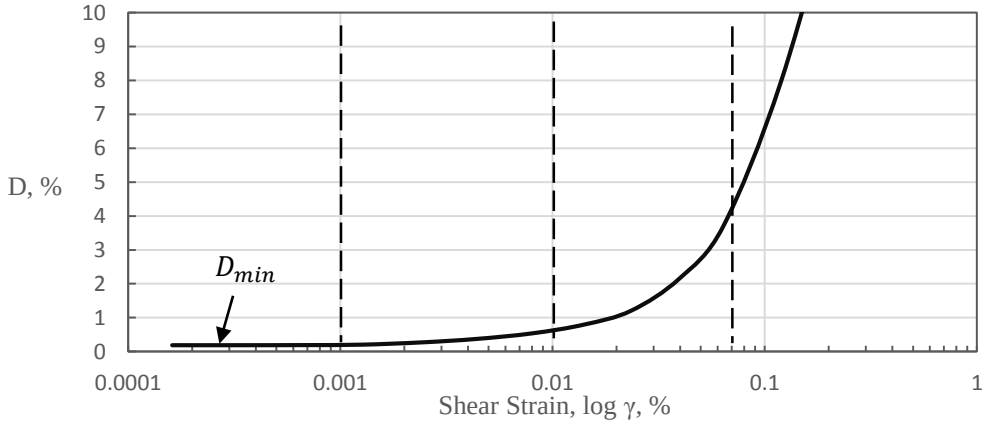

(c) Material Damping Ratio – Log Shear Strain Curve

Figure 2.2 Generalized Nonlinear Dynamic Properties of a Granular Soil Confined at a Pressure of One Atmosphere (after Kacar, 2014)

respectively. The normalized shear modulus, G/G_{max}, is equal to one in this strain range. Above γ_t^e in the nonlinear "elastic" range, G and G/G_{max} decreases with increasing shear strain while D increases with increasing shear strain as shown in Figure 2.2. The upper bound of the second strain range is denoted by the cyclic threshold strain, γ_t^c. At strains above γ_t^c, the tendency for volume change begins which also creates changes in the material skeleton. Hence, above γ_t^c, the term "elastic" is no longer used because permanent changes in the granular material begin to occur. In the third strain range, the moderately nonlinear range, G and D are changing significantly with shear strains. The value of γ_t^e varies with soil type, but 0.001 % can be assumed as a representative value if soil type is unknown and the confining pressure is around one atmosphere.

Many other factors can affect the dynamic properties of soil. For example, confining pressure, void ratio, geologic age, cementation, over-consolidation, plastic index, strain rate and number of loading cycles can effect G and D. In Table 2.1, the impacts of each factor on G_{max}, G/G_{max} and D are given by Dobry and Vucetic. The two specific kinds of soil involved in this study are both cohesionless soils. Thus, details about the dynamic properties of sandy soils are the focus of the discussions in the following sections.

2.3.2 Small-Strain Dynamic Properties of Sandy Soil

As mentioned above, even though the small-strain dynamic properties of sandy

Table 2.1 Factors Affecting Dynamic Properties of Natural Soils (from Dobry and Vucetic, 1987)

Affecting Factor	G_{max}	G/G_{max}	D
Confining Pressure, σ_o	increases with σ_o	stays constant or increases with σ_o	stays constant or decreases with σ_o
Void Ratio, e	decreases with e	increases with e	decreases with e
Geologic Age, t	increases with t	may increase with t	decreases with t
Cementation, c	increases with c	may increase with c	may decrease with c
Overconsolidation, OCR	increase with OCR	not affected	not affected
Plasticity Index, PI	increases with PI if OCR > 1 stays about constant if OCR = 1	increases with PI	decreases with PI
Cyclic Strain, γ_c	-	decreases with γ_c	increases with γ_c
Strain Rate, $\dot{\gamma}$ (Frequency of Cyclic Loading)	increases with $\dot{\gamma}$	G increases with $\dot{\gamma}$ G/G_{max} probably not affected if G and G_{max} are measured at same $\dot{\gamma}$	stays constant or may increase with $\dot{\gamma}$
Number of Loading Cycles, N	decreases with N at large γ_c but recovers later with time	decreases with N at large γ_c (G_{max} measured before N cycles)	not significant for moderate γ_c and N

Note: In these cases, all changes in G_{max}, G/G_{max} and D noted in the columns are for the "factor" in Column #1 increasing.

soil are independent of shear strain, there are many other factors that can affect G_{max} and D_{min}. An early investigation of G_{max} of reconstituted sandy soils was performed by Hardin and Richart (1963). They found that both mean effective confining pressure (σ_0') and void ratio (e) affect G_{max}. From their studies, a generalized equation was recommended for G_{max}:

$$G_{max} = C_G F(e)(\sigma_0')^{n_G} \tag{2.6}$$

where $F(e)$ is a function of e, and C_G and n_G are constants. C_G equals the value of G_{max} when $F(e) = 1.0$ and $\sigma_0' = 1\ atm$. According to their test results, G_{max} increases with increasing σ_0' and decreasing e. Commonly used functions for $F(e)$ are:

$$F(e) = \frac{(2.97 - e)^2}{1 + e}\ by\ Hardin\ and\ Black\ (1968), and \tag{2.7}$$

$$F(e) = \frac{1}{0.3 + 0.7e^2}\ by\ Hardin\ (1978). \tag{2.8}$$

For most clean sand, Hardin and Black (1968) found that n_G, the exponent of σ_0', has a value generally close to 0.5. However, for different types of sandy soils, C_G and n_G can vary somewhat. Several researchers have done studies on n_G and C_G values in Equation 2.6, and some results are presented in Table 2.2.

Table 2.2 Values of n_G and C_G of Several Sandy Soils (Kokusho, 1987; Ishihahra, 1996)

Referebce	F (e)	C_G (kPa)	n_G	Soil description
Hardin and Richart (1963)	$\frac{(2.17-e)^2}{1+e}$	7000	0.5	Round grain Ottawa sand
	$\frac{(2.97-e)^2}{1+e}$	3300	0.5	Angular grained crushed quartz
Iwasaki et al. (1978)	$\frac{(2.17-e)^2}{1+e}$	9000	0.38	Eleven kinds of clean sand
Kokusho (1980)	$\frac{(2.17-e)^2}{1+e}$	8400	0.5	Toyoura sand
Yu and Richart (1984)	$\frac{(2.17-e)^2}{1+e}$	7000	0.5	Three kinds of clean sand

In the Hardin and Richart's equation, only σ_0' and e are considered as numerical factors that can affect G_{max}. The impacts of other factors are attributed to either the constant C_G or the change of e. To include other important characteristics of granular soils in the G_{max} equation, such as median grain size (D_{50}) and uniformity coefficient (C_u), Menq (2003) tested 59 reconstituted sandy and gravelly specimens. In Menq's dissertation, he suggested the following modified equations based on Hardin and Richart's equation:

$$G_{max} = C_{G3} \times {C_u}^{b1} \times e^x \times \left(\frac{\sigma_0'}{P_a}\right)^{n_G} \tag{2.9}$$

where $C_{G3} = 67.1\ MPa\ (1400\ ksf)$,

$b1 = -0.2$,

$x = -1 - (D_{50}/20)^{0.75}$,

$n_G = 0.48 \times C_u^{0.09}$

C_u = uniformity coefficient, and,

e = void ratio

From Menq's study, the main factors that influence G_{max} are σ_0', e and D_{50}. The effect caused by C_u is minor, and is mostly due to the changes of e caused by changes in C_u. According to Menq's equation, G_{max} increases with increasing values of σ_0', D_{50} and C_u and decreasing e.

The small-strain material damping ratio (D_{min}) of soil has been more difficult to measure than G_{max} because of the interference from ambient background noise and equipment-generated damping in the material damping values measured in resonant column (RC) tests. Using early work by Hwang (1997), Laird (1994) utilized metal specimens, which have very small D_{min}, to measure equipment-generated damping at each frequency and developed an equation to calculate equipment-generated damping. By subtracting equipment-generated damping from the material damping measured in the RC tests, D_{min} can be obtained. Based on the measured D_{min} of dry granular soil (washed mortar sand), Laird (1994) then developed an equation for the calculation of D_{min} as:

$$D_{min} = C_D F(e) \left(\frac{\sigma_0'}{P_a}\right)^{n_D} \tag{2.10}$$

where C_D is the dimensionless material damping ratio coefficient and n_D is the effective isotropic stress exponent. $F(e)$ is a function of e and commonly used in the form of Equation 2.8. From the equation, the main factors that influence D_{min} are σ_0' and e.

Menq (2003) also developed an equation for the calculation of D_{min} from his study on 59 reconstituted sandy and gravelly specimens. Menq's equation is:

$$D_{min} = 0.55 \times {C_u}^{0.1} \times {D_{50}}^{-0.3} \times \left(\frac{\sigma_0'}{P_a}\right)^{-0.08} \tag{2.11}$$

According to Equation 2.11, D_{min} increases with decreasing D_{50} and σ_0', and increasing C_u. However, the influences of C_u and σ_0' are much smaller than that of D_{50}.

In this study, the following equations are applied to G_{max} and D_{min} in the first fitting of the test data to permit easy comparisons to readily be made:

$$G_{max} = A_G \left(\frac{\sigma_0'}{P_a}\right)^{n_G} \tag{2.12}$$

$$D_{min} = A_D \left(\frac{\sigma_0'}{P_a}\right)^{n_D} \tag{2.13}$$

where A_G and A_D are the values of these parameter at σ_0' equal to one atmosphere (P_a).

2.3.2 Nonlinear Dynamic Properties of Sandy Soils

As mentioned earlier, the shear modulus (G) and normalized shear modulus (G/G_{max}) decrease and the material damping ratio (D) increases with increasing shear strain (γ) above the elastic threshold, γ_t^e. These changes in G, G/G_{max} and D_{min} are illustrated in Figure 2.2 where the nonlinear range is subdivided into four parts. Other factors can also affect the nonlinear behavior of sandy soils as discussed by Hardin and Drnerich (1972) and in Chapters Five and Six in this study.

The cyclic threshold strain (γ_t^c) and the reference strain (γ_r), where the G/G_{max} is 0.5, are effective strain levels for comparison of mild ("elastic") and moderate nonlinearity, respectively. Seed et al. (1986) presented a study that showed sandy soils behave more linearly than gravelly soils in the mild and moderate nonlinear ranges of shear strains. This difference in response means that sandy soils have larger values of γ_t^c and γ_r than gravelly soils. For instance, in Figure 2.3, the mean value of γ_r of sandy soils is about 0.036 % while the mean value of γ_r of gravelly soils is about 0.012 % at $\sigma_0' \sim 1\ atm$. However, this trend is not well shown in the $D - \log\gamma$ curves in the Seed at al. data; that is, the D values of gravelly soils cover a wide range in D values which, for the testing results, also encompass the D values of sandy soils.

Tanaka et al. (1978) showed how isotropic confining pressure (σ_0') and gravel content influenced the nonlinear behavior of gravelly soil. As seen in Figure 2.4, as confining pressure increases and gravel content decreases, both the $G/G_{max} - \log\gamma$ and

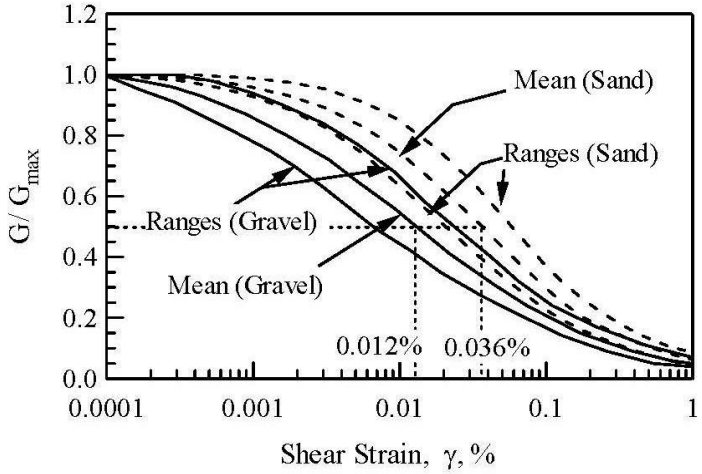

(a) Normalized Shear Modulus – Log Shear Strain Relationships in the Nonlinear Range

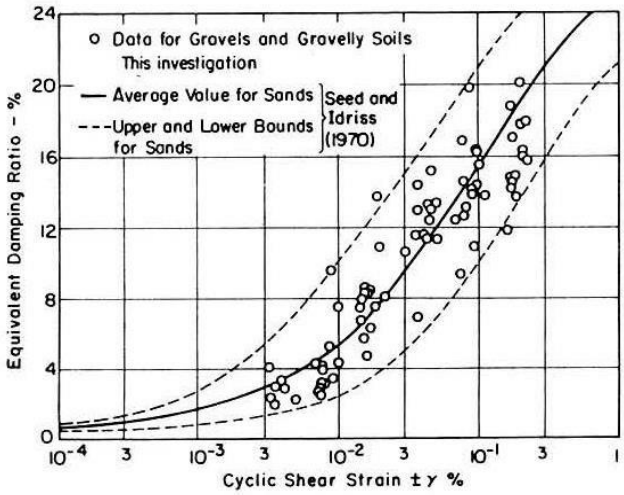

(b) Material Damping Ratio – Log Shear Strain Relationships in the Nonlinear Range

Figure 2.3 $G/G_{max} - \log\gamma$ and $D - \log\gamma$ Curves of Sandy and Gravelly Soils as Suggested by Seed et al. (1986). Note: Darendeli (2001) and Menq (2003) show that these $G/G_{max} - \log\gamma$ relationships actually represent soils at σ_0'~1atm.

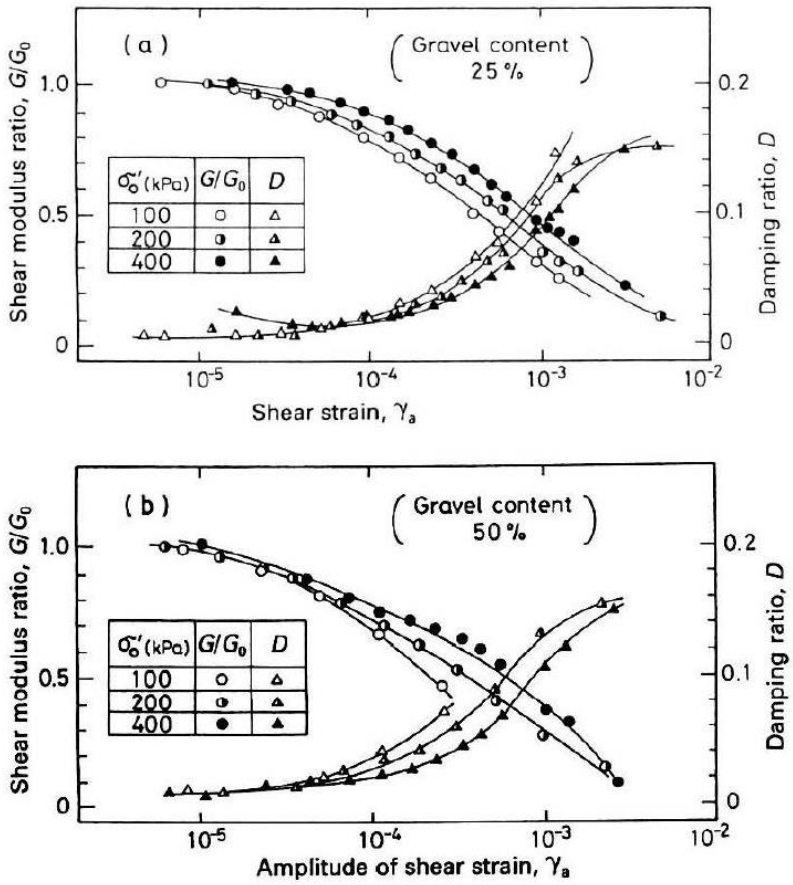

Figure 2.4 Comparison of the Effects of Effective Isotropic Confining Pressure and Gravel Content on $G/G_{max} - \log\gamma$ and $D - \log\gamma$ Curves of Reconstituted Gravelly Materials (from Tanaka et al. 1987)

$D - \log\gamma$ curves move to the right (to higher shear strains) and γ_r increases, which means the soil behaves more linearly.

Menq (2003) applied the modified hyperbolic model (Darendeli, 2001) to the study of the nonlinear behavior of sandy and gravelly soils. The G/G_{max} equation for Darendeli's modified hyperbolic model is:

$$\frac{G}{G_{max}} = \frac{1}{1 + \left(\frac{\gamma}{\gamma_r}\right)^a} \tag{2.14}$$

where: $a =$ curvature coefficient.

Menq found that, in addition to σ_0', another main factor which affects the nonlinear shear modulus of sandy and gravelly soils is the uniformity coefficient (C_u). As shown in Figure 2.4, with increasing C_u, sandy and gravelly soils behave more nonlinearly and γ_r decreases. In Menq's tests of 59 reconstituted sandy and gravelly soil specimens, he presented the recommended equations for calculating the parameters in Darendeli's modified hyperbolic model (γ_r and a) for nonlinear shear modulus:

$$\gamma_r = 0.12 \times {C_u}^{-0.6} \times \left(\frac{\sigma_0'}{P_a}\right)^{0.5 \times {C_u}^{-0.15}} \tag{2.15}$$

$$a = 0.86 + 0.1 \times \log\left(\frac{\sigma_0'}{P_a}\right) \tag{2.16}$$

According to Darendeli (2001), the nonlinear material damping ratio for sandy and gravelly soils can be described well with the modified "Masing behavior" as shown in following equations:

$$(D - D_{min}) = b \cdot \left(\frac{G}{G_{max}}\right)^{0.1} \cdot D_{Masing} \tag{2.17}$$

$$D_{Masing,a=1.0}\,(\%) = \frac{100}{\pi}\left[4\frac{\gamma - \gamma_r \ln\left(\frac{\gamma+\gamma_r}{\gamma_r}\right)}{\frac{\gamma^2}{\gamma+\gamma_r}} - 2\right] \quad (2.18)$$

$$D_{Masing}\,(\%) = c_1 D_{Masing,a=1.0} + c_2 {D_{Masing,a=1.0}}^2 + c_3 {D_{Masing,a=1.0}}^3 \quad (2.19)$$

where: D_{Masing} = material damping ratio determined from the "Masing behavior",

b = scaling coefficient ($= 0.6329 - 0.0057 \times \ln(N)$),

$c_1 = -1.1143a^2 + 1.8618a + 0.2523$,

$c_2 = 0.0805a^2 - 0.0710a - 0.0095$, and

$c_3 = -0.0005a^2 + 0.0002a + 0.0003$.

Menq's tests of sandy and gravelly soils also supported Equations 2.17 and 2.18.

With the $(D - D_{min}) - G/G_{max}$ relationship, the $(D - D_{min}) - \log\gamma$ relationship can be obtained based on the $G/G_{max} - \log\gamma$ relationship. Finally, the $D - \log\gamma$ curve can be calculated by adding D_{min} to the $(D - D_{min}) - \log\gamma$ relationship.

2.4 BACKGROUND INFORMATION ON THE LIQUEFIABLE SAND AND CALCAREOUS SAND TESTED IN THIS STUDY

2.4.1 Liquefiable Sand

Liquefiable sand is sand that almost completely loses strength and stiffness under sudden large changes (decreases) in the effective stress condition, usually caused by earthquake shaking and the generation of large pore water pressure. Soil liquefaction generally happens in saturated or nearly saturated ($S_r > 99.6\%$) loose sands. When a

shear load is suddenly applied to the saturated loose sand, water in the sand has no time to drain so that an undrained condition occurs and pore water pressure increases. Since effective stress equals total stress minus pore water pressure, the effective stress decreases as pore pressure increases. When the pore water pressure is close to the total stress, the effective stress will be nearly zero and the soil will lose the ability to support loads. In earthquakes, soil liquefaction can lead to serious consequences. The term "liquefied" was first mentioned by Hazen (1920). And since then, many studies and much research have been conducted on this subject.

Liquefiable sand tested in this study is from Christchurch, New Zealand. In 2010-2011, the city of Christchurch experienced widespread liquefaction, which was caused by a series of powerful earthquakes. Significant damage covering large areas was caused by the serious liquefaction around the city and the surrounding suburbs. The layers composed of liquefiable sand are generally at or below the ground water table. Disturbed samples of the liquefiable fine sands and silty sands that were tested in this study were obtained from trenches that were dug at several sites. Significant dewatering was required to permit the trenches (less than about 3 m deep) to be dug. The samples were air dried before shipping to the University of Texas at Austin.

2.4.2 Calcareous Sand

Calcareous sand is sand which contains a large proportion of calcium carbonate and is usually formed by complex interactions among biological, mechanical, physical,

and chemical factors. Many special features of calcareous sand have been found, such as remarkable void space inside the particles and very angular particle shapes. As a result, calcareous sand usually has a large void ratio, large compressibility and high susceptibility to crushing. During previous studies, calcareous sand has been proven to behave differently compared to other siliceous sands.

The calcareous sand involved in this study comes from Puerto Rico. This sand was kindly provided to this project by Professor Christorpher Baxter at the University of Rhode Island. The sand had been air dried before shipping to UT. Information about many physical properties of the sand was also supplied by Professor Baxter and his students. However, no more details about the sampling are available at this time.

2.5 SUMMARY

The theory of wave propagation is a basic principle used in dynamic laboratory testing to determining dynamic soil properties. (This theory is not used in slow cyclic testing because "inertia" does not enter the data analysis in slow loading) In previous investigations of small-strain dynamic properties of sandy soil, Hardin and Richart's equation for G_{max}, Laird's equation for D_{min} and Menq's equations for G_{max} and D_{min} are discussed. To describe the nonlinear dynamic properties of sandy soil, the studies from Seed et al. (1986) Tanaka et al. (1978), and Menq (2003) are presented. An explanation of Menq's equations used to model G and D of sandy and gravelly soils is also presented. Finally, the two specific types of sandy soils dynamically tested in this

project – liquefiable sand from Christchurch and calcareous sand from Puerto Rico - are briefly introduced.

CHAPTER THREE

OVERVIEW OF THE RESONANT COLUMN TESTING DEVICE AND DATA ANALYSIS

3.1 INTRODUCTION

The resonant-column (RC) test equipment and methodology of analyzing the test data are described in this chapter. The RC test has been employed as a prime tool to investigate the dynamic characteristics of soil specimens in the shear strain range of 0.0001 to 0.1 %, mainly shear modulus (G) and material damping ratio in shear (D) for many decades. In this study, the dynamic properties of two specific kinds of sandy soil are investigated using the RC test equipment. In Section 3.2, details of the RC device are introduced. The data analysis method used in the RC test is discussed in Section 3.3.

3.2 OVERVIEW OF THE RESONANT COLUMN TESTING DEVICE

3.2.1 General Information

The resonant column (RC) test has been used for more than 38 years in the Soil and Rock Dynamics Laboratory at University of Texas at Austin by Dr. Stokoe and his graduate students; for instance, Isenhower, 1979, Lodde, 1982, Ni, 1987, Kim, 1991, Hwang, 1997, Darendeli, 2001 and Menq, 2003. The basic principle in RC testing is to vibrate a cylindrical specimen of material in first-mode torsional motion. The simplest

configuration involves a soil specimen that is free to move in torsional motion at the top and is fixed by a rigid base pedestal at the bottom. Sinusoidal torsional excitation is applied to the top of the specimen over a range of frequencies in a downward, stepped-wise sweep. The torsional motion of the top of the specimen is recorded and a dynamic response curve is created. The RC configuration is called a fixed-free RC test; because the top of the specimen freely vibrates while the bottom of the specimen remains fixed (remains stationary). This type of RC testing was performed in this study.

The fixed-free RC device used herein can be divided into four basic subsystems. These subsystems are: (1) a confinement system that applies confining pressure to the specimen, (2) a drive system that is used to apply sinusoidal torsional excitation at the top of the specimen, (3) a height monitoring system that is used to measure the height-change of the specimen during confinement, and (4) a motion monitoring system that is used to measure the torsional response at the top of the specimen. The confinement system is operated manually while the other three systems are controlled by an automated computer system with data acquisition and processing. Details of each system are discussed in following subsections.

The RC test equipment is calibrated annually to assure proper maintenance and accurate measurement during normal operation. A large number of RC tests (>800) have been performed in the Soil and Rock Dynamics Laboratory at University of Texas at Austin. Therefore, the RC test equipment is well suited, properly calibrated, and qualified for use in this study.

3.2.2 RC Confinement System

The RC confinement system consists of a stainless steel chamber, air-pressure sources and air pressure gages to measure the confining pressure inside the chamber. Stainless steel is used for the chamber to minimize forces of attraction between the magnets attached to the drive plate in the RC drive system and the chamber walls. A 10-inch, OD hollow cylinder, four fixing rods, a top plate and a base plate together enclose the confined space in which the specimen is placed (see Figure 3.1). Compressed air (or nitrogen gas) is introduced into the confining chamber to create the cell pressure. Rubber O-rings are used between the ends of the hollow cylinder and the two end plates to create seals at the top and bottom of the chamber. The base plate is firmly attached to the table on which the RC test device is placed.

The RC confinement chamber was designed to be capable of handling air pressure as high as 460 psi (about 31 atm). There are two air sources for the confinement system; the building air pressure source and a high-pressure (~2000 psi) nitrogen tank. The supplied pressure from the building can go up to about 80 psi and, after that, the supplied pressure from the nitrogen tank is used for higher confining pressures. Different pressure gages are used for the different pressure sources considering the proper resolution and range. Annual calibration is required for the pressure gages to ensure the accuracy of the readings. In Figure 3.1, a simplified schematic of the RC confinement system is presented. In Figure 3.2, a photograph of the actual RC confinement system is presented.

In this study, the sandy soil specimens were reconstituted on the base pedestal using a split mold. Once the required height of the specimen was reached, a metal top cap was placed on top of the specimen. A membrane with a pre-selected thickness was utilized around the specimen to transfer the confinement from the air pressure to the specimen. Sealing the specimen was done with vacuum grease and O-rings at the ends of the membrane on both the top cap and base pedestal. One or two drainage vents through the base pedestal and the base plate connected the pore pressure inside the specimen to the outside atmosphere and made sure that drained conditions would exist during the RC test.

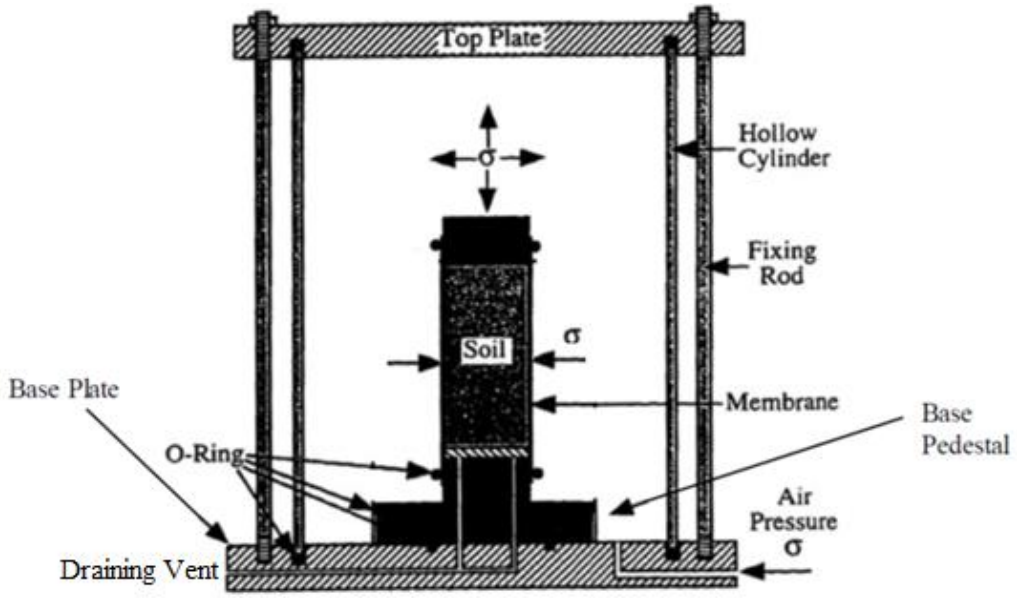

Figure 3.1 Simplified Schematic of RC Confining System (from Hwang, 1997)

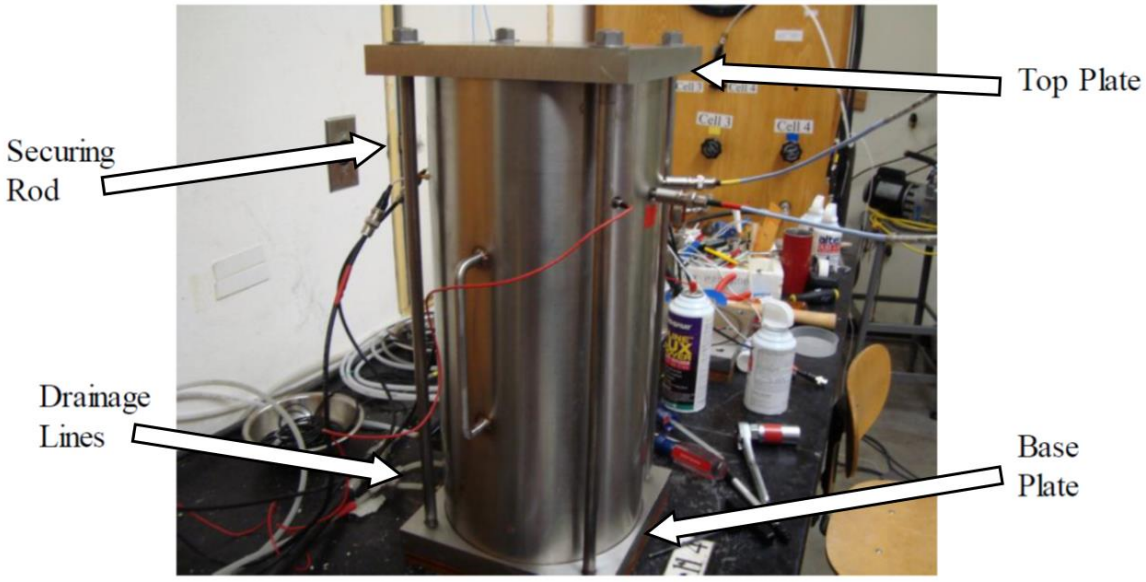

Figure 3.2 Photograph of Confining Chamber Used in RC Testing at UT (from Umberg, 2012)

3.2.3 RC Drive System

The drive system in the RC device consists of a rigid drive plate, a function generator and a power amplifier. The rigid drive plate has four arms with one permanent magnet firmly fixed at the end of each arm as shown in Figure 3.3. Each permanent magnet is encircled with two sets of drive coils which do not touch the magnet. The central portion of the drive plate is attached to the top cap on the specimen using four screws. During each RC test, sinusoidal electrical current passes through the total of eight coils. The electrical current creates sinusoidal torsional excitation, which in turn

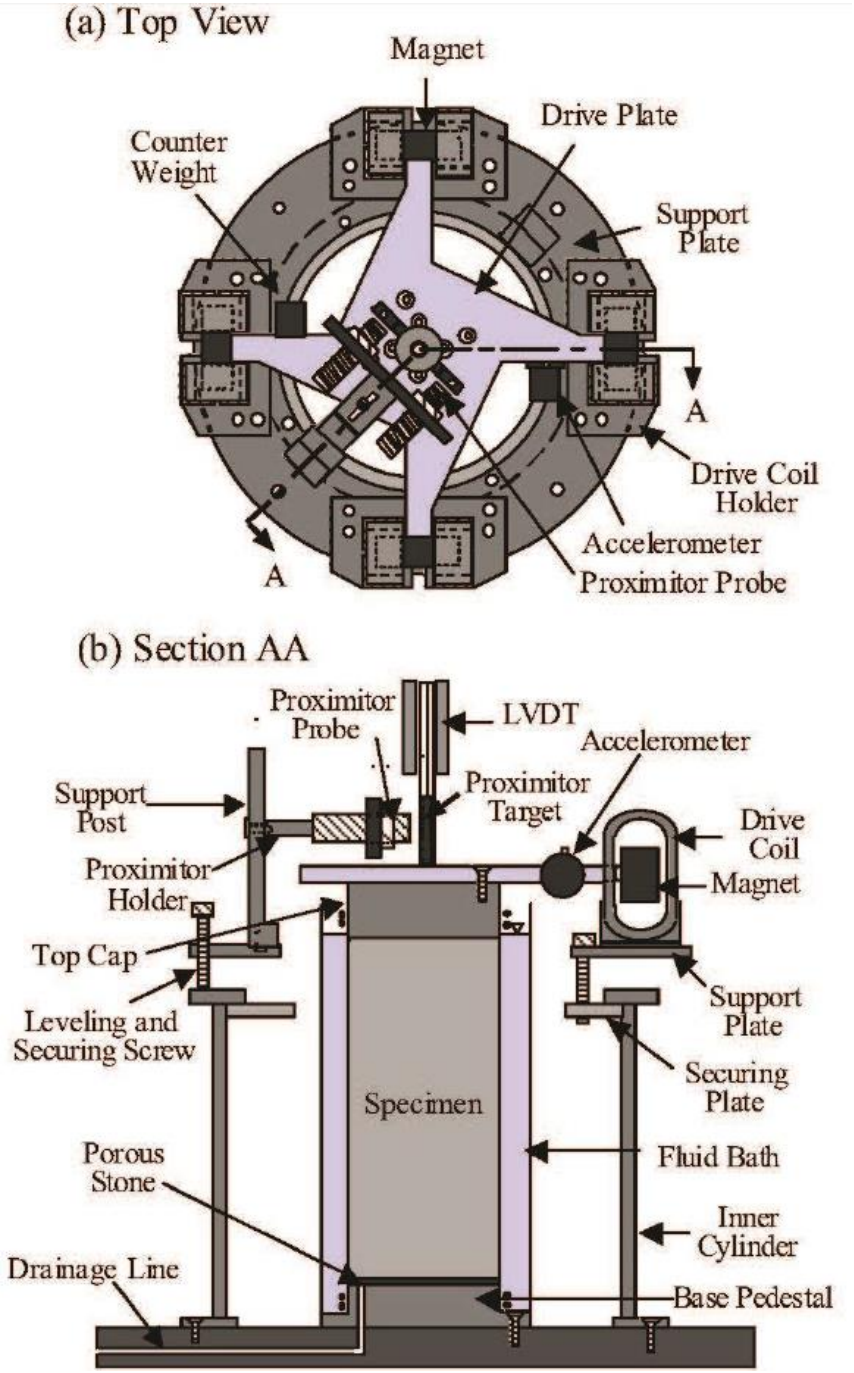

Figure 3.3 Drive System Used in the RC test: (a) Top View and (b) Cross-Sectional View (from Ni, 1989)

generates torsional motion at the top of the specimen. The magnitude of torque generated by the drive plate is dependent on the strength of the permanent magnets, the size and resistance of the drive coils, the size of the air gap between the magnets and coils, the length of the drive plate arms and the power of the electrical current that passes through the coils. The function generator is the device that generates the sinusoidal current going to the coils.

In one RC test to evaluate G and D at one time under a given confining pressure, the function generator produces three kinds of signals. These three kinds of signals are used to perform the following: (1) a "rough" sweep over a pre-selected frequency range, (2) then a "fine" sweep around the resonant frequency and (3) then free-vibration decay tests. The "rough" sweep is used to find a "rough" value of the resonant frequency. The "fine" sweep is used to obtain an accurate value of the resonant frequency as well as the shape of the response curve to allow determination of the half-power bandwidth. The free-vibration decay tests are used to evaluate the material damping ratio. The half-power bandwidth method is also used as a complementary method to the free-vibration tests to evaluate D_{min} at small strains. The power amplifier is used to amplify the current signal to obtain larger values of torque during higher-amplitude testing. The drive plate, function generator and power amplifier are all checked annually for calibration compliance.

3.2.4 Specimen-Height Monitoring System

The specimen-height monitoring system consists primarily of a linear variable differential transformer (LVDT) (see Figure 3.3). An output voltage signal is obtained after an input voltage signal is sent to the LVDT. This output voltage is combined with the calibration factor from the annual calibration and the height of the specimen at the time of the measurement is determined. This process is repeated many times during RC testing at each confining pressure. The height of the specimen at all times during testing is needed in the data analysis for the estimation of changes in void ratio and total unit weight of the specimen during the total duration of confinement.

The LVDT is shown in the Figure 3.3 b. The LVDT core is attached to the drive plate, which moves together with the top cap on the specimen. The LVDT coils are supported by a holding arm that is fixed to the base plate of the RC system so that the LVDT coils remain in a fixed position during testing. The LVDT core, which is located inside the LVDT coils, does not touch the coils. When the height of the specimen changes, the relative position of the core inside the coils will change too, and a different LVDT reading will be obtained.

3.2.5 Specimen-Motion Monitoring System

The specimen-motion monitoring system is composed of an accelerometer, a charge amplifier, a frequency counter, a digital voltmeter and a digital oscilloscope. All

components in the motion monitoring system are calibrated annually to ensure accurate measurements.

As shown in Figure 3.3, the accelerometer is attached to the drive plate and generates an electrical signal created by the torsional motions of the specimen. The recorded signal from the accelerometer is then conditioned by the charge amplifier after which the digital voltmeter is used to read this voltage at each frequency measured by the frequency counter. The amplitude of torsional motion at each frequency can then be obtained from which a frequency response curve is plotted. The resonant frequency of the specimen is obtained from the frequency at maximum motion. After the resonant-frequency measurement has been successfully and accurately performed, the drive system then applies a sinusoidal torsional excitation at the resonant frequency of the specimen. Once this resonant motion becomes steady state, the computer suddenly shuts off the current so that a free-vibration decay curve is captured by the digital oscilloscope. The frequency response curve and free-vibration decay curve are used in the data analysis to calculate the shear modulus and material damping ratio, respectively. This procedure is discussed below.

3.3 DATA ANALYSIS FOR RESONANT COLUMN TESTING

3.3.1 Shear Modulus Calculation

An example frequency response curve obtained at one measurement time in the RC test is shown as Figure 3.4. The frequency response curve is “bell-like” and has a

peak at the first-mode resonant frequency. By inserting the resonant circular frequency, ω_r ($\omega_r = 2\pi f_r$), in the following equation, the shear wave velocity, V_s, can be calculated:

$$\frac{I}{I_0} = \frac{\omega_r \cdot h}{V_s} \tan \frac{\omega_r \cdot h}{V_s} \tag{3.1}$$

where I = mass polar moment of inertia of the soil specimen,

I_0 = mass polar moment of inertia of the top cap and drive system,

h = height of the soil specimen,

ω_r = circular resonant frequency ($\omega_r = 2\pi f_r$), and

V_s = shear wave velocity of the soil specimen.

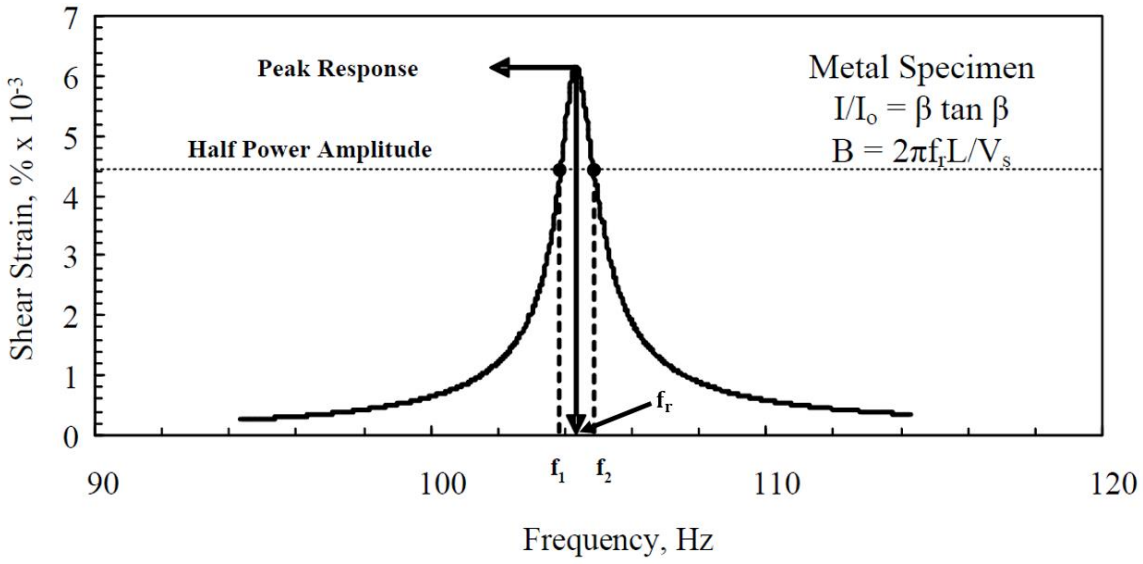

Figure 3.4 Typical Dynamic Response Curve Obtained in a Small-Strain Resonant Column Test (from Stokoe et al, 1994)

The relationship between shear wave velocity and shear modulus in the wave propagation theory discussed in Chapter 2 is then used to calculate the shear modulus from the shear wave velocity and the total unit weight of the specimen at the time of the measurement. This relationship is presented in Equation 2.3.

3.3.2 Calculation of the Material Damping Ratio

There are two different ways of obtaining the material damping ratio (D) of the specimen in the RC test. These two ways differ in principle. The first way is calculating D from the width of the dynamic frequency response curve. This method is called the half-power bandwidth method and is illustrated in Figure 3.4. The value of D is calculated using the following equation (Van Hoff, 1993) based on linear behavior:

$$D = \frac{f_1 - f_2}{2f_r} \tag{3.2}$$

where f_1 = the lower frequency where the shear strain amplitude is equal to the half power of the maximum shear strain (0.707 A_{max}),

f_2 = the higher frequency where the shear strain amplitude is equal to the half power of the maximum shear strain (0.707 A_{max}),

f_r = the resonant frequency of the specimen, and,

A_{max} = the amplitude at f_r.

When the dynamic frequency response curve is symmetrical, which means that the RC test is exciting the specimen in the linear range, the values of D from the half-power bandwidth method and from the free-vibration decay method are in good agreement. However, as the shear strains excited in the specimens move into the nonlinear range, the dynamic frequency response curve becomes nonsymmetrical and tilts towards the lower frequency. This change in shape of the response curve can cause a serious error in the calculation of D by the half power bandwidth method. After this negative effect, the free-vibration decay curve is used as the only method of calculation of D. The free-vibration decay curve is obtained by suddenly stopping the current to the drive coils during the constant vibration at the resonant frequency. A typical free-vibration decay curve is presented in Figure 3.5. The log decrement, δ, is calculated by:

$$\delta = \ln \frac{A_n}{A_{n+1}} \tag{3.3}$$

where A_n= peak strain amplitude of the $(n)\ th$ circle, and

A_{n+1}= peak strain amplitude of the $(n+1)\ th$ circle.

The value of D is calculated by:

$$D = \sqrt{\frac{\delta^2}{4\pi^2 + \delta^2}} \tag{3.4}$$

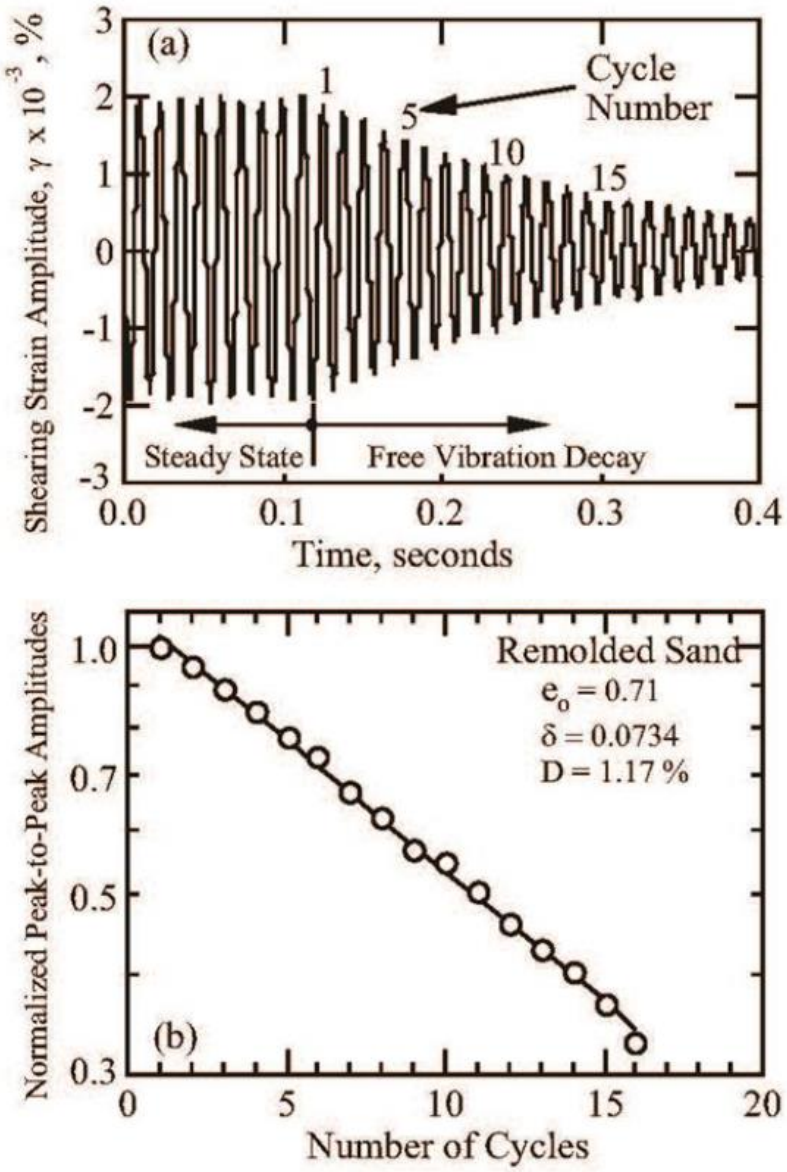

Figure 3.5 Material Damping Ratio Measurement in RC testing from the Free-Vibration Decay Curve: (a) the Free Vibrations and (b) the Log Decrement Evaluation (from Stokoe et al, 1994)

During small-strain RC testing, the measurement of D using the free-vibration decay curve can easily be disturbed if a high level of background noise exists. As the shear strain becomes larger, the effect of background noise is no longer a problem compared to the large motions of the specimen. Therefore, in small-strain RC testing, D is often more accurately measured by the half-power bandwidth method. On the other hand, for the larger-strain RC testing into the nonlinear range, the free-vibration decay curve must be used to measure D because the dynamic response curve becomes asymmetrical which causes erroneous values of D (Ni, 1987).

Equipment-generated damping is also created by the coil-magnet system. This type of damping is evaluated with metal specimens. Since metal specimens have very low D, the measured D from metal specimens is mainly created by equipment-generated damping. The RC equipment is annually calibrated for this effect. Equipment-generated damping is then subtracted from the total measurement of damping, D_{total}, to determine D of the soil specimen.

3.4 SUMMARY

The RC test device used in this study is called a fixed-free device. The RC device includes four basic subsystems: (1) a confinement system, (2) a drive system, (3) a height-monitoring system, and (4) a motion-monitoring system. The confinement system is operated manually and the other three systems are controlled by an automated computer system with data acquisition and processing capabilities. The RC-test

equipment is calibrated annually to make sure that the system is operating properly and accurate measurements of soil stiffness and material damping are being performed.

Shear modulus (G) is calculated from the dynamic frequency response curve. Material damping ratio (D) is obtained either from the half-power bandwidth method, or the free-vibration decay curve, depending on the magnitude of shear strains. In the linear strain range, both the half-power bandwidth method and the free-vibration decay method are generally used together. In the nonlinear strain range, only the free-vibration decay curve is used to evaluate D. In all cases, equipment-generated damping is measured using metal specimens during the annual calibration process and this value is subtracted from the initially measured D value at each frequency.

CHAPTER FOUR

SAMPLE PREPARATION AND EXPERIMENTAL PROGRAM

4.1 INTRODUCTION

The purpose of this study is to use resonant column equipment to investigate the dynamic properties of two specific kinds of sandy soil: (1) a liquefiable sand from Christchurch, New Zealand, and (2) a calcareous sand from Puerto Rico. The physical properties of both sandy soils are presented in Section 4.2. The procedure of preparing the reconstituted soil specimens for RC testing is described in Section 4.3. Finally, the RC testing program for each kind of sandy soil are discussed in Section 4.4.

4.2 DESCRIPTION OF TEST MATERIALS

4.2.1 Physical Properties of Liquefiable Sand from Christchurch, NZ

The liquefiable sand was sampled from two sites in Christchurch, New Zealand. The soil samples were air-dried before they were shipped to Texas. The two sites are designated as Site 3 and Site 6 in the overall NSF-supported project (Stokoe and Cox, 2013). At both sites, the samples were recovered from the natural soil test panels identified as NS. The samples from Site 6 are: 6-NS-2 meaning from a 2 m depth and 6-NS-3 indicating recovery from a depth of 3 m. The samples from Site 3 are: 3-NS-2.5 from a 2.5 m depth and 3-NS-3 from a 3 m depth. These samples are also designated in

the figures in this thesis as S6(2m), S6(3m), S3(2.5m) and S3(3m), respectively. In order to determine the material composition of these samples, sieve analyses (ASTM D6913-04) were performed to obtain the grain size distribution of each sample. The grain size distribution curves of the samples are presented in Figure 4.1. Based on the Unified Soil Classification System (USCS) (ASTM D2487-11), the boundaries for the different soil types are also plotted. As seen in Figure 4.1, the liquefiable sands from Christchurch are mostly fine sand with less than 5 % fines. These sands classify as SP in the USCS.

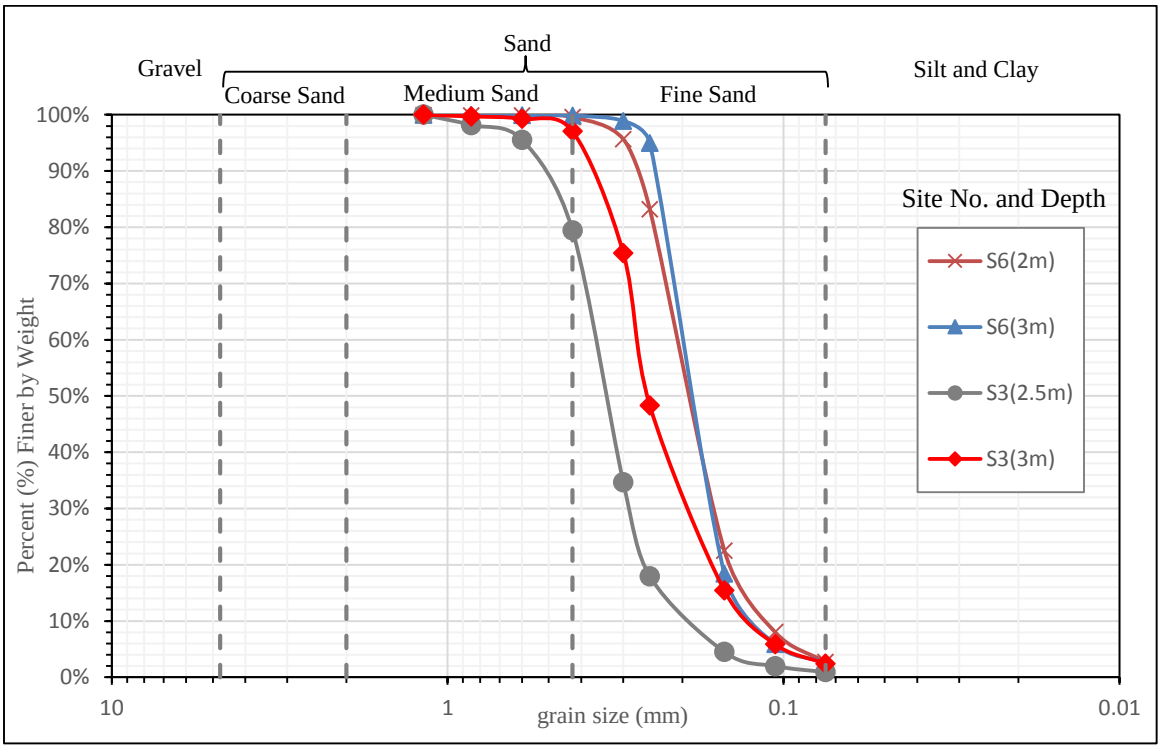

Figure 4.1 Grain Size Distribution of Liquefiable Sand from Christchurch, New Zealand

The values of percent passing for various grain diameters, D, were obtained from the grain size distribution curves. These values are presented in Table 4.1. The uniformity coefficient, C_u, was then calculated from:

$$C_u = \frac{D_{60}}{D_{10}} \tag{4.1}$$

where D_{60} = the grain size corresponding to 60% passing, and

D_{10} = the grain size corresponding to 10% passing in the grain-size distribution curve.

The values of C_u range from 1.55 to 2.13 as presented in Table 4.1.

Electron microscope images of sands from the natural soil (NS) test panel at Site 3 are shown in Figure 4.2 for sands from depths of 2.5 and 3 m. The particle shapes of the sands from the 2.5-m and 3-m depths at Site 3 range between sub-rounded and sub-angular shapes in the writer's judgment. No electron microscope images of sands for Site 6 are available, but the particle shapes are expected to be similar to those of sands from Site 3. The assumption is made by all researchers in the New Zealand study that these sands were sampled from the liquefiable sand layer at each site, and this layer is believed to be continuous throughout the test sites. Using the estimated Roundness ($R = \frac{minimum\ radius\ of\ the\ particle\ edges}{inscribed\ radius\ of\ the\ entire\ particle}$) and Youd's recommended estimation of e_{min} and e_{max} from gradational and particle shape characteristics in Figure 4.3, the e_{min} and e_{max} values can be estimated. The e_{min} and e_{max} values can also be estimated from

Table 4.1: Grain Size Information of the Liquefiable Sand from Site 3 and 6 in Christchurch, New Zealand

Site	Depth (m)	D_{10}	D_{30}	D_{50}	D_{60}	D_{95}	C_u	Estimation[1]		Estimation[2]	
		(mm)						e_{min}	e_{max}	e_{min}	e_{max}
6-NS-2	2.0	0.114	0.162	0.192	0.206	0.295	1.81	0.46	0.96	0.55	0.98
6-NS-3	3.0	0.128	0.164	0.186	0.198	0.250	1.55	0.50	1.0	0.61	1.04
3-NS-2.5	2.5	0.193	0.289	0.335	0.360	0.590	1.87	0.45	0.95	0.54	0.94
3-NS-3	3.0	0.128	0.194	0.255	0.273	0.402	2.13	0.42	0.89	0.50	0.88

Note: 1. Based on Youd, 1973 (Figure 4.3)
2. Based on Menq, 2003 (Figure 4.4)

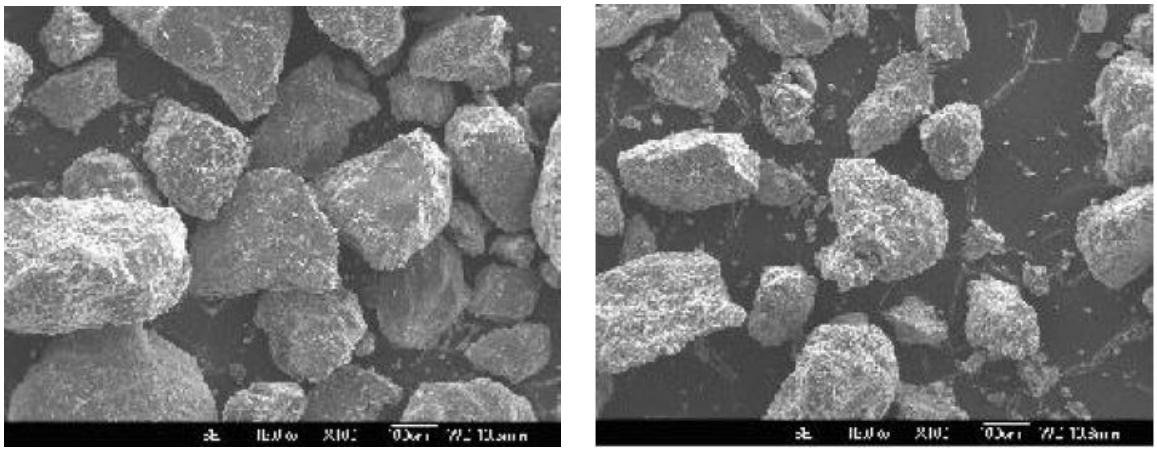

(a) Site 3-NS-1 at 2.5 m depth (b) Site 3-NS-1 at 3.0 m depth

Figure 4.2 Electron Microscope Images of Sand from Site 3-NS-1 (Ground Improvement Trials Report, 2014)

Menq, 2003 which is based on earlier work presented by Rix, 1984, Winterkorn and Fang, 1975, Kokusho et al., 1994, and Kokusho et al., 1995. This relationship is presented in Figure 4.4 and equations for the trend lines of e_{min} and e_{max} is presented as:

$$e_{max} = 0.95 \times (1/C_u) + 0.43 \quad (4.2)$$

$$e_{min} = 0.60 \times (1/C_u) + 0.22 \quad (4.3)$$

where $200 \geq C_u \geq 1.0$. These trend lines were developed by Rix, 1984, Winterkorn and Fang, 1975, Kokusho et al., 1994 – 1995, and Menq, 2003. The estimated values of e_{max} and e_{min} are presented in Table 4.1.

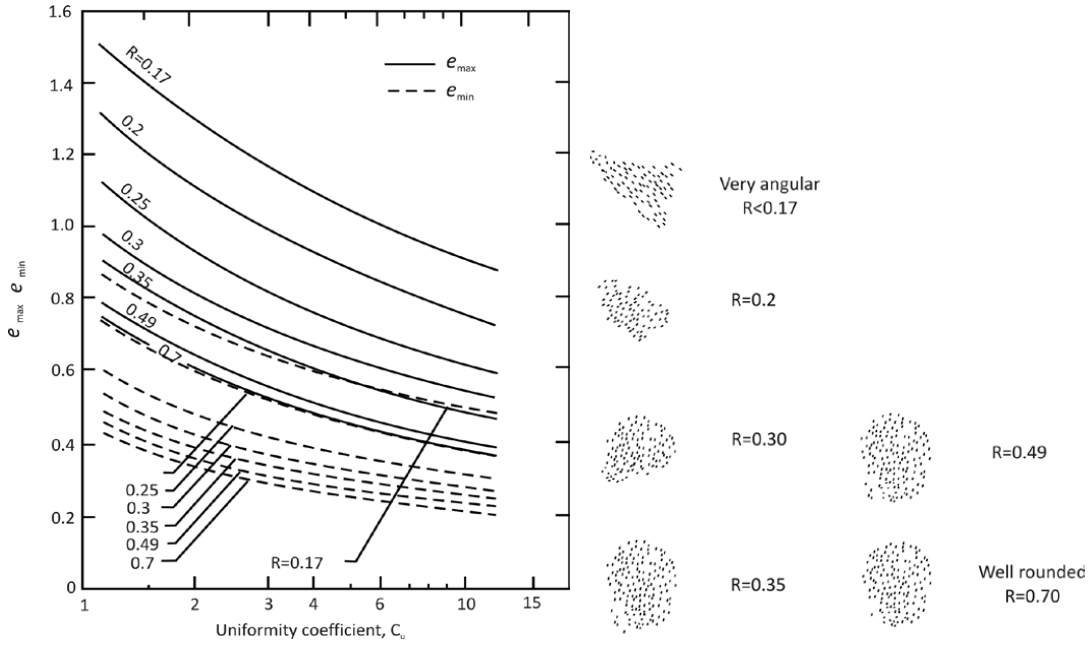

Figure 4.3 Youd's Recommended Estimation of e_{min} and e_{max} from Gradational and Particle Shape Characteristics and General range of R (Youd, 1973)

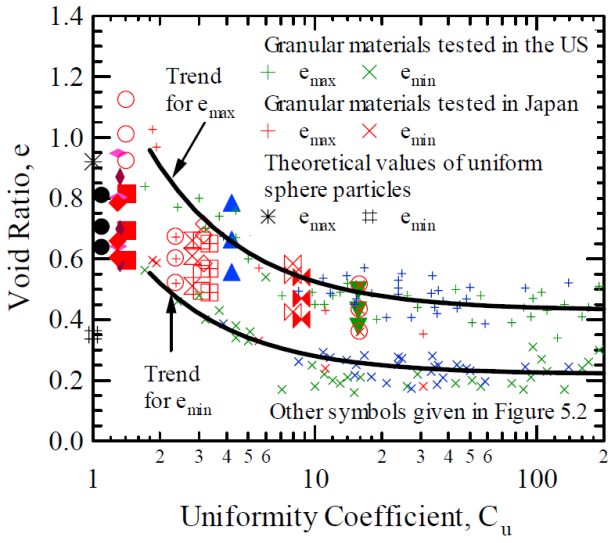

Figure 4.4 Variation between Void Ratio and Uniformity Coefficient, C_u, for Reconstituted Granular Materials (from Menq, 2003)

Finally, the specific gravity of all liquefiable sands is assumed to be 2.65.

4.2.2 Physical Properties of Calcareous Sand from Puerto Rico

The calcareous sand from Puerto Rico was air-dried before delivery to UT. The sand, the grain-size distribution curve and other soil properties were provided by Professor Christorpher Baxter at the University of Rhode Island. The physical properties of the calcareous sand from Puerto Rico are presented in Table 4.2, and the grain-size distribution curve is shown in Figure 4.4. This calcareous sand classifies as SP in the USCS.

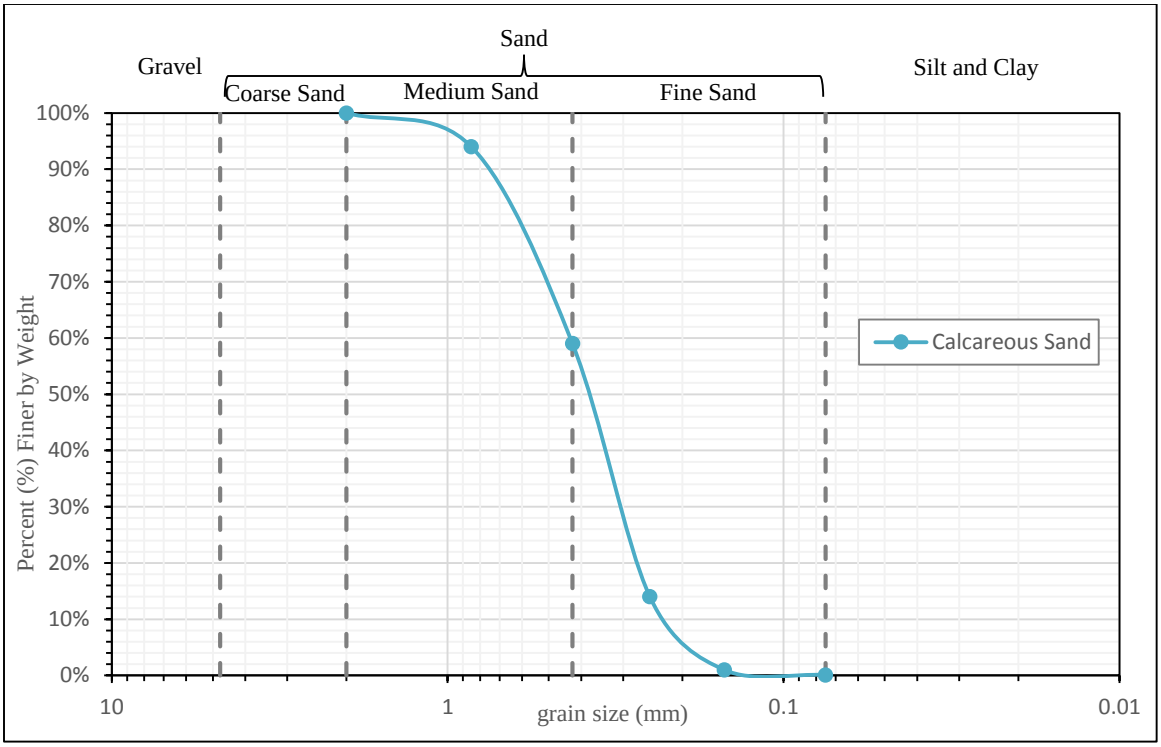

Figure 4.5 Grain-Size Distribution of Calcareous Sand from Puerto Rico

Table 4.2: Physical Properties of the Calcareous Sand from Puerto Rico (Baxter (2013); data included with sand shipped to UT)

	$\rho_{d\ max}$ (g/cc)	e_{min}	e_{max}	D_{10} (mm)	D_{30} (mm)	D_{60} (mm)	C_u	C_c	G_s
Calcareous Sand	1.22	1.34	1.75	0.24	0.3	0.42	1.75	0.89	2.87

4.3 SPECIMEN RECONSTITUTION

Both the liquefiable sand from NZ and the calcareous sand from Puerto Rico were reconstituted as cylindrical specimens with a diameter of about 2 in. and a height of 4 in. The under-compaction method (Ladd, 1978) was applied to build the specimens to the target uniform density. The specimen was compacted in 5 layers and each layer had a target height which was calculated using the under-compaction method. A split, stainless steel mold with an inner diameter slightly greater than 2 in. was used to hold the specimen during reconstitution. A small, stainless steel tamper with slightly less than a diameter of 1 in. was used to tamp the specimen to the target height in each step. The split mold and small tamper are shown in Figure 4.6.

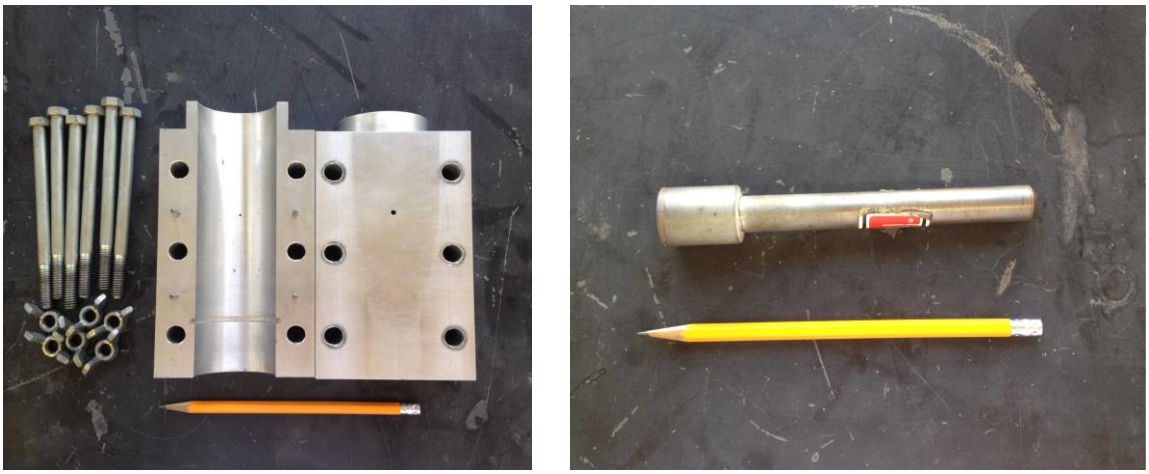

(a) Split Compaction Mold (b) Small Compaction Tamper

Figure 4.6 Compaction Mold with an Inside Diameter Slightly More than 2 in. and Compaction Tamper with a Compacting Foot Slightly Less than 1 in.

Each specimen was compacted using moist sand. For the specimens of the liquefiable sand from Christchurch, the target relative densities were 80% and 40%, and the target degree of saturation was 20%. For the specimens of the calcareous sand from Puerto Rico, the target relative densities were 80% and 40%, and the target degree of saturation was 50%. The relative density, D_r, degree of saturation, S_r, water content, w_c, void ratio, e, and total unit weight, γ_t of the reconstituted specimens are presented in Tables 4.3 and 4.4 for the liquefiable sand and calcareous sand, respectively. Each specimen was wrapped with two membranes to keep the water context of the specimens as constant as possible and to minimize the movement of air used as the confining pressure through the specimens during RC testing. The membranes should be thin enough

Table 4.3: Relative Density, Degree of Saturation, Water Content, Void Ratio and Total Unit Weight of the Specimens of the Liquefiable Sand from Christchurch, NZ

Specimen ID.[1]	Test ID.	Relative Density, D_r[2], (%)	Degree of Saturation, S_r, (%)	Water Content, w_c, (%)	Void Ratio, e[3]	Total Unit Weight, $\gamma_t, g/cm^3$
S6(2m)	YWKH03	75	19	4.5	0.62	1.71
	YWKH04	38	22	6.6	0.79	1.58
S6(3m)	YWKH01	78	17	4.2	0.64	1.68
	YWKH02	38	21	6.4	0.80	1.57
S3(2.5m)	YWKH05	74	20	4.6	0.62	1.71
	YWKH06	45	21	5.9	0.75	1.60
S3(3m)	YWKH07	71	19	4.4	0.60	1.73
	YWKH08	37	20	5.7	0.75	1.60

Notes:
1. The format is: site location (depth).
2. $D_r = \frac{e_{max} - e_{measured}}{e_{max} - e_{min}} \times 100\ \%$.
3. The void ratio is measured at the start of testing.

Table 4.4: Relative Density, Degree of Saturation, Water Content, Void Ratio and Total Unit Weight of the Specimens of the Calcareous Sand from Puerto Rico

Test ID.	Relative Density, D_r, (%)	Degree of Saturation, S_r[1], (%)	Water Content, w_c, (%)	Void Ratio, e[2]	Total Unit Weight, $\gamma_t, g/cm^3$
YW02	78	49	24.5	1.43	1.47
YW03	76	49	24.7	1.44	1.47
YW05	54	50	26.8	1.53	1.44
YW07	79	49	24.3	1.43	1.47
YW08	42	51	27.9	1.58	1.42

Notes:
1. $D_r = \frac{e_{max} - e_{measured}}{e_{max} - e_{min}} \times 100\ \%$.
2. The void ratio is measured at the start of testing.

to not affect the properties of the specimens and thick enough to withstand the highest confining pressure in the RC tests. For both the liquefiable and calcareous sands, each membrane had a thickness of 0.012 in.

4.4 EXPERIMENTAL PROGRAM

4.4.1 Experimental Program of Testing the Liquefiable Sand from Christchurch, NZ

Both low-amplitude resonant column (RC-LA) tests and high-amplitude resonant column (RC-HA) tests were performed to evaluate the dynamic properties of the liquefiable sand from Christchurch, NZ.

Six levels of confining pressures were applied to these sand specimens. The pressures were: 2, 4, 8, 16, 32 and 64 psi. The test procedure was divided into three parts: (1) the loading RC-LA tests, (2) the unloading RC-LA tests and (3) the unloading RC-

HA test at the final pressure of 8 psi. In the loading RC-LA part, the confining pressures were increased in steps following the six confining pressure levels. At each confining pressure, RC-LA tests were performed for about 65 minutes to obtain the variation of dynamic properties with time. After RC-LA testing was completed at the highest confining pressure of 64 psi, the confining pressure applied to the specimen was unloaded in steps from 64 to 8 psi. RC-LA tests were again performed at each unloading pressure, but just for 35 minutes. At the unloading pressure of 8 psi, which was approximately twice the in-situ confining pressure, RC-HA tests were performed to investigate the nonlinear behavior of the specimens. The RC-HA test began at approximately 100 minutes after the test confining pressure was applied to minimize time effects on the dynamic properties. The pressure of 8 psi was selected to minimize potential slipping of the top cap at the larger values of torque applied to the specimen during the final stages

Table 4.5: RC Test Schedule for Evaluating the Dynamic Properties of the Liquefiable Sand from Christchurch

	Isotropic Confining Pressure, σ_0, psi								
	Loading[1]						Unloading[2]		
	2	4	8	16	32	64	32	16	8
RC-LA	X	X	X	X	X	X	X	X	X
RC-HA									X[3]

Notes:
1. Low-amplitude testing was performed for about 65 minutes at each loading pressure.
2. Low-amplitude testing was performed for about 35 minutes at each unloading pressure.
3. Only one set of high-amplitude RC tests was performed because the high-amplitude cycling permanently changed the material skeleton.

of high-amplitude loading. The RC test schedule for the liquefiable sand is presented in Table 4.5.

4.4.2 Experimental Program of Testing the Calcareous Sand from Puerto Rico

Both low-amplitude resonant column (RC-LA) tests and high-amplitude resonant column (RC-HA) tests were also performed to evaluate the dynamic properties of the calcareous sand from Puerto Rico.

Seven levels of confining pressure were applied to these sand specimens. The pressures were: 2.25, 4.5, 9, 18, 36 and 72 psi. Since no in-situ confining pressure was provided, a representative in-situ confining pressure of 18 psi was used. The confining pressures were applied to each specimen in steps from 2.25 psi to 72 psi as shown in Table 4.6. At each confining pressure, RC-LA tests were performed for 65 minutes to

Table 4.6: RC Test Schedule for Evaluating the Dynamic Properties of the Calcareous Sand from Puerto Rico

	Isotropic Confining Pressure, σ_0, psi					
	2.25	4.5	9	18	36	72
RC-LA[1]	X	X	X	X	X	X
RC-HA[2]		X		X		X

Notes:
1. Low-amplitude testing was performed for about 65 minutes at each loading pressure.
2. How-amplitude tests were stopped at G/G_{max} = 0.9 and 0.8 at σ_0 = 4.5 and 18 psi, respectively, to not damage the specimen. At σ_0 = 72 psi, testing was conducted to the full torque of the RC device.

obtain the variations of dynamic properties with time.

RC-HA tests were performed at 4.5 psi, 18 psi and 72 psi on the same loading sequence as the RC-LA tests. The RC-HA tests were conducted after the RC-LA tests at 100 minutes. At 4.5 psi, the RC-HA tests were stopped at G/G_{max} = 0.9 to avoid too much unrecoverable damage to the specimens which would have adversely affected the following RC tests. With increase confining pressure, G/G_{max} can be evaluated to higher strains without adversely affecting the specimens. At 18 psi, RC-HA tests were stopped at G/G_{max} = 0.8 for the same reason. At the highest confining pressure of 72 psi, RC-HA tests were conducted to the largest strain to obtain as much of the nonlinear dynamic behavior as possible. The RC-HA test schedule for the calcareous sand is also presented in Table 4.6.

4.5 SUMMARY

The material composition of both the liquefiable sand from Christchurch and the calcareous sand from Puerto Rico are discussed in this chapter. Both materials classify as SP materials in the USCS and have less than 5 % fines. The grain-size distribution, specific gravity, and estimations of the minimum and maximum void ratios are presented. Additionally, preparation of the reconstituted specimens and the target specimen information including relative density, water content, and void ratio are discussed. The under-compaction method was used for sample reconstitution. Lastly, the testing programs were composed of RC-LA tests and RC-HA tests for both the liquefiable sand

and the calcareous sand. The testing programs are outlined. Slightly different test schedules were applied to the liquefiable sand and the calcareous sand.

CHAPTER FIVE

DYNAMIC PROPERTIES OF LIQUEFIABLE SAND FROM CHRISTCHURCH, NZ

5.1 INTRODUCTION

In this chapter, the dynamic properties of liquefiable sand from Christchurch, NZ that were determined by RC testing are discussed. The dynamic properties of the liquefiable sand in the small-strain range are discussed in Section 5.2. The dynamic properties of the sand in the nonlinear strain range are then discussed in Section 5.3. Finally, a summary of the dynamic properties is given in Section 5.4.

5.2 SMALL-STRAIN DYNAMIC PROPERTIES OF THE LIQUEFIABLE SAND

The low-amplitude tests using the resonant column device were performed to determine the dynamic properties (V_S, G_{max} and D_{min}) of the liquefiable sand in the small-strain range, $\gamma < 0.0006\,\%$. These tests were performed at the following six isotropic confining pressures: 2, 4, 8, 16, 32 and 64 psi. The variations of shear wave velocity, shear modulus and material damping ratio with isotropic confining pressure for the eight sand specimens are discussed in Sections 5.2.1, 5.2.2 and 5.2.3, respectively.

5.2.1 Variation of Small-Strain Shear Wave Velocity with σ_0 and e

The variations in low-amplitude shear wave velocity with isotropic confining pressure from RC testing of the eight sand specimens from Sites 3 and 6 are shown in Figure 5.1. Since the specimens were in the drained state during testing, the confining pressure, σ_0, is estimated to equal the effective isotropic confining pressure, σ_0'; hence any negative capillary stresses are assumed to be small. From Figure 5.1, it can be seen that the low-amplitude shear wave velocities (V_S) of all specimens increase with effective isotropic confining pressures (σ_0'), just as shown in numerous previous studies. The first point readily observed in Figure 5.1 is that the denser specimens are stiffer (have larger V_S values at all σ_0's) than the looser specimens. The second point is that the $\log V_S - \log \sigma_0'$ relationships are well represented either by a single line (a single linear relationship) or by two lines (a bi-linear relationship), with the first line having a "flatter slope" in the bi-linear relationship. Each one of these points is discussed below.

To observe and compare the $\log V_S - \log \sigma_0'$ relationship of each specimen in the pair of specimens (looser and denser specimens) for each specimen depth at Sites 3 and 6, Figures 5.2 and 5.3, respectively, have been prepared. In these figures, the single linear relationship shown by each denser specimen is easily seen, with the exception of Specimen YWKH01 at the lowest pressure. The bi-linear relationship for all four looser specimens is also readily seen. The single linear $\log V_S - \log \sigma_0'$ relationship of the denser specimens indicates that those specimens were exhibiting a behavior similar to a normally consolidated (NC) specimen. On the other hand, the bi-linear $\log V_S - \log \sigma_0'$

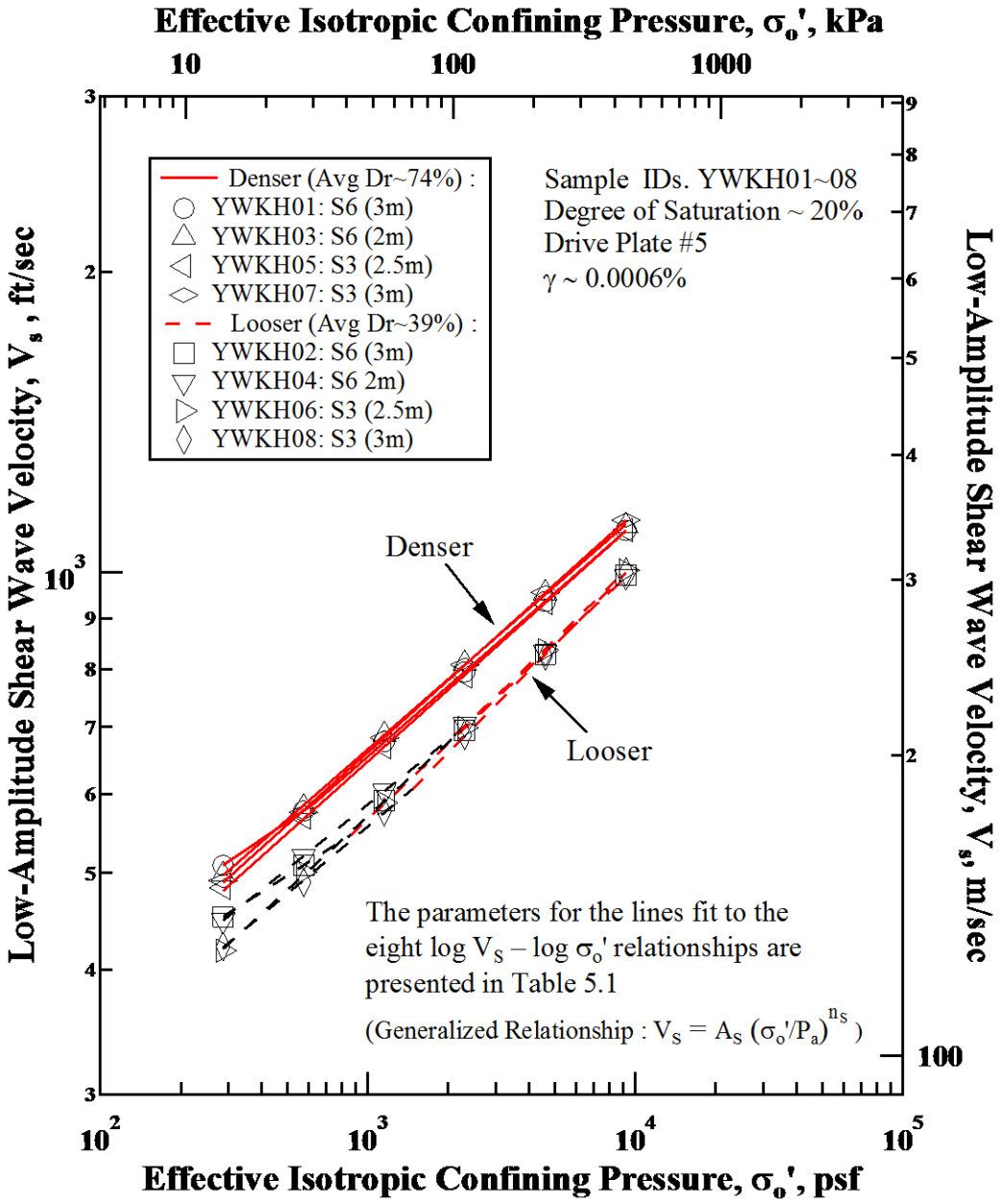

Figure 5.1 Variations in the Low-Amplitude Shear Wave Velocity with Effective Isotropic Confining Pressure from Resonant Column Tests of Eight Sand Specimens from Sites 3 and 6.

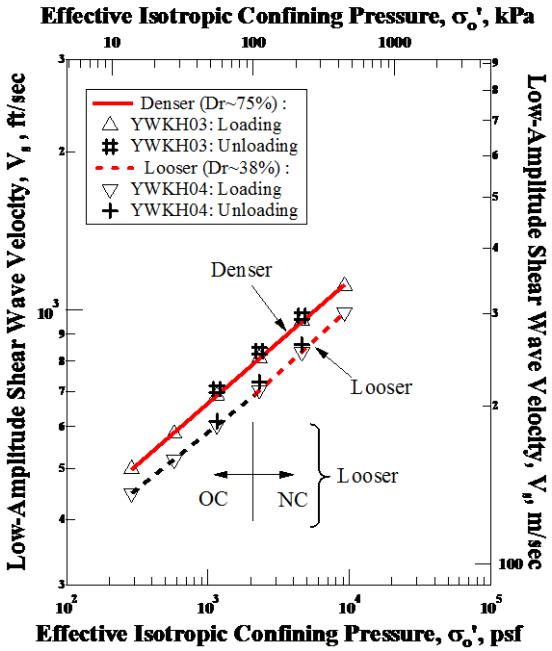

a. Soil from a depth of 2 m

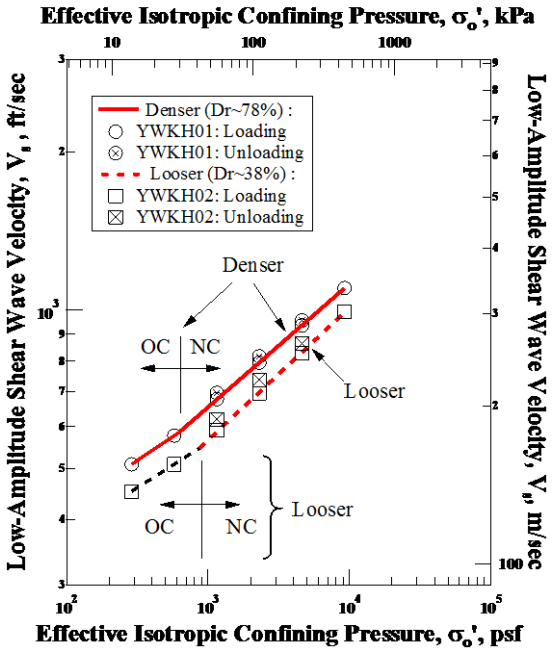

b. Soil from a depth of 3 m

Figure 5.2 Comparisons of the Variations in the $\text{Log}\, V_S - \text{Log}\, \sigma_0'$ Relationships for Each Pair of Looser and Denser Specimens from Site 6.

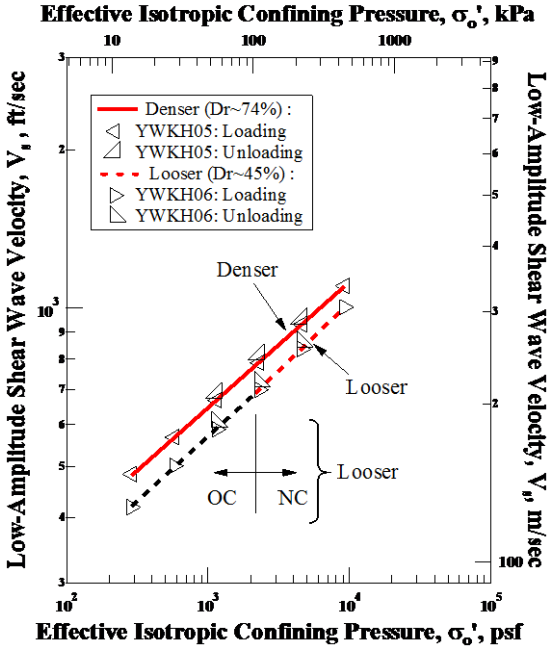

a. Soil from a depth of 2.5 m

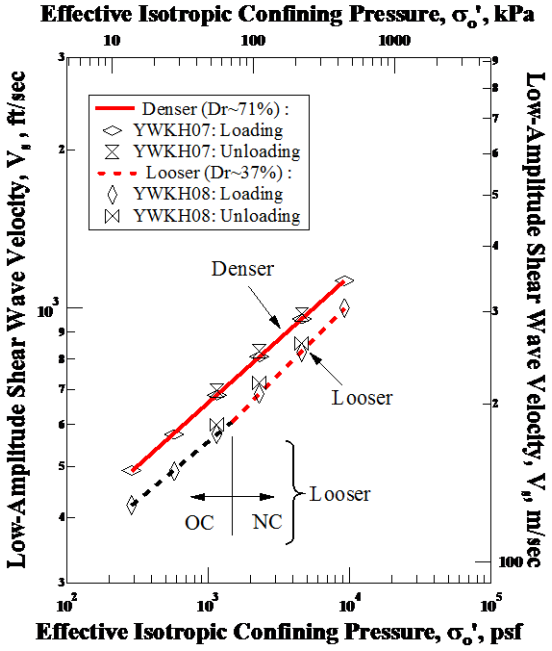

b. Soil from a depth of 3 m

Figure 5.3 Comparisons of the Variations in the $\text{Log}\, V_S - \text{Log}\, \sigma_0'$ Relationships for Each Pair of Looser and Denser Specimens from Site 3.

relationship indicates that the looser specimens were exhibiting a behavior similar to specimens that are behaving like overconsolidated (OC) specimens at lower pressures and then become normally consolidated at higher pressures. The equation that can be used to represent each linear segment in the $\log V_S - \log \sigma_0'$ relationship is:

$$V_S = A_S(\sigma_0'/P_a)^{ns} \tag{5.1}$$

in which A_S equals the value of V_S at σ_0' equal to one atmosphere (hence, V_{S1}) and P_a

Table 5.1: Parameters Fit to Each Linear Section of the Eight $\text{Log } V_S - \text{Log } \sigma_0'$ Relationships from Resonant Column Tests of Sand Specimens from Sites 3 and 6.

Specimen ID.	Test ID.	Estimated Relative Density, D_r[1], (%)	Consolidation State	V_S[2]	
				A_S (fps)	n_S
S6 (2m)	YWKH03	75	NC[3]	793	0.234
	YWKH04	38	OC[4]	688	0.216
			NC	689	0.246
S6 (3m)	YWKH01	78	OC	730	0.181
			NC	780	0.234
	YWKH02	38	OC	636	0.171
			NC	685	0.251
S3 (2.5m)	YWKH05	74	NC	774	0.238
	YWKH06	45	OC	685	0.246
			NC	683	0.262
S3 (3m)	YWKH07	71	NC	791	0.241
	YWKH08	37	OC	658	0.224
			NC	670	0.272

Notes:
1. $D_r = (e_{max} - e)/(e_{max} - e_{min}) \times 100\%$, e_{max} and e_{min} are estimates based on Youd, 1973, and Menq, 2003,
2. $V_s = A_s(\sigma_0'/P_a)^{ns}$, $P_a = one\ atmosphere$,
3. NC = normally consolidated state,
4. OC = overconsolidated state.

is equal to one atmosphere with the same units as σ_0'. Each linear segment of the $\log V_S - \log \sigma_0'$ relationships shown in Figures 5.2 and 5.3 has been best-fit with Equation 5.1 using the least squares regression method. The resulting best-fit values of the parameters (A_S and n_S) are presented in Table 5.1. The r^2 values for the best-fits to determine A_S and n_S range from 0.9987 to 0.9999 and average 0.9996.

Void ratio (e) has an influence on the low-amplitude shear wave velocity in the general way that denser soil fabrics form a stiffer soil skeleton. The denser specimens with smaller e alway have higher V_S values than the looser specimens with larger e at the same σ_0' level. For the sand specimens tested from New Zealand, the void ratio of a given specimen changed less 1.83 % during the time it was confined at each test pressure. The change in e with $\log \sigma_0'$ is shown for the four specimens from Site 6 in Figure 5.4a and for the four specimens from Site 3 in Figure 5.4b. As the confining pressure increases, e of each specimens decrease a little because the soil skeleton densifies. In terms of the average values of V_S at σ_0' of one atmosphere for the two similar specimens (denser vs. looser) from each site, the comparisons are as follows. At Site 6, average $A_{S,denser}$ is 786 ft/sec and average $A_{S,looser}$ is 687 ft/sec. This comparison is only for the NC portion of the relationship because the overconsolidated portion was caused by the compaction effect and does not relate to the in-situ condition unless the sand is overconsolidated. Also the values of the void ratios at σ_0' of one atmosphere are 0.63 and 0.80 for $A_{S,denser}$ and $A_{S,looser}$, respectively. The same relative comparison at Site 3 gives an average $A_{S,denser}$ of 782 ft/sec and an average $A_{S,looser}$ of 677 ft/sec.

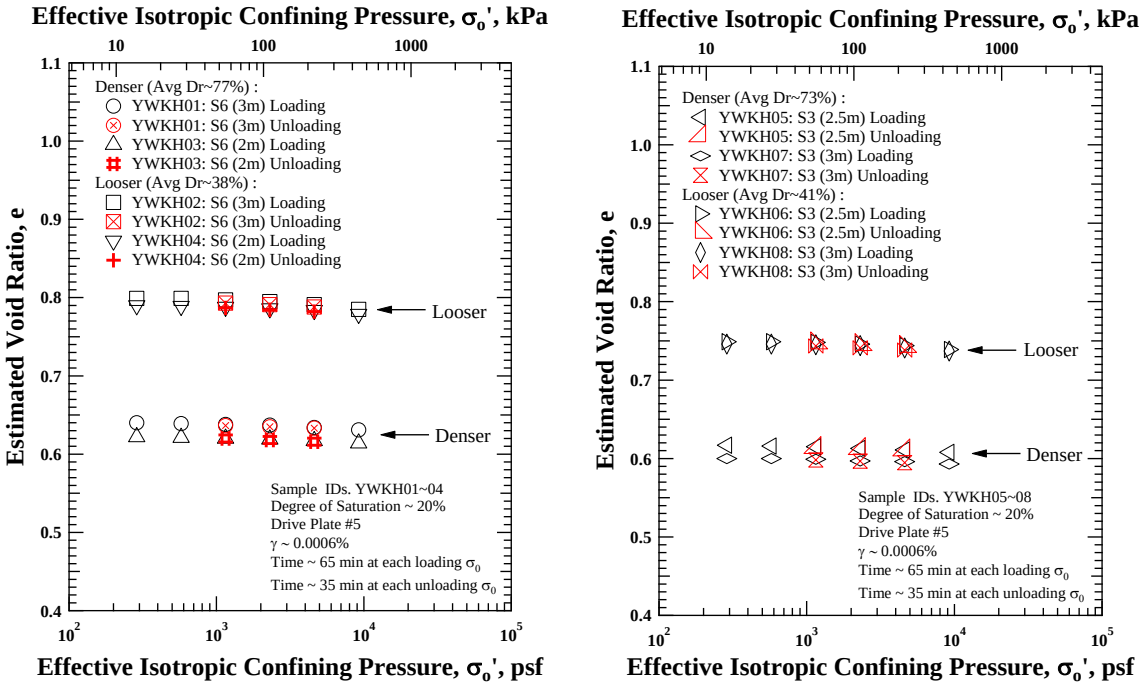

a. Soil from Site 6 b. Soil from Site 3

Figure 5.4 Variation in Void Ratio with Effective Isotropic Confining Pressure Determined during Resonant Column Testing of all Sand Specimens from Sites 3 and 6.

The associated values of the void ratios at σ_0' of one atmosphere are 0.61 and 0.75 for $A_{S,denser}$ and $A_{S,looser}$, respectively.

In Table 5.1, the value of n_S is also affected slightly by the value of e since denser specimens always have slightly smaller values of n_S than looser specimens for the same kind of liquefiable sand. In terms of the average values of n_S for the two pairs of specimens (denser vs. looser) from each site, the comparison is as follows. At Site 6, the average $n_{S,denser}$ is 0.234 and the average $n_{S,looser}$ is 0.249. This comparison is only for the NC portion of the relationship because the overconsolidated portion was

caused by the compaction effect and is assumed not to relate to the in-situ condition as noted above. The same relative comparison at Site 3 gives average $n_{S,denser}$ of 0.241 and average $n_{S,looser}$ of 0.267. The relative difference is reasonable because looser specimens are easier to densify than denser specimens. With the same increment of σ_0', looser specimens have slightly larger changes in e and V_S than denser specimens.

Void-ratio-adjusted shear wave velocities, $V_S/\sqrt{F(e)}$ ($F(e)$ is calculated using Equation 2.8), for all specimens are plotted versus σ_0' on a log-log scale in Figure 5.5. In order to view the results more clearly, comparisons of looser and denser specimens at each site depth are shown in Figure 5.6 for Site 6 and in Figure 5.7 for Site 3. The NC portion of the $\log V_S/\sqrt{F(e)} - \log \sigma_0'$ relationships are shown in Figures 5.6 and 5.7. The best-fit of the NC portion was done using Equation 5.1 and the least squares

Table 5.2: Parameters Fit to NC Portion of the Log $V_S/\sqrt{F(e)}$ − Log σ_0' Relationships from Resonant Column Tests of all Sand Specimens from Sites 3 and 6.

Specimen ID.	Test ID.	Estimated Relative Density, D_r[1], (%)	Initial Void Ratio, e	$V_S/\sqrt{F(e)}^2$	
				A_{Se} (fps)	n_{Se}
S6 (2m)	YWKH03	75	0.62	597	0.232
	YWKH04	38	0.79	590	0.242
S6 (3m)	YWKH01	78	0.64	596	0.232
	YWKH02	38	0.80	590	0.246
S3 (2.5m)	YWKH05	74	0.62	581	0.237
	YWKH06	45	0.75	568	0.258
S3 (3m)	YWKH07	71	0.60	586	0.240
	YWKH08	37	0.75	556	0.268

Notes:
1. $D_r = (e_{max} - e)/(e_{max} - e_{min}) \times 100\%$, e_{max} and e_{min} are estimates based on Youd, 1973, and Menq, 2003,
2. $V_S/\sqrt{F(e)} = A_{se}(\sigma_0'/P_a)^{n_{Se}}$, $P_a = one\ atmosphere.$

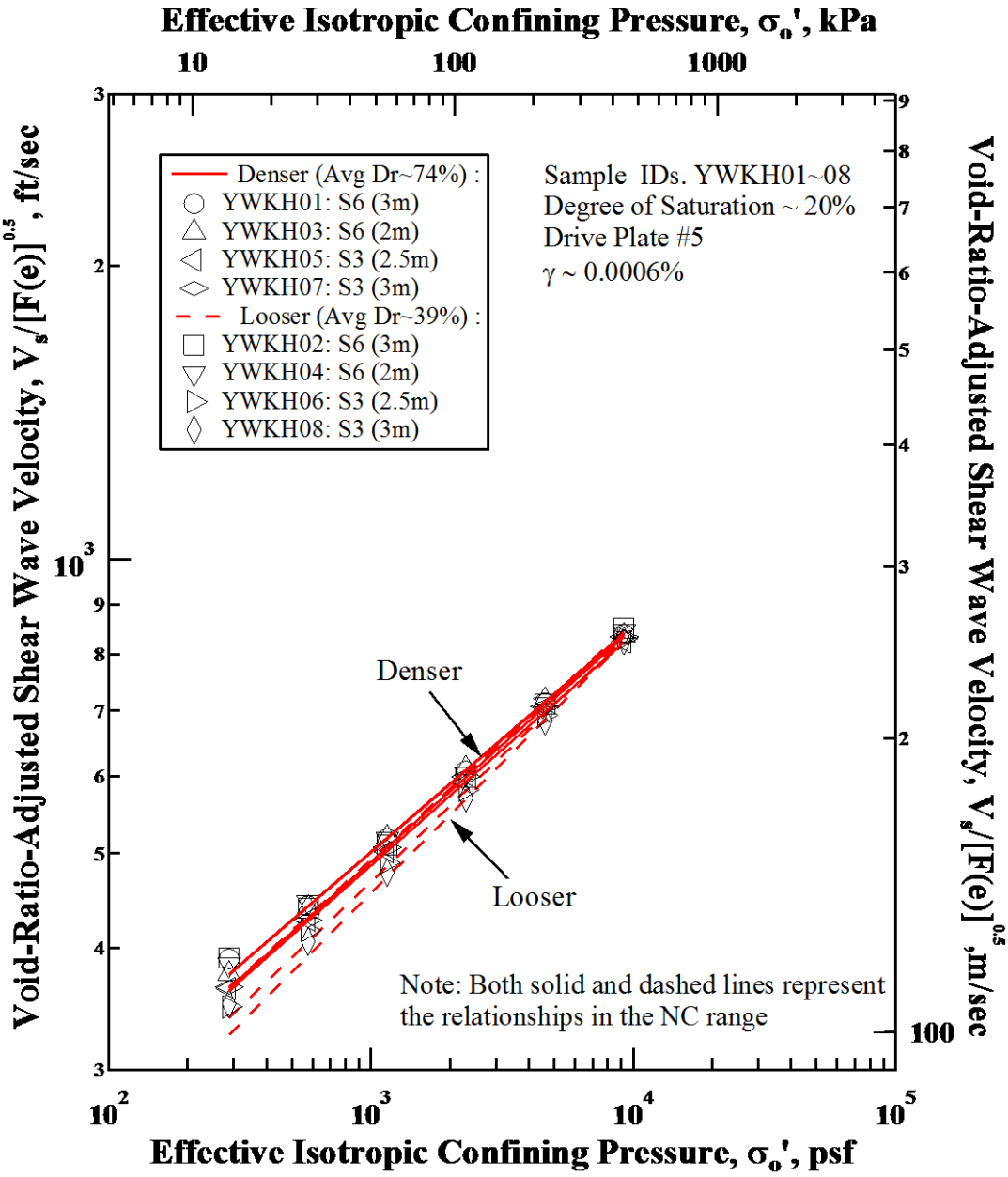

Figure 5.5 Variation in Void-Ratio-Adjusted Shear Wave Velocity ($V_S/\sqrt{F(e)}$) with Effective Isotropic Confining Pressure from Resonant Column Tests of the Eight Sand Specimens Relationships Fit to the Normally Consolidated State from Sites 3 and 6.

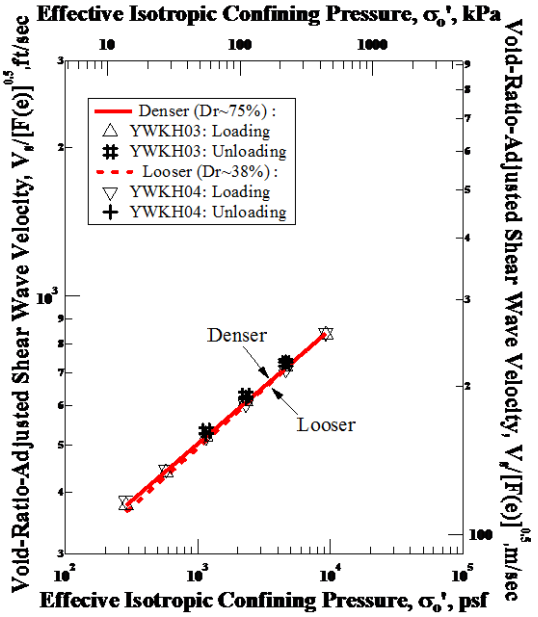

a. Soil from a depth of 2m

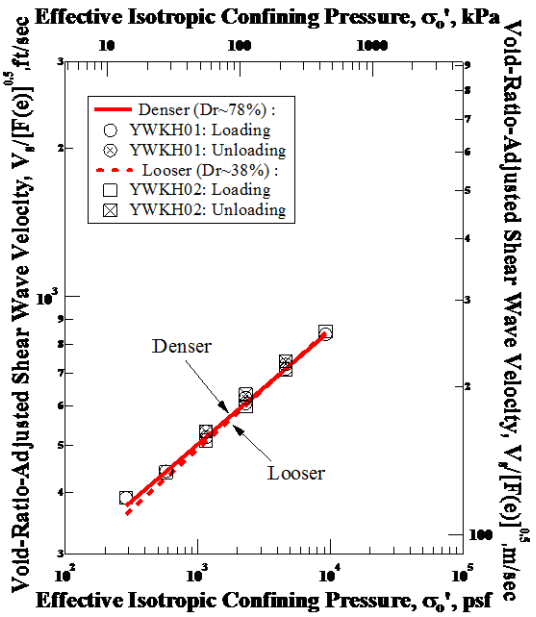

b. Soil from a depth of 3 m

Figure 5.6 Comparisons of the Variations in the $\text{Log}\, V_S/\sqrt{F(e)} - \text{Log}\, \sigma_0'$ Relationships for Each Pair of Looser and Denser Specimens Tested in the Normally Consolidated State from Site 6.

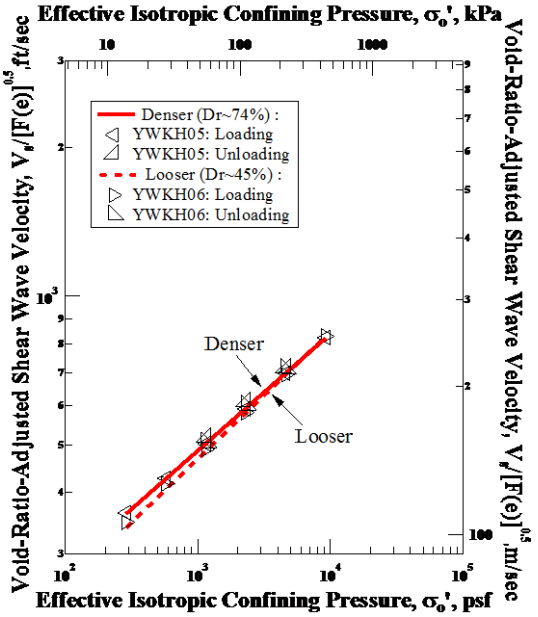

a. Soil from a depth of 2.5 m

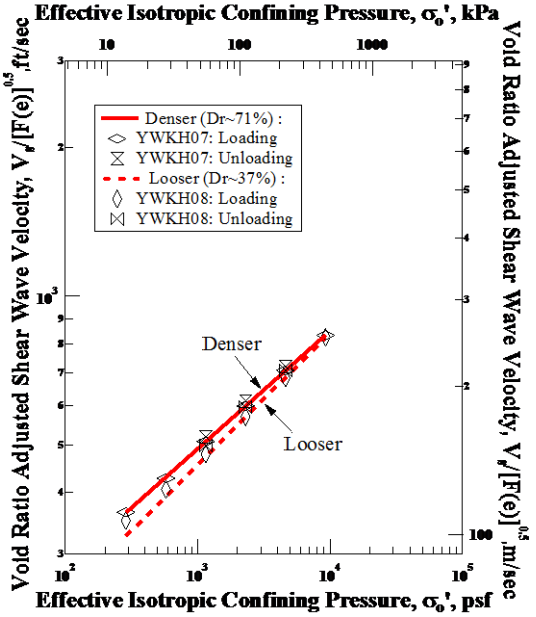

b. Soil from a depth of 3 m

Figure 5.7 Comparisons of the Variations in the $\text{Log}\, V_S/\sqrt{F(e)} - \text{Log}\, \sigma_0'$ Relationships for Each Pair of Looser and Denser Specimens Tested in the Normally Consolidated State from Site 3.

regression method. The resulting values of the parameters (A_{Se} and n_{Se}) are presented in Table 5.2.

In terms of the average values of $V_S/\sqrt{F(e)}$ at σ_0' of one atmosphere for the two similar specimens (denser vs. looser) from each site, the comparison is as follows. At Site 6, the average $A_{Se,denser}$ is 597 ft/sec (the value is the same for both denser specimens) and the average $A_{Se,looser}$ is 590 ft/sec (the value is the same for both looser specimens). The reason for the same value of A_{Se} for the same void ratio is that the gradation curves are the same (see Figure 4.1). On the other hand, at Site 3, the average value of $A_{Se,denser}$ is 583 ft/sec and the average value of $A_{Se,looser}$ is 562 ft/sec. In the case of Site 3, the average values are truly average values and differ from the values of A_{Se} in each pair because the gradation curve of the soil recovered from a depth of 2.5 m differs somewhat from that of the soil recovered from a depth of 3 m. After the void ratio adjustment, the value of $A_{Se,denser}$ becomes close to the value of $A_{Se,looser}$ for both Sites 3 and 6, which makes the relationships plot close together as seen in Figures 5.7 and 5.8.

In terms of the average values of n_{Se} for the two similar specimens (denser vs. looser) from each site, the comparison is as follows. At Site 6, the average $n_{Se,denser}$ is 0.232 and the average $n_{Se,looser}$ is 0.244, a difference of less than 5%. At Site 3, the average $n_{Se,denser}$ is 0.239 and the average $n_{Se,looser}$ is 0.263, a difference of about 10%. The difference of n_{Se} values between denser and looser specimens does not change significantly from the comparison of n_S values discussed earlier. This

comparison shows that $\sqrt{F(e)}$ is an important factor in evaluating A_S, but another factor is needed in normalizing n_S.

The two liquefiable sands, one from Site 6 and one from Site 3, differ only slightly in D_{50}, C_u and $\%\,fines$. They are shown to behave very similarly in the $\log V_S - \log \sigma_0'$ relationships at a given relative density. This finding is quite reasonable since the sand type, D_{50}, etc. are not different enough to create a distinguishable correlation with the low-amplitude shear wave velocity.

5.2.2 Small-Strain Shear Modulus of Liquefiable Sand

The small-strain shear modulus can be calculated from the shear wave velocity and total unit weight of the specimen at the time of the measurement using the relationship between shear wave velocity and shear modulus in the wave propagation theory discussed in Chapter 2. The variations in small-strain shear modulus with effective isotropic confining pressure from RC testing of the eight sand specimens from Sites 3 and 6 are shown in Figure 5.8. Since the specimens were in the drained state during testing, the confining pressure, σ_0, is estimated to equal the effective isotropic confining pressure, σ_0'; hence any negative capillary stresses are assumed to be small.

It can be seen in Figure 5.8 that the small-strain shear moduli of all specimens (G_{max}) increase with effective isotropic confining pressures (σ_0'), just as shown in numerous previous studies. Similar to the $\log V_S - \log \sigma_0'$ relationships shown in Figure

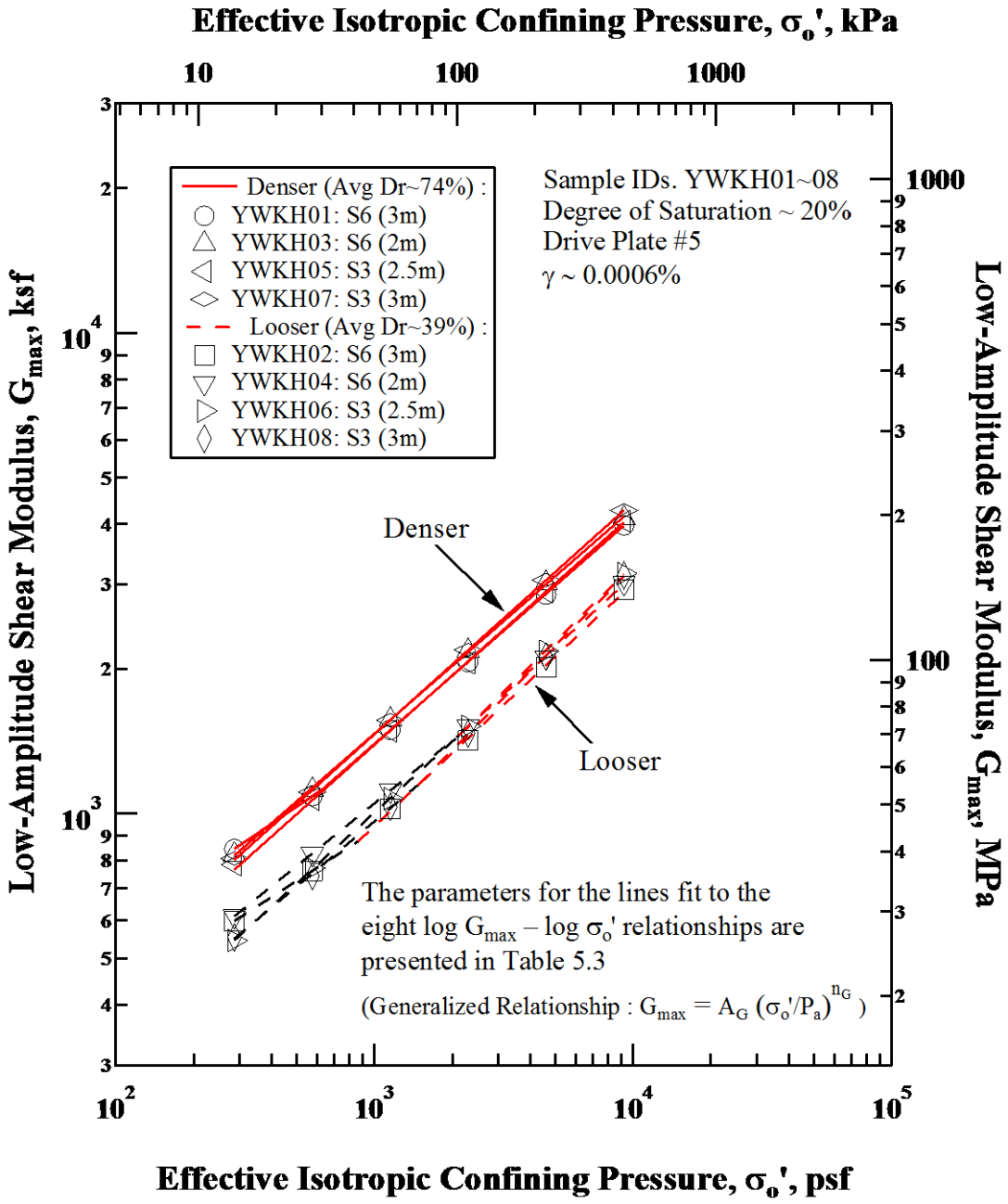

Figure 5.8 Variations in Small-Strain Shear Modulus with Effective Isotropic Confining Pressure from Resonant Column Tests of Eight Sand Specimens from Sites 3 and 6.

5.1, the first point readily observed in Figure 5.8 is that the denser specimens are stiffer (have larger G_{max} values at all σ_0's) than the looser specimens. The second point is that the $\log G_{max} - \log \sigma_0'$ relationships are well represented either by a single line (a single linear relationship) or by two lines (a bi-linear relationship), with the first line having a "flatter slope" in the bi-linear relationship. This behavior is essentially the same as exhibited by the $\log V_S - \log \sigma_0'$ relationships, except that γ_t is needed in calculating G_{max}. The $\log G_{max} - \log \sigma_0'$ relationships are discussed in more detail below.

To observe and compare the $\log G_{max} - \log \sigma_0'$ relationship of each specimen in the pair of specimens (looser versus denser specimens) for each depth at Sites 6 and 3, Figures 5.9 and 5.10, respectively, have been prepared. In these figures, the linear relationship shown by each denser specimen is easily recognized, with the exception of Specimen YWKH01 at the lowest pressure. The bi-linear relationship for all four loose specimens is readily seen. The single linear $\log G_{max} - \log \sigma_0'$ relationship of the denser specimens indicates that those specimens were exhibiting a behavior similar to a normally consolidated (NC) specimen. On the other hand, the bi-linear $\log G_{max} - \log \sigma_0'$ relationship indicates that the looser specimens were exhibiting a behavior similar to specimens that are behaving like overconsolidated (OC) specimens at low pressures and then become normally consolidated at higher pressures. The equation that can be used to represent each linear segment in the $\log G_{max} - \log \sigma_0'$ relationship is:

$$G_{max} = A_G(\sigma_0'/P_a)^{n_G} \tag{5.2}$$

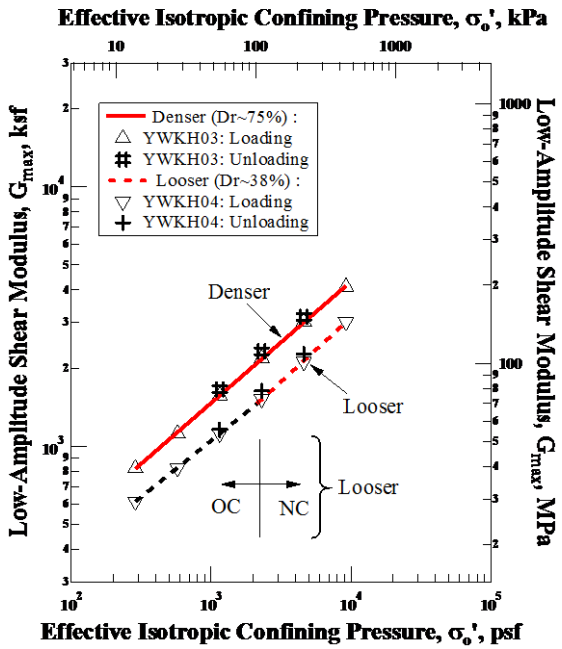

a. Soil from a depth of 2 m

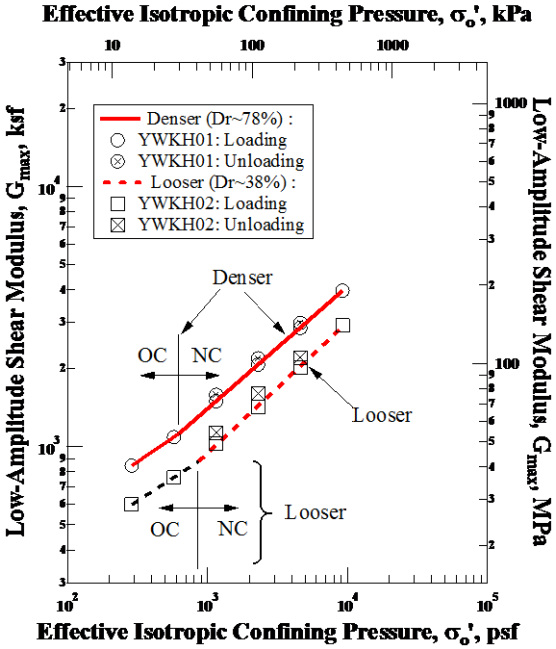

b. Soil from a depth of 3 m

Figure 5.9 Comparisons of the Variations in the $\text{Log}\, G_{max} - \text{Log}\, \sigma_0'$ Relationships for Each Pair of Looser and Denser Specimens from Site 6.

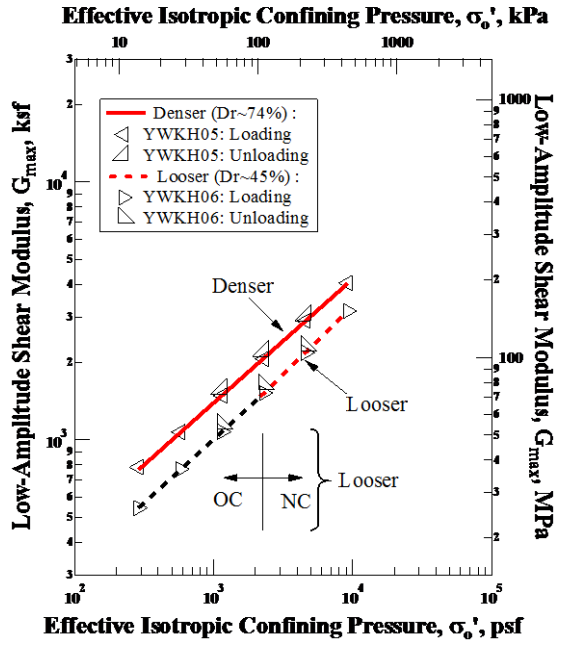

a. Soil from a depth of 2.5 m

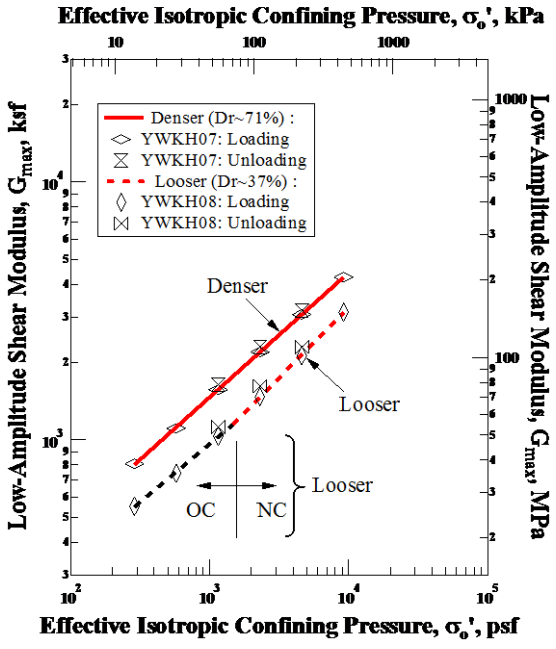

b. Soil from a depth of 3 m

Figure 5.10 Comparisons of the Variations in the $\text{Log}\, G_{max} - \text{Log}\, \sigma_0'$ Relationships for Each Pair of Looser and Denser Specimens from Site 3.

Table 5.3: Parameters Fit to Each Linear Segment of the Eight Log G_{max} − Log σ'_0 Relationships from Resonant Column Tests of Eight Sand Specimens from Sites 3 and 6.

Specimen ID.	Test ID.	Estimated Relative Density, D_r[1], (%)	Consolidation State	G_{max}[2]	
				A_G (ksf)	n_G
S6 (2m)	YWKH03	75	NC[3]	2090	0.468
	YWKH04	38	OC[4]	1450	0.434
			NC	1450	0.494
S6 (3m)	YWKH01	78	OC	1750	0.365
			NC	1990	0.470
	YWKH02	38	OC	1200	0.347
			NC	1380	0.505
S3 (2.5m)	YWKH05	74	NC	2000	0.475
	YWKH06	45	OC	1450	0.491
			NC	1450	0.527
S3 (3m)	YWKH07	71	NC	2100	0.483
	YWKH08	37	OC	1350	0.451
			NC	1400	0.545

Notes:
1. $D_r = (e_{max} - e)/(e_{max} - e_{min}) \times 100\%$, e_{max} and e_{min} are estimates based on Youd, 1973, and Menq, 2003,
2. $G_{max} = A_G(\sigma'_0/P_a)^{n_G}$, $P_a = one\ atmosphere$,
3. NC = normally consolidated state,
4. OC = overconsolidated state.

in which A_G equals the value of G_{max} at σ'_0 equal to one atmosphere (hence, G_{max1}) and P_a is equal to one atmosphere with the same units as σ'_0. Each linear segment of the $\log G_{max} - \log \sigma'_0$ relationships shown in Figures 5.9 and 5.10 has been best-fit with Equation 5.2 using the least squares regression method. The resulting best-fit values of the parameters (A_G and n_G) are presented in Table 5.3. The r^2 values for the best-fits to determine A_G and n_G range from 0.9990 to 0.9999 and average 0.9997.

As with void ratio (e) having an effect on small-strain V_S through the stiffening effect of denser soil skeletons, void ratio also has an influence on the small-strain shear

modulus. The effect is even more pronounced because the effect is further increased by the fact that total unit weight enters the calculation of shear modulus ($G = (\gamma_t/g)V_S^2$). Denser specimens of the same material with lower values of e and higher values of γ_t always have larger G_{max} values than the looser specimens with higher values of e and lower values of γ_t at the same σ_0' level. In terms of the average values of G_{max} at σ_0' of one atmosphere for the pairs of specimens (denser vs. looser) from each site, the comparison is as follows. At Site 6, average $A_{G,denser}$ is 2040 ksf and average $A_{G,looser}$ is 1415 ksf. This comparison is only for the NC portion of the relationship because the overconsolidated portion was caused by the compaction effect and is assumed not to relate to the in-situ condition. The same relative comparison at Site 3 gives the average $A_{G,denser}$ of 2045 ksf and the average $A_{G,looser}$ of 1425 ksf. In Table 5.3, n_G is also affected by e and γ_t since denser specimens always have smaller values of n_G than looser specimens for the same kind of sand. In terms of the average values of n_G for the two similar specimens (denser vs. looser) from each site, the comparison is as follows. At Site 6, the average $n_{G,denser}$ is 0.469 and the average $n_{G,looser}$ is 0.500. This comparison is only for the NC portion of the relationship because the overconsolidated portion was caused by the compaction effect and is assumed not to relate to the in-situ condition. The same relative comparison at Site 3 gives the average $n_{G,denser}$ of 0.482 and the average $n_{G,looser}$ of 0.536. These relative values are reasonable because looser specimens are easier to be densified than denser specimens. With the same increment in σ_0', looser specimens should have larger changes in e, γ_t and G_{max} than denser

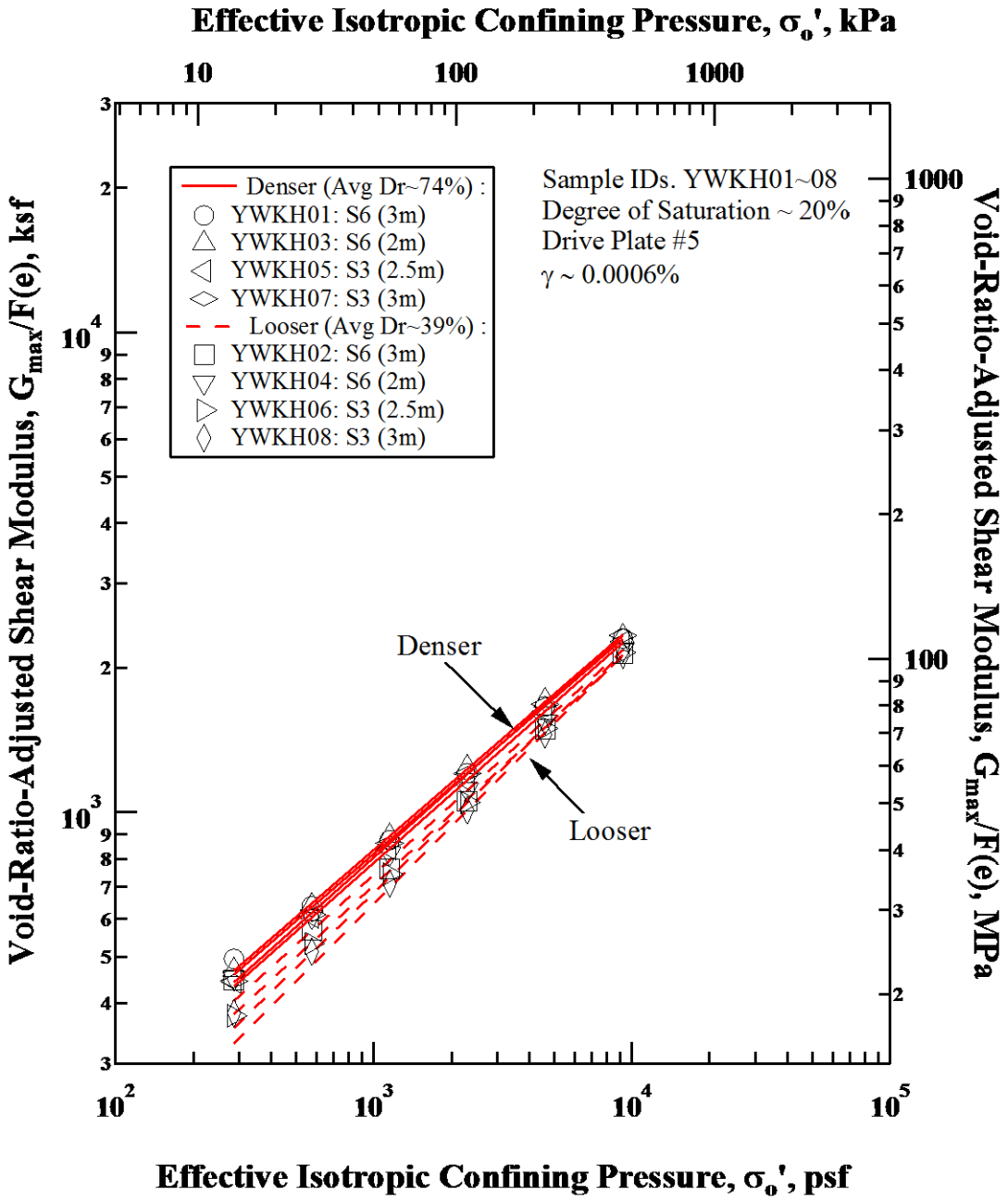

Figure 5.11 Variation in Void-Ratio-Adjusted Shear Modulus ($G_{max}/F(e)$) with Effective Isotropic Confining Pressure from Resonant Column Tests of all Sand Specimens Tested in the Normally Consolidated State from Sites 3 and 6.

specimens.

Void-ratio-adjusted shear modulus, $G_{max}/F(e)$ ($F(e)$ is calculated using Equation 2.8), for all specimens were plotted versus σ_0' on a log-log scale in Figure 5.11. To view the results more clearly, comparisons of looser and denser specimens for each site depth are presented in Figures 5.12 and 5.13. The NC portion of the $\log G_{max}/F(e) - \log \sigma_0'$ relationships shown in Figures 5.12 and 5.13 has been best-fit with Equation 5.2 using the least squares regression method. The resulting best-fit values of the parameters (A_{Ge} and n_{Ge}) are presented in Table 5.4.

Table 5.4: Parameters Fit to the NC Portion of the $\text{Log}\, G_{max}/F(e) - \text{Log}\ \sigma_0'$ Relationships from Resonant Column Tests of all Sand Specimens from Sites 3 and 6.

Specimen ID.	Test ID.	Estimated Relative Density, D_r[1], (%)	Initial Void Ratio, e	$G_{max}/F(e)$ [2]	
				A_{Ge} (ksf)	n_{Ge}
S6 (2m)	YWKH03	75	0.62	1184	0.465
	YWKH04	38	0.79	1067	0.486
S6 (3m)	YWKH01	78	0.64	1161	0.465
	YWKH02	38	0.80	1021	0.496
S3 (2.5m)	YWKH05	74	0.62	1122	0.476
	YWKH06	45	0.75	1003	0.519
S3 (3m)	YWKH07	71	0.60	1154	0.480
	YWKH08	37	0.75	962	0.538

Notes:
1. $D_r = (e_{max} - e)/(e_{max} - e_{min}) \times 100\%$, e_{max} and e_{min} are estimates based on Youd, 1973, and Menq, 2003,
2. $G_{max}/F(e) = A_{Ge}(\sigma_0'/P_a)^{n_G}$, $P_a = one\ atmosphere$.

In terms of the average values of $G_{max}/F(e)$ at σ_0' of one atmosphere for the pairs of similar specimens (denser vs. looser) from each site, the comparison is as follows. At Site 6, the average $A_{Ge,denser}$ is 1174 ksf and the average $A_{Ge,looser}$ is 1044

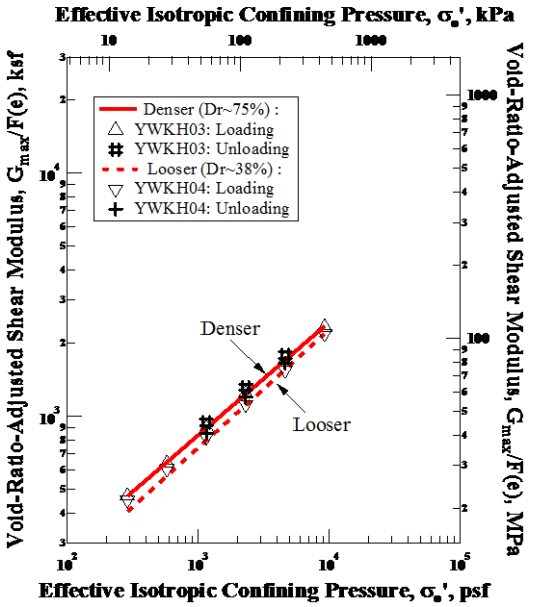

a. Soil from a depth of 2 m

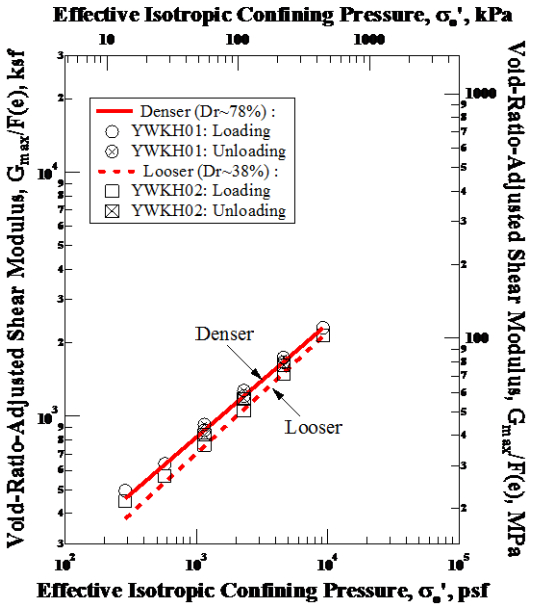

b. Soil from a depth of 3 m

Figure 5.12 Comparisons of the Variations in the $\text{Log}\, G_{max}/F(e) - \text{Log}\, \sigma_0'$ Relationships for the Pairs of Looser and Denser Specimens Tested in the Normally Consolidated State from Site 6.

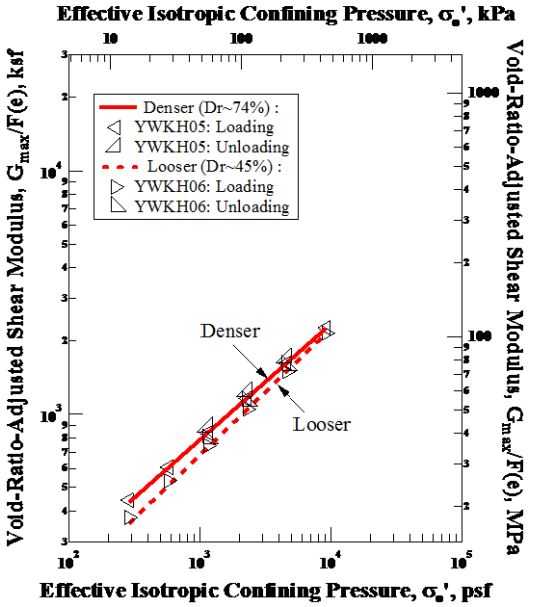

a. Soil from a depth of 2.5 m

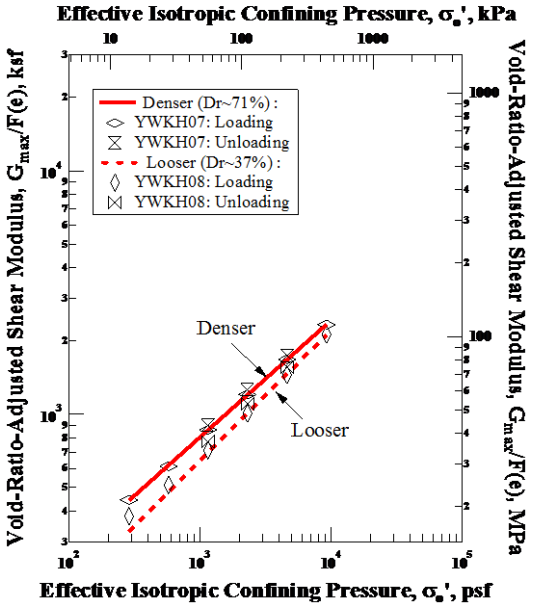

b. Soil from a depth of 3 m

Figure 5.13 Comparisons of the Variations in the $\text{Log}\, G_{max}/F(e) - \text{Log}\, \sigma_0'$ Relationships for the Pairs of Looser and Denser Specimens Tested in the Normally Consolidated State from Site 3.

ksf. At Site 3, the average $A_{Ge,denser}$ is 1138 ksf and the average $A_{Ge,looser}$ is 983 ksf. After the void ratio adjustment, $A_{Ge,denser}$ become closer to $A_{Ge,looser}$ for both Sites 3 and 6, which makes the relationships plot closer together. In terms of the average values of n_{Ge} for the two similar specimens (denser vs. looser) from each site, the comparison is as follows. At Site 6, the average $n_{Ge,denser}$ is 0.465 and the average $n_{Ge,looser}$ is 0.491. At Site 3, the average $n_{Ge,denser}$ is 0.478 and the average $n_{Ge,looser}$ is 0.529. The difference of n_{Ge} values between denser and looser specimens does not change significantly compared with the difference in the n_G comparison. This comparison shows that $F(e)$ is an important factor in evaluating A_G, but another factor seems to be needed in normalizing n_G.

To investigate the influence of total unit weight on small-strain shear modulus, a combined total unit weight and void ratio adjusted shear modulus, $G_{max}/[F(e) * \gamma_t/\gamma_w]$ ($F(e)$ was calculated using Equation 2.8, and γ_w equals the unit weight of water) is calculated. It should be noted that the unit weight factor is simply a normalized total unit weight defined as γ_t/γ_w. This "adjusted" G_{max} for all specimens is plotted versus σ_0' on a log-log scale in Figure 5.14. To view the results more clearly, comparisons of pairs of looser and denser specimens for each site depth are shown in Figures 5.15 and 5.16 for Sites 6 and 3, respectively. The NC portions of the $\log G_{max}/[F(e) * \gamma_t/\gamma_w] - \log \sigma_0'$ relationships in Figures 5.15 and 5.16 have been best-fit with Equation 5.2 using the least squares regression method. The resulting best-fit values of the parameters ($A_{Ge\gamma}$ and $n_{Ge\gamma}$) are presented in Table 5.5.

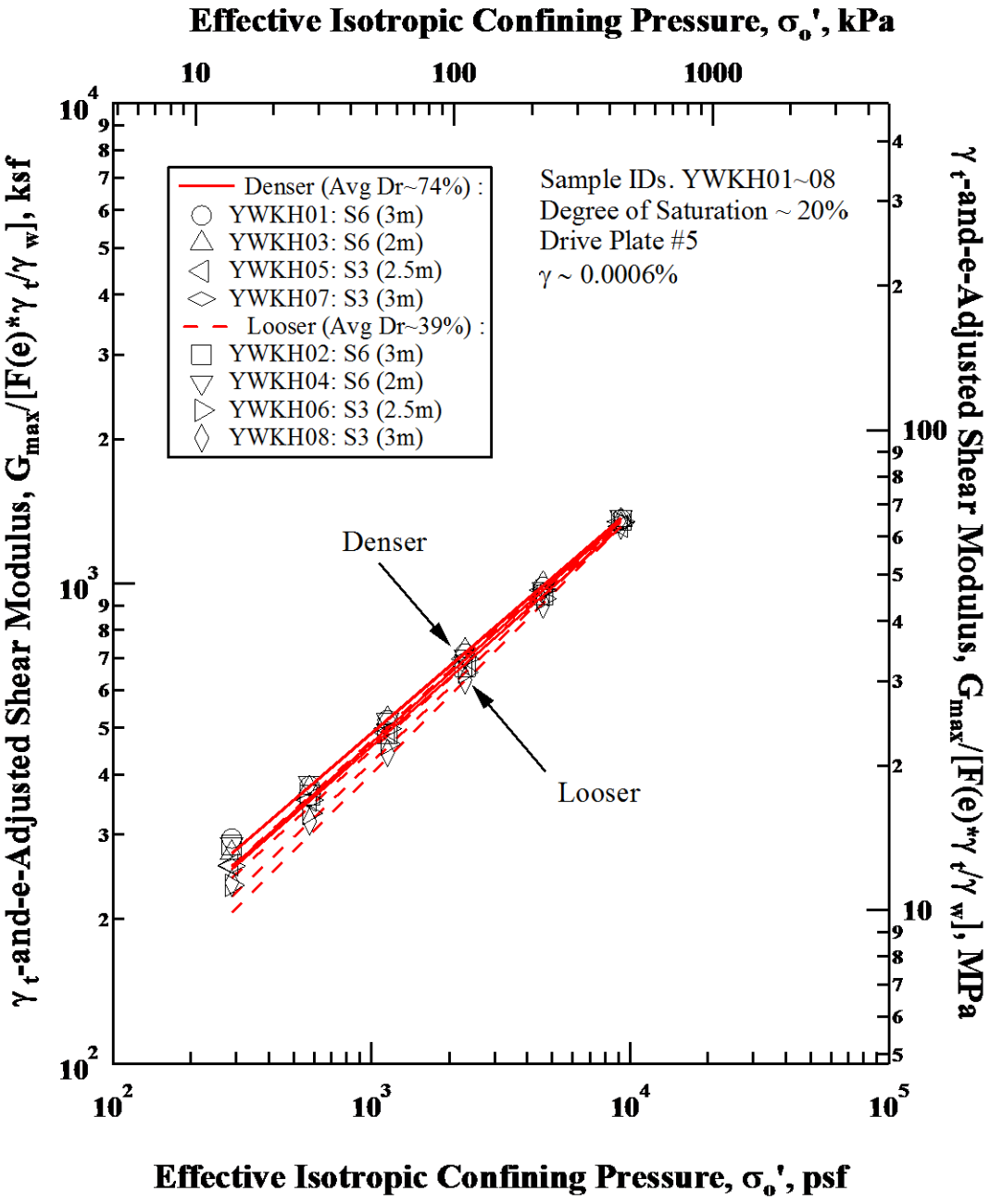

Figure 5.14 Variation in Total-Unit-Weight-and-Void-Ratio-Adjusted Shear Modulus ($G_{max}/[F(e) * \gamma_t/\gamma_w]$) with Effective Isotropic Confining Pressure from Resonant Column Tests of all Sand Specimens Tested in the Normally Consolidated State from Sites 3 and 6.

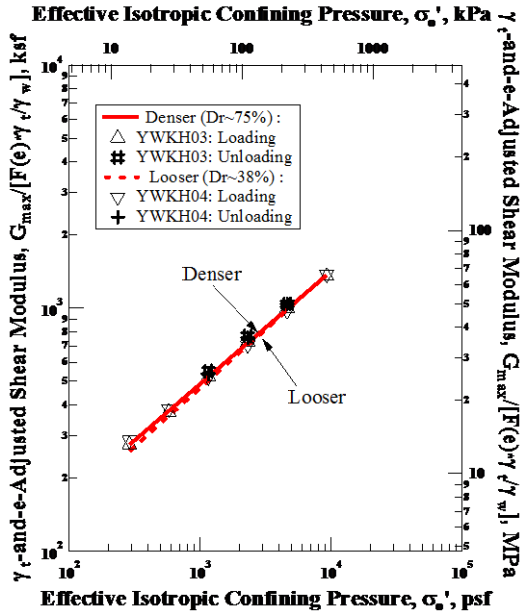

a. Soil from a depth of 2 m

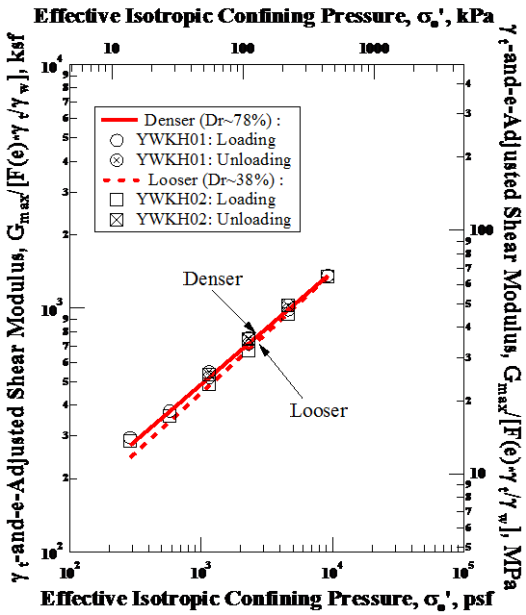

b. Soil from a depth of 3 m

Figure 5.15 Comparisons of the Variations in the $\text{Log}\, G_{max}/[F(e) * \gamma_t/\gamma_w] - \text{Log}\, \sigma_0'$ Relationships for the Pairs of Looser and Denser Specimens Tested in the Normally Consolidated State from Site 6.

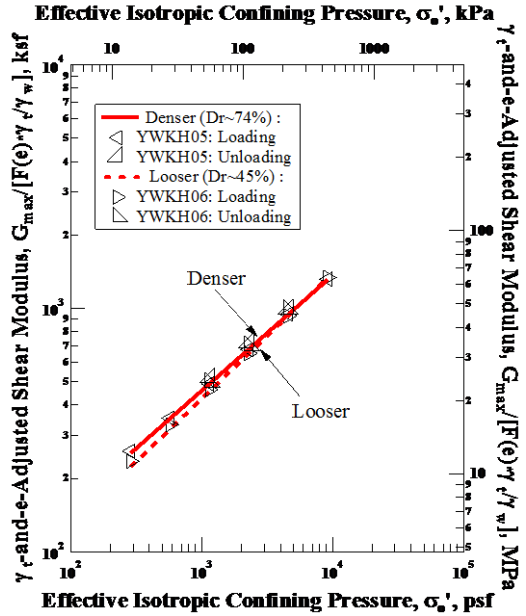

a. Soil from a depth of 2.5 m

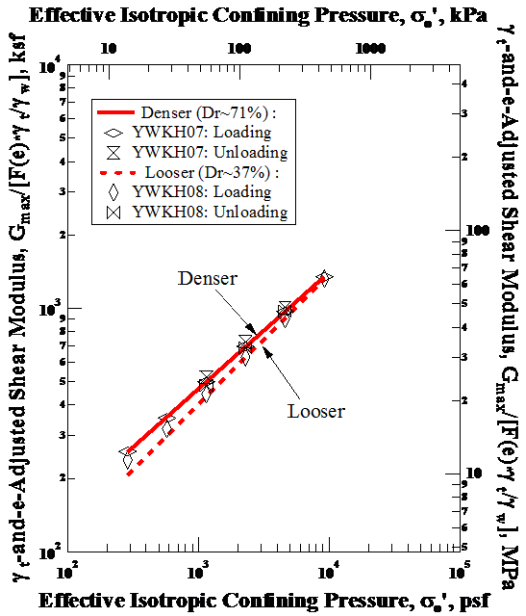

b. Soil from a depth of 3 m

Figure 5.16 Comparisons of the Variations in the $\text{Log}\, G_{max}/[F(e) * \gamma_t/\gamma_w] - \text{Log}\, \sigma_0'$ Relationships for the Pairs of Looser and Denser Specimens Tested in the Normally Consolidated State from Site 3.

Table 5.5: Parameters Fit to the NC Portion of the Log $G_{max}/[F(e)*\gamma_t/\gamma_w]$ − Log σ_0' Relationships from Resonant Column Tests of all Sand Specimens from Sites 3 and 6.

Specimen ID.	Test ID.	Relative Density, D_r[1], (%)	Initial Total Unit Weight γ_t, (g/cm^3)	$G_{max}/[F(e)*\gamma_t/\gamma_w]$ [2]	
				$A_{Ge\gamma}$ (ksf)	$n_{Ge\gamma}$
S6 (2m)	YWKH03	75	1.71	692	0.464
	YWKH04	38	1.58	675	0.482
S6 (3m)	YWKH01	78	1.68	688	0.463
	YWKH02	38	1.57	650	0.493
S3 (2.5m)	YWKH05	74	1.71	653	0.474
	YWKH06	45	1.60	624	0.516
S3 (3m)	YWKH07	71	1.73	667	0.479
	YWKH08	37	1.60	599	0.535

Notes:
1. $D_r = (e_{max} - e)/(e_{max} - e_{min}) \times 100\%$, e_{max} and e_{min} are estimates based on Youd, 1973, and Menq, 2003,
2. $G_{max}/[F(e)*\gamma_t/\gamma_w] = A_{Ge\gamma}(\sigma_0'/P_a)^{n_{Ge\gamma}}$, $P_a = one\ atmosphere,\ \gamma_w = water\ unit\ weight.$

In terms of the average values of $G_{max}/[F(e)*\gamma_t/\gamma_w]$ at σ_0' of one atmosphere for the pairs of similar specimens (denser vs. looser) from each site, the comparison is as follows. At Site 6, the average $A_{Ge\gamma,denser}$ is 690 ksf and the average $A_{Ge\gamma,looser}$ is 663 ksf. At Site 3, the average $A_{Ge\gamma,denser}$ is 660 ksf and the average $A_{Ge\gamma,looser}$ is 612 ksf. After the γ_t-and-e-adjustment, $A_{Ge\gamma,denser}$ becomes closer to $A_{Ge\gamma,looser}$ for both Sites 3 and 6, which make the relationships plot close together. In terms of the average values of $n_{Ge\gamma}$ for the pairs of similar specimens (denser vs. looser) from each site, the comparison is as follows. At Site 6, the average $n_{Ge\gamma,denser}$ is 0.464 and the average $n_{Ge\gamma,looser}$ is 0.488. At Site 3, the average $n_{Ge\gamma,denser}$ is 0.477 and the average $n_{Ge\gamma,looser}$ is 0.526. The difference in $n_{Ge\gamma}$ values between denser and looser

specimens does not change significantly compared with the n_{Ge} values. This comparison seems to show that, like $F(e)$, the γ_t is also an important factor in evaluating A_G, but another factor is needed in normalizing n_G.

The liquefiable sands at Sites 3 and 6 with somewhat different sand types and D_{50} values behaved very similarly in terms of the $\log G_{max} - \log \sigma_0'$ relationship at a given relative density. It seems that sand type, C_u, and D_{50} are so similar that they cannot be used to develop correlations that distinguish between the small-strain shear modulus of these liquefiable sands.

Table 5.6: Comparison of $\text{Log}\, G_{max} - \text{Log}\, \sigma_0'$ Relationships in the NC portion between the RC Test Results and Menq's (2003) Prediction[1].

Specimen ID.	Test ID.	Relative Density, D_r[1], (%)	RC Test		Menq's Prediction[1]	
			A_G (ksf)	n_G	A_G (ksf)	n_G
S6 (2m)	YWKH03	75	2085	0.468	2035	0.506
	YWKH04	38	1453	0.494	1585	0.506
S6 (3m)	YWKH01	78	1989	0.470	2031	0.499
	YWKH02	38	1376	0.505	1614	0.499
S3 (2.5m)	YWKH05	74	1993	0.480	2037	0.509
	YWKH06	45	1452	0.527	1669	0.509
S3 (3m)	YWKH07	71	2101	0.483	2045	0.514
	YWKH08	37	1399	0.545	1622	0.514

Notes:
1. $D_r = (e_{max} - e)/(e_{max} - e_{min}) \times 100\%$,
   e_{max} and e_{min} are estimates based on Youd, 1973, and Menq, 2003,
2. $G_{max} = C_{G3} \times {C_u}^{b1} \times e^x \times \left(\frac{\sigma_0'}{P_a}\right)^{n_G}$,
   where $C_{G3} = 67.1\, MPa\ (1400\, ksf)$,
   $b1 = -0.2$,
   $x = -1 - (D_{50}/20)^{0.75}$,
   $n_G = 0.48 \times {C_u}^{0.09}$,
   C_u = uniformity coefficient, and,
   e = void ratio

Comparison of the NC portion of the $\log G_{max} - \log \sigma_0'$ relationships between the RC tests measured results and the predicted results using Menq's (2003) equation are presented in Table 5.6. For the denser specimens with $D_r \approx 75$ %, Menq's equation gives close values of A_G with the RC test results, with the average value of $A_G = 2042\ ksf$ from RC tests and the average value of $A_G = 2037\ ksf$ from Menq's equation. However, for the looser specimens with $D_r \approx 40$ %, Menq's equation gives higher values of A_G than the RC test results, with the average value of $A_G = 1420\ ksf$ from RC tests and the average value of $A_G = 1623\ ksf$ from Menq's equation. This difference makes Menq's prediction somewhat unconservative. Also Menq's equation does not consider changes in n_G caused by changes in e, which does show affects on n_G even though the influence is not large.

To compare the RC test results from this study with test data from previous studies, the average C_G and n_G values in Equation 2.6 are calculated from the RC test results. This comparison is shown in the Table 5.7. The liquefiable sand from Christchurch has a normal average value of C_G about 6500 and a very common n_G range from 0.48 to 0.52.

5.2.3 Small-Strain Material Damping Ratio of Liquefiable Sand

Small-strain material damping ratios (D_{min}) of liquefiable sand were also measured during low-amplitude resonant column (RC) testing. The variations of (D_{min})

Table 5.7: Comparison of C_G and n_G Values[1, 2] of between Liquefiable Sand from Christchurch with Sandy Soils from Previous Studies.

Source	$F(e)$	C_G	n_G	Soil description
Hardin and Richart (1963)	$\frac{(2.17-e)^2}{1+e}$	7000	0.5	Round grain Ottawa sand
	$\frac{(2.97-e)^2}{1+e}$	3300	0.5	Angular grained crushed quartz
Iwasaki et al. (1978)	$\frac{(2.17-e)^2}{1+e}$	9000	0.38	Eleven kinds of clean sand
Kokusho (1980)	$\frac{(2.17-e)^2}{1+e}$	8400	0.5	Toyoura sand
Yu and Richart (1984)	$\frac{(2.17-e)^2}{1+e}$	7000	0.5	Three kinds of clean sand
This Thesis	$\frac{(2.17-e)^2}{1+e}$	7300	0.48	Dense liquefiable sand
		5700	0.52	Loose liquefiable sand

Notes:
1. $G_{max} = C_G \cdot F(e) \cdot (\sigma_0')^{n_G}$,
2. G_{max} and σ_0' are in kPa

with effective isotropic confining stress (σ_0') from the eight specimens are presented in Figure 5.17 in terms of $\log D_{min}$ versus $\log \sigma_0'$. Since the specimens were in the drained state during testing, the confining pressure, σ_0, is estimated to equal the effective isotropic confining pressure, σ_0'; hence any negative capillary stresses are assumed to be small.

It can be seen in Figure 5.17 that the small-strain material damping ratios of all specimens (D_{min}) decrease with effective isotropic confining pressures (σ_0'), just as shown in numerous previous studies. The first point readily observed in Figure 5.17 is that the trend for the variation of D_{min} is more complex than those of V_S and G_{max} and the relationships for denser and looser specimens are closer together than those for

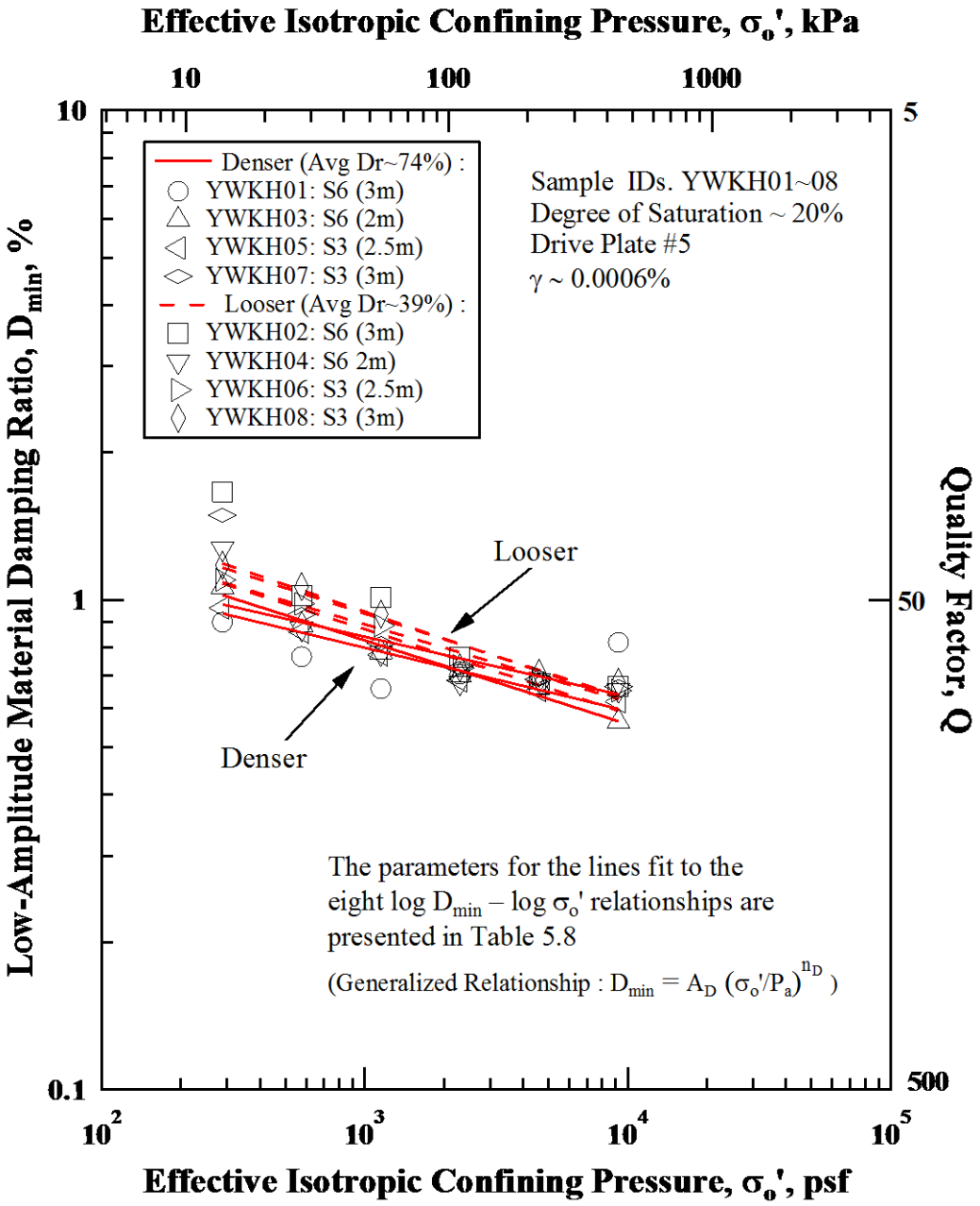

Figure 5.17 Variations in Low-Amplitude Material Damping Ratio with Effective Isotropic Confining Pressure from Resonant Column Tests of Eight Sand Specimens from Sites 3 and 6.

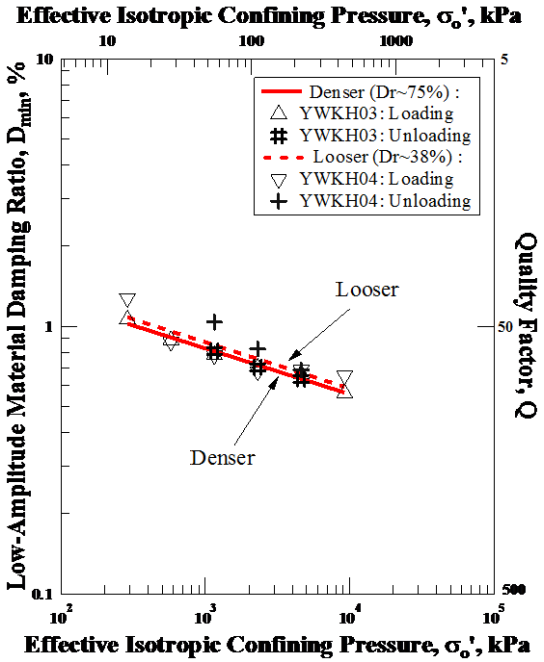

a. Soil from a depth of 2 m

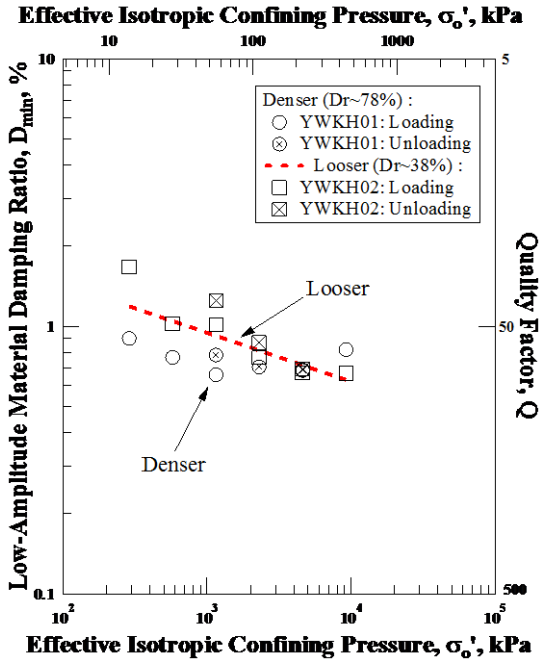

b. Soil from a depth of 3 m

Figure 5.18 Comparisons of the Variations in the $\text{Log}\, D_{min} - \text{Log}\, \sigma_0'$ Relationships for Each Pair of Looser and Denser Specimens from Site 6.

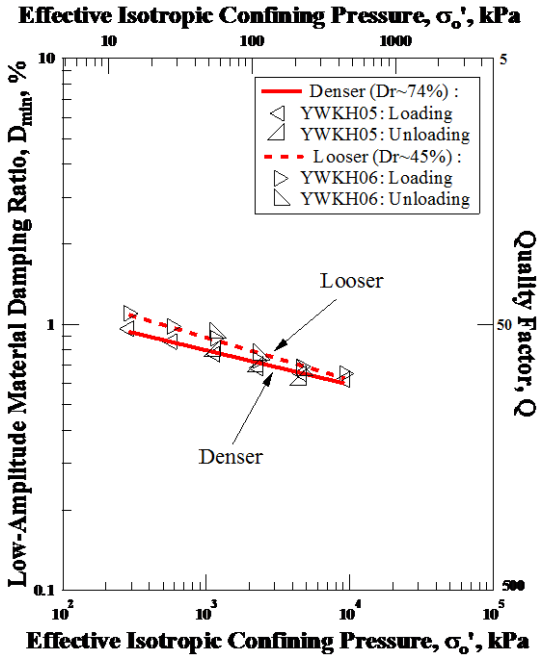

a. Soil from a depth of 2.5 m

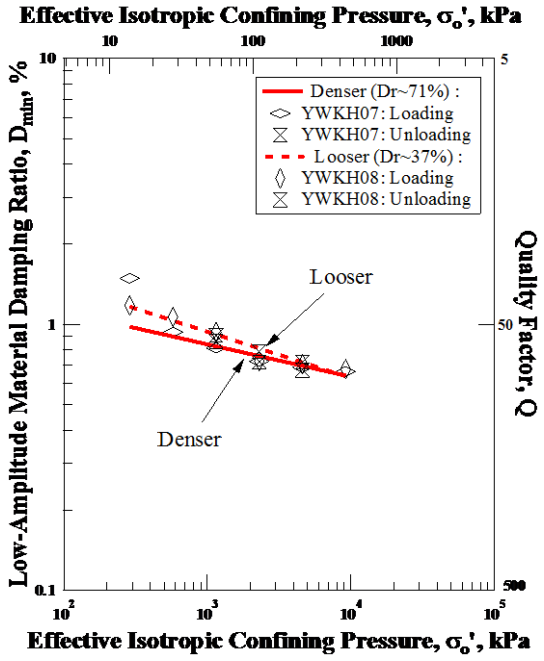

b. Soil from a depth of 3 m

Figure 5.19 Comparisons of the Variations in the $\text{Log}\, D_{min} - \text{Log}\, \sigma_0'$ Relationships for Each Pair of Looser and Denser Specimens from Site 3.

V_S and G_{max}. The second point is that denser specimens generally have smaller D_{min} values at all σ_0's than the looser specimens. This relationship may be opposite to the expected relationship and may be affected by the water in the specimens. Given the variability of the measurement caused by the ambient background noise, the influence caused by the consolidation state is relatively minor. Then each $\log D_{min} - \log \sigma_0'$ relationship is represented by a single line (a single linear relationship) for convenience.

To observe and compare the $\log D_{min} - \log \sigma_0'$ relationship of each specimen in the pair of specimens (looser versus denser specimens) for each depth at Sites 3 and 6, Figures 5.18 and 5.19, respectively, have been prepared. In these figures, the linear relationship shown by each specimen, with the exception of Specimen YWKH01, is generally easy to recognize, but contains more scatter (variability) than found in the V_S and G_{max} measurements. The equation that can be used to represent each linear segment in the $\log D_{min} - \log \sigma_0'$ relationship is:

$$D_{min} = A_D(\sigma_0'/P_a)^{n_D} \tag{5.3}$$

in which A_D equals the value of D_{min} at σ_0' equal to one atmosphere (hence, D_{min1}) and P_a is equal to one atmosphere with the same units as σ_0'. Each linear segment of the $\log D_{min} - \log \sigma_0'$ relationships shown in Figures 5.18 and 5.19 has been best-fit with Equation 5.3 using the least squares regression method. The resulting best-fit values of the parameters (A_D and n_D) are presented in Table 5.8. The r^2 values for the best-fits to determine A_D and n_D range from 0.7838 to 0.9778 and average 0.9263, among

which r^2 value of Specimen YWKH04 (Site 6 (2m)) is 0.7838 and r^2 value of Specimen YWKH02 (Site 6 (3m)) is 0.8848.

Table 5.8: Parameters Fit to Each Linear Segment of the Eight Log D_{min} − Log σ_0' Relationships from Resonant Column Tests of Eight Sand Specimens from Sites 3 and 6.

Specimen ID.	Test ID.	Estimated Relative Density, D_r[1], (%)	D_{min}[2]	
			A_D (%)	n_D
S6 (2m)	YWKH03	75	0.727	-0.171
	YWKH04	38	0.765	-0.173
S6 (3m)	YWKH01	78		
	YWKH02	38	0.824	-0.183
S3 (2.5m)	YWKH05	74	0.724	-0.129
	YWKH06	45	0.792	-0.159
S3 (3m)	YWKH07	71	0.767	-0.122
	YWKH08	37	0.823	-0.174

Notes:
1. $D_r = (e_{max} - e)/(e_{max} - e_{min}) \times 100\%$, e_{max} and e_{min} are estimates based on Youd, 1973, and Menq, 2003
2. $D_{min} = A_D(\sigma_0'/P_a)^{n_D}$, $P_a = one\ atmosphere$,

During the small-strain resonant column test for specimen YWKH01, D_{min} at confining pressures from 16 psi to 64 psi seem to be out of the general trend and thus discarded. This may also result from environmental vibration or small structural changes, which does not affect G_{max}, in specimen YWKH01 during the resonant column test because damping ratio is more sensitive than shear modulus in resonant column test. In test YWKH02 and YWKH07, D_{min} at the lowest confining pressure 2 psi is affected by background noise to be unusually high and thus discarded.

As with void ratio (e) having an effect on small-strain V_S and G_{max}, through the stiffening effect of denser soil skeletons, void ratio also has an influence on the small-

strain material damping ratio. Denser specimens of the same material with lower values of e generally have smaller D_{min} values than the looser specimens with higher values of e at the same σ_0' level. In terms of the average values of D_{min} at σ_0' of one atmosphere for the pairs of specimens (denser vs. looser) from each site, the comparison is as follows. At Site 6, the average $A_{D,denser}$ is 0.73 % and the average $A_{D,looser}$ is 0.80 %. The same relative comparison at Site 3 gives the average $A_{D,denser}$ of 0.75 % and the average $A_{D,looser}$ of 0.81 %. In Table 5.8, n_D is also affected by e since denser specimens always have smaller absolute values of n_D than looser specimens for the same kind of sand. In terms of the average values of n_D for the two similar specimens (denser vs. looser) from each site, the comparison is as follows. At Site 6, the average $n_{D,denser}$ is -0.17 and the average $n_{D,looser}$ is -0.18. The same relative comparison at Site 3 gives the average $n_{D,denser}$ of -0.13 and the average $n_{D,looser}$ of -0.17.

Comparison of $D_{min} - \sigma_0'$ relationships using Equation 2.11 between the RC test results and Menq's (2003) prediction are presented in Table 5.9. Menq's equation gives a little higher A_D values than the RC tests because Menq's equation is based on the dry granular sand and the specimens tested in RC devices are with degree of saturation about 20 %. According to Madhusudhan and Kumar (2013), for fine sand, after the optimum degree of saturation (S_r), damping ratio will increase with decreasing in S_r. It is reasonable that A_D from Menq's equation is a little higher than the RC tests. However, n_D in Menq's equation is a constant of -0.08, which is different from n_D values from

the RC tests. When σ_0' goes high, Menq's prediction will give higher D_{min} than the RC tests due to the flatter slope in $D_{min} - \sigma_0'$ plot obtained from Menq's equation, which will be somewhat unconservative. From the RC tests, it does show that e has an influence on both A_D and n_D.

Table 5.9: Comparison of $\log D_{min} - \log \sigma_0'$ Relationships in the NC portion between the RC Test Results and Menq's Prediction.

Specimen ID.	Test ID.	Estimated Relative Density, D_r[1], (%)	RC Test		Menq's Prediction[2]	
			A_D (%)	n_D	A_D (%)	n_D
S6 (2m)	YWKH03	75	0.727	-0.171	0.952	-0.08
	YWKH04	38	0.765	-0.173	0.952	-0.08
S6 (3m)	YWKH01	78			0.958	-0.08
	YWKH02	38	0.824	-0.183	0.958	-0.08
S3 (2.5m)	YWKH05	74	0.724	-0.129	0.813	-0.08
	YWKH06	45	0.792	-0.159	0.813	-0.08
S3 (3m)	YWKH07	71	0.767	-0.122	0.894	-0.08
	YWKH08	37	0.823	-0.174	0.894	-0.08

Notes:
1. $D_r = (e_{max} - e)/(e_{max} - e_{min}) \times 100\%$, e_{max} and e_{min} are estimates based on Youd, 1973, and Menq, 2003
2. $D_{min} = 0.55 \times {C_u}^{0.1} \times {D_{50}}^{-0.3} \times \left(\frac{\sigma_0'}{P_a}\right)^{-0.08}$, where C_u = uniformity coefficient, and, D_{50} = median grain size

D_{min} measurements from previous studies are rare because of difficulties of eliminating the background noise and equipment-generated damping. The average C_D and n_D in the equation 2.10 are calculated from the RC test results. Comparison with washed Mortar sand is shown in the Table 5.10. The liquefiable sand from Christchurch has a higher C_D and a lower absolute value of n_D than washed Mortar sand.

Table 5.10: Comparison of C_D and n_D of between Liquefiable Sand from Christchurch and Washed Mortar Sand.

Source	$F(e)$	C_D	n_D	Soil description
Boonam Shin (2014)	$\frac{1}{0.3+0.7e^2}$	0.73	-0.16~-0.23	Washed Mortar sand
This Thesis	$\frac{1}{0.3+0.7e^2}$	1.82	-0.122~-0.2	Liquefiable sand from Christchurch

Notes: 1. $D_{min} = C_D F(e) \left(\frac{\sigma_0'}{P_a}\right)^{n_D}$

5.3 NONLINEAR DYNAMIC PROPERTIES OF THE LIQUEFIABLE SAND

5.3.1 Nonlinear Shear Moduli of Liquefiable Sand

High-amplitude resonant column (RC) tests were performed to obtain the dynamic properties of the liquefiable sand specimens in the nonlinear shear strain range. These tests were performed at only one effective isotropic confining pressure (σ_0') that was equal to 8 psi. The nonlinear testing was performed after the low-amplitude unloading tests were performed. Variations in shear modulus (G) with shear strain (γ) of the eight sand specimens from Sites 3 and 6 are shown in Figure 5.20.

The first point observed in Figure 5.20 is that the shear moduli of all specimens decrease with increasing shear strain (γ), just as shown in numerous previous studies. The second point observed in Figure 5.20 is that the specimens divide into two groups, with the denser specimens being stiffer (have larger G values at all shearing strains) than the looser specimens. The third point is that the $G - \log\gamma$ relationships are well represented by a hyperbolic model. To observe and compare the $G - \log\gamma$ relationship of each

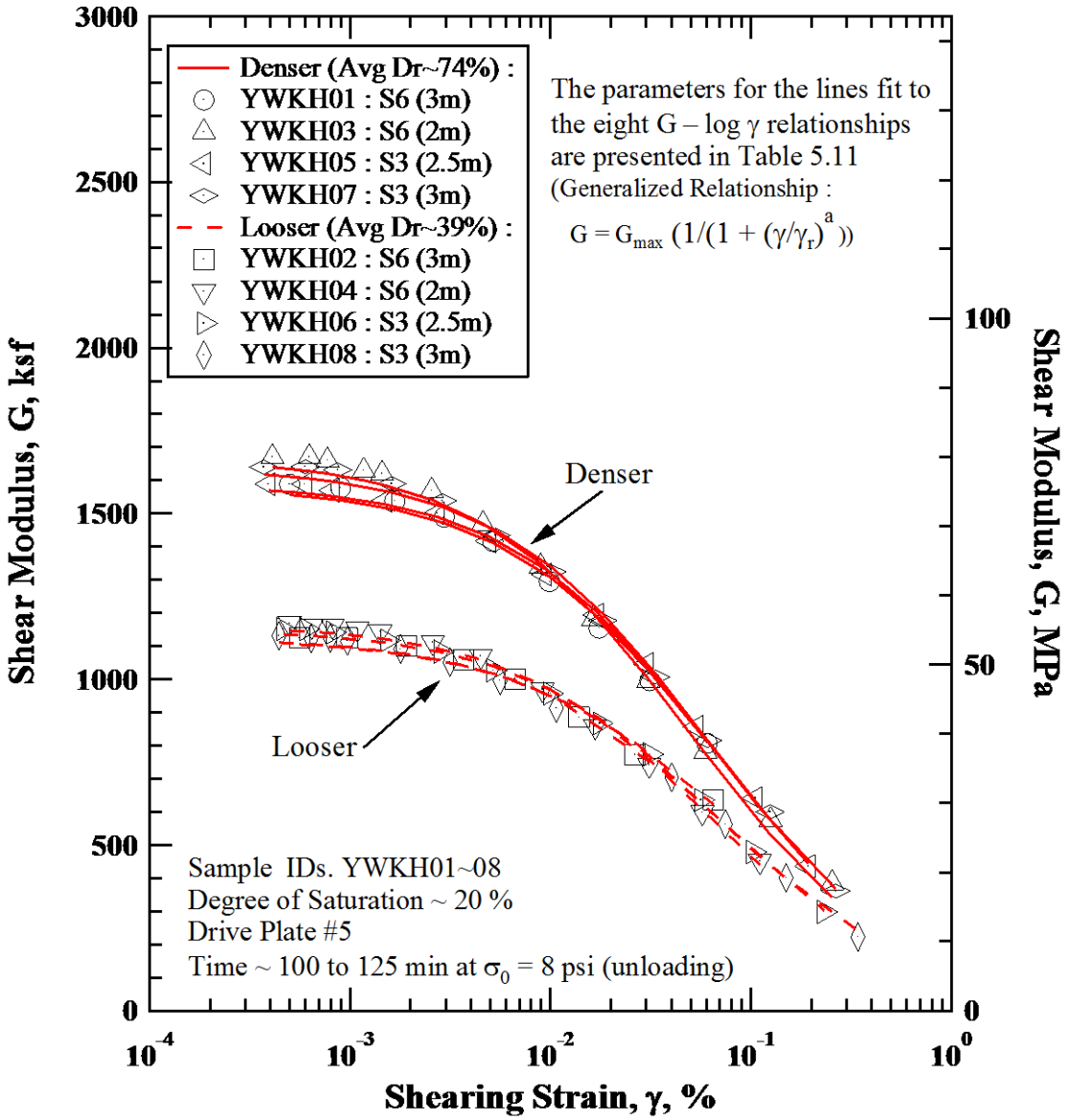

Figure 5.20 Variations in Shear Modulus with Shearing Strain at an Unloading Effective Isotropic Confining Pressure of 8 psi from Resonant Column Tests of Eight Sand Specimens from Sites 3 and 6.

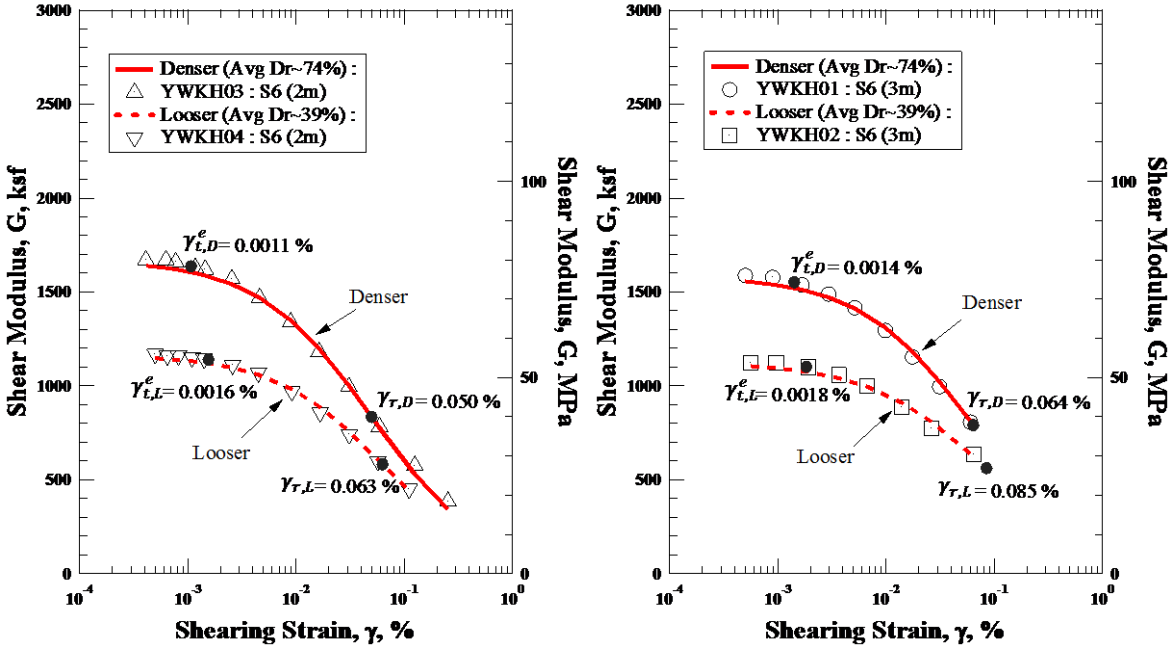

a. Soil from a depth of 2 m b. Soil from a depth of 3 m

Figure 5.21 Comparisons of the Variations in the $G - \mathrm{Log}\,\gamma$ Relationships for Each Pair of Looser and Denser Specimens from Site 6.

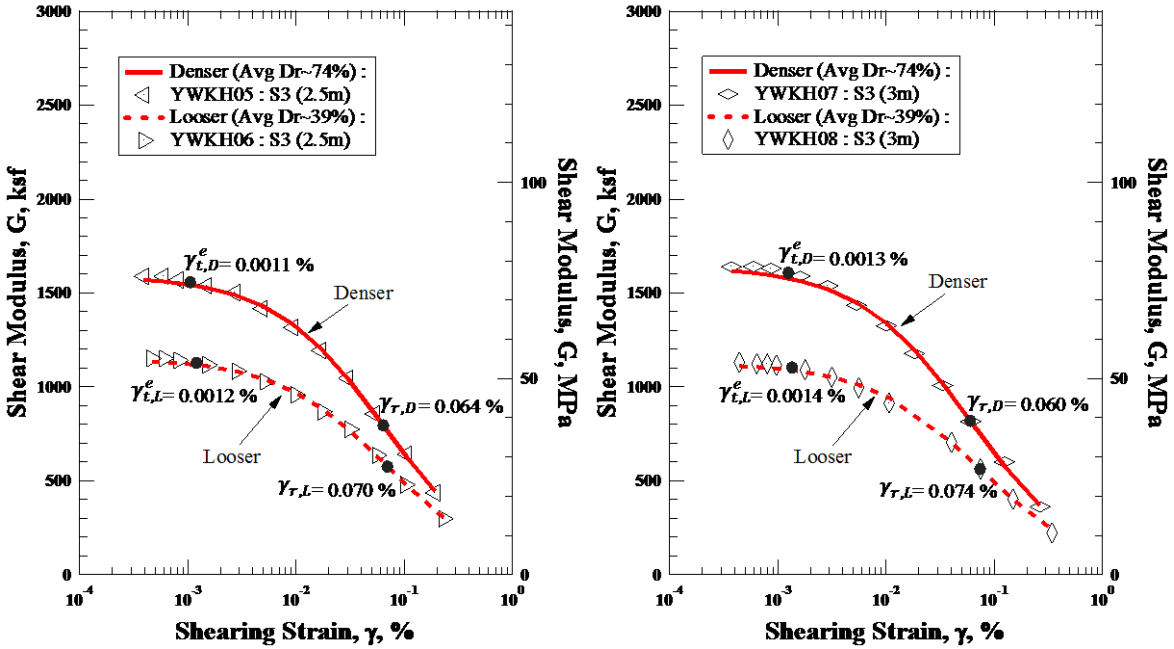

a. Soil from a depth of 2.5 m b. Soil from a depth of 3 m

Figure 5.22 Comparisons of the Variations in the $G - \mathrm{Log}\,\gamma$ Relationships for Each Pair of Looser and Denser Specimens from Site 3.

specimen in the pair of specimens (looser and denser specimens) for each depth at Sites 6 and 3, Figures 5.21 and 5.22, respectively, have been prepared. Darendeli's (2001) equation was used to represent each hyperbolic curve in the $G - \log\gamma$ relationship as:

$$\frac{G}{G_{max}} = \frac{1}{1 + \left(\frac{\gamma}{\gamma_r}\right)^a} \tag{5.4}$$

in which G_{max} is equal to the shear modulus in the small-strain range at an unloading effective isotropic confining stress of 8 psi, γ_r is equal to the reference shear strain at which shear modulus equals half of G_{max}, and a is a curvature coefficient. Each $G -$

Table 5.11: Parameters Fit to the $G - \text{Log}\,\gamma$ Relationships from Resonant Column Tests of all Sand Specimens from Sites 3 and 6.

Specimen ID.	Test ID.	Estimated Relative Density, D_r[1], (%)	Initial Void Ratio, e	Elastic Threshold γ_t^{e2} (%)	Modified Hyperbolic Relationship[3]	
					γ_r (%)	a
S6 (2m)	YWKH03	75	0.62	0.0011	0.050	0.834
	YWKH04	38	0.79	0.0016	0.063	0.879
S6 (3m)	YWKH01	78	0.64	0.0014	0.064	0.838
	YWKH02	38	0.80	0.0018	0.085	0.805
S3 (2.5m)	YWKH05	74	0.62	0.0011	0.064	0.857
	YWKH06	45	0.75	0.0012	0.070	0.857
S3 (3m)	YWKH07	71	0.60	0.0013	0.060	0.837
	YWKH08	37	0.75	0.0014	0.074	0.847

Notes:
1. $D_r = (e_{max} - e)/(e_{max} - e_{min}) \times 100\%$,
   e_{max} and e_{min} are estimates based on Youd, 1973, and Menq, 2003,
2. $\gamma_t^e =$ shear strain at which $G/G_{max} =$ 0.98,
3. Modified hyperbolic relationship:
   $G/G_{max} = 1/(1 + (\gamma/\gamma_r)^a)$,
   where G_{max} = small-strain shear modulus
   γ_r = reference shear strain, and,
   a = curvature coefficient.

$\log\gamma$ relationship shown in Figures 5.21 and 5.22 has been best-fit with Equation 5.4 using the least-squares regression method. The resulting best-fit values of the parameters (γ_r and a) are presented in Table 5.11. The r^2 values for the best-fits to determine γ_r and a ranged from 0.9686 to 0.9985 and averaged 0.9926.

In $G - \log\gamma$ plots, denser specimens always have a higher shear modulus at given shear strains than the looser specimens, and this difference is mainly caused by the higher G_{max} of the denser specimens. To eliminate the effect of G_{max} on the nonlinear shear modulus behavior, the variations in normalized shear modulus (G/G_{max}) with shear strain (γ) from RC testing of the eight sand specimens from Sites 3 and 6 are compared. This comparison is presented in Figure 5.23. To observe and compare the $G/G_{max} - \log\gamma$ relationship of each specimen in the pair of specimens (looser and denser specimens) for each depth at Sites 3 and 6, Figures 5.24 and 5.25, respectively, have been prepared.

In these figures, it can be seen that looser specimens and denser specimens have same values of G/G_{max} $(= 1.0)$ when the shear strain is in linear small-strain range. When the normalized shear modulus begins to exhibit the nonlinearity, this strain is taken as the elastic threshold strain (γ_t^e). The average threshold shear strains for the two pairs of specimens (denser and looser pair) from each site show the following comparison. At Site 6, average $\gamma_{t,denser}^e$ is 0.0013 % and average $\gamma_{t,looser}^e$ is 0.0017 %. The same relative comparison at Site 3 gives an average $\gamma_{t,denser}^e$ of 0.0012 % and the average $\gamma_{t,looser}^e$ of 0.0013 %. The looser specimens have slightly higher values of the elastic

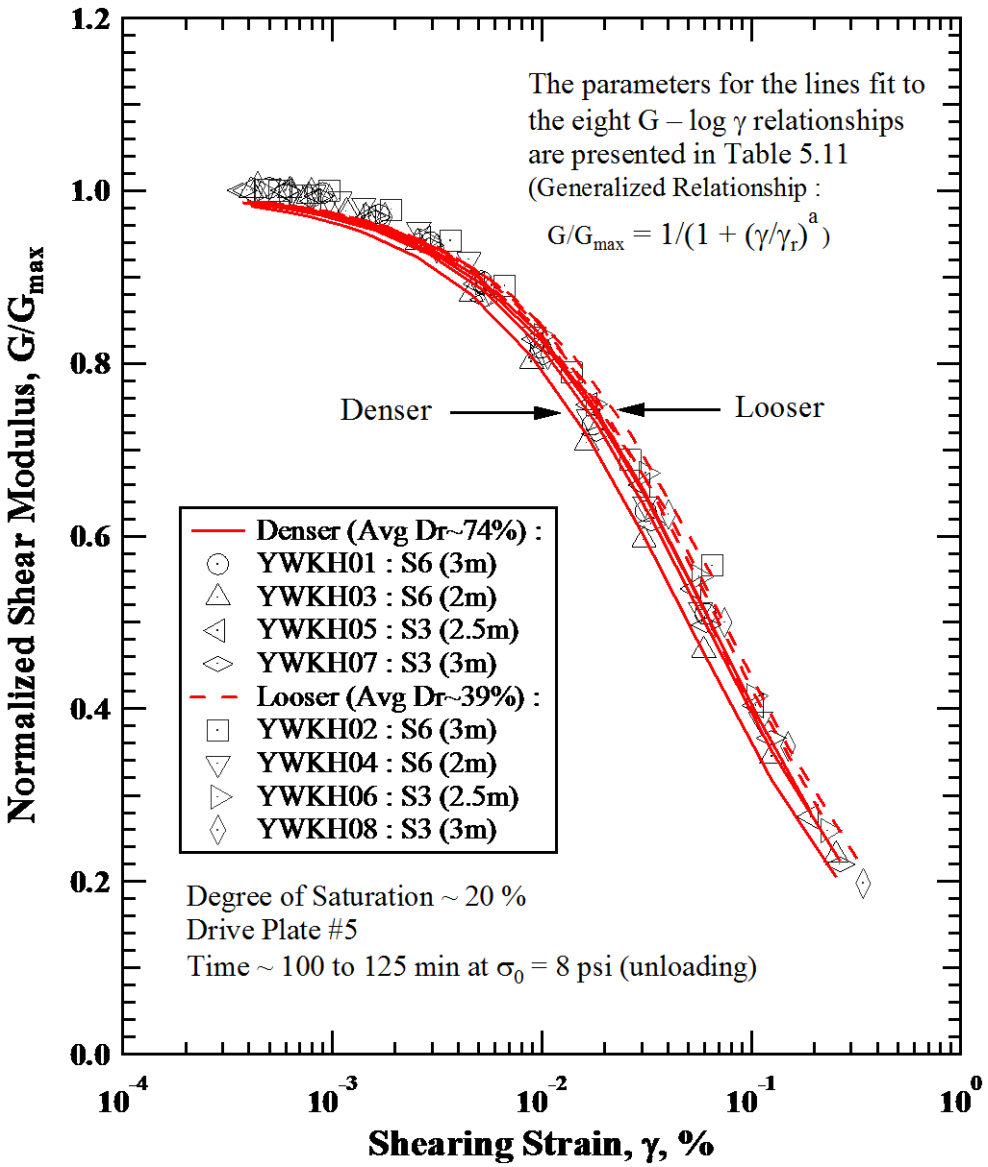

Figure 5.23 Variations in Normalized Shear Modulus with Shearing Strain at an Unloading Effective Isotropic Confining Pressure of 8 psi from Resonant Column Tests of Eight Sand Specimens from Sites 3 and 6.

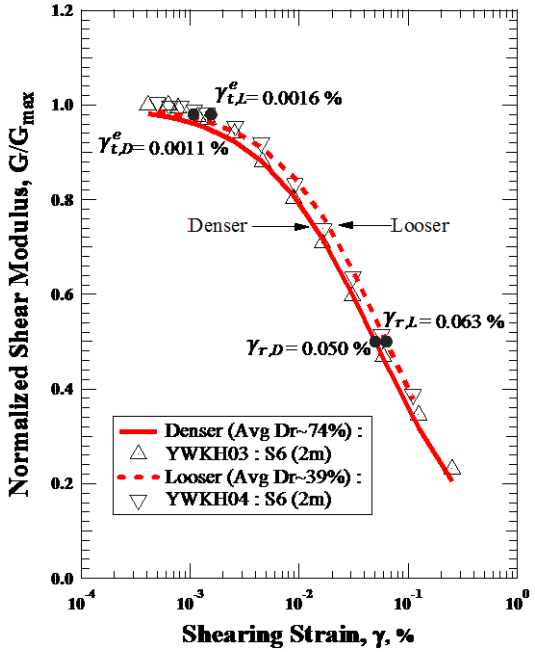

a. Soil from a depth of 2 m

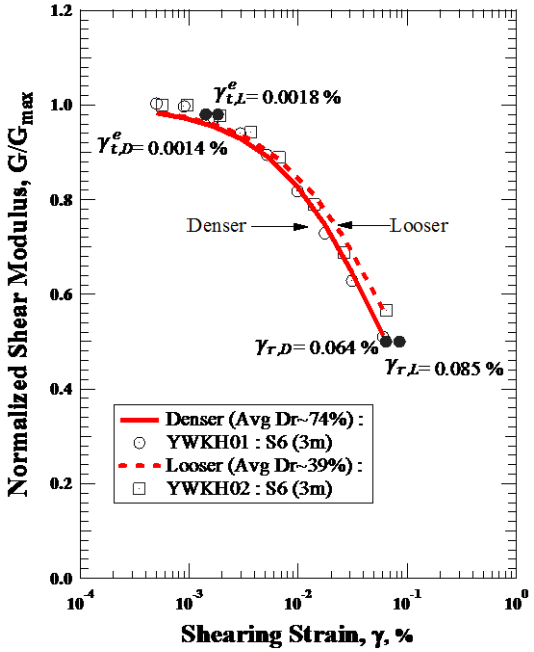

b. Soil from a depth of 3 m

Figure 5.24 Comparisons of the Variations in the $G/G_{max} - \mathrm{Log}\,\gamma$ Relationships for Each Pair of Looser and Denser Specimens from Site 6.

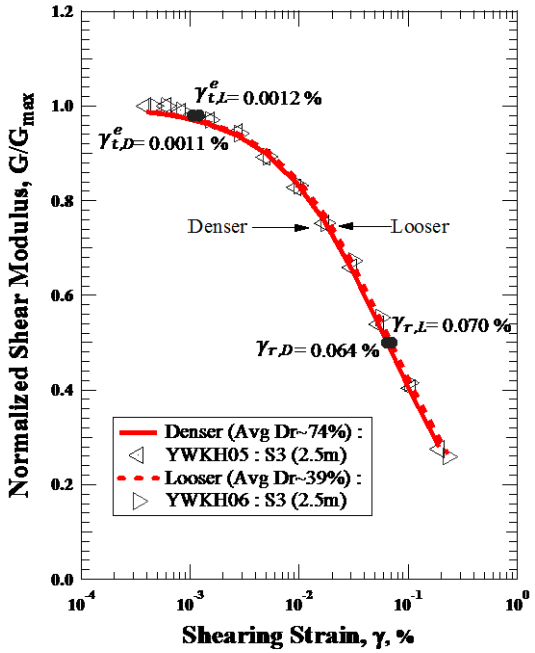

a. Soil from a depth of 2.5 m

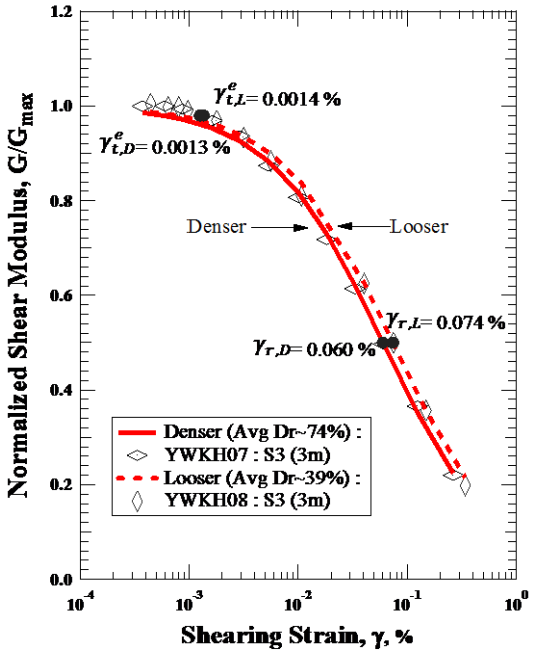

b. Soil from a depth of 3 m

Figure 5.25 Comparisons of the Variations in the $G/G_{max} - \mathrm{Log}\,\gamma$ Relationships for Each Pair of Looser and Denser Specimens from Site 3.

threshold than the denser specimens, which means looser specimens have higher values of G/G_{max} than denser specimens at each γ in the nonlinear elastic range. As the shear strain increases from the linear to the moderately nonlinear and then to the highly nonlinear range, looser specimens have higher values of G/G_{max} than denser specimens at each γ. In terms of the average values of reference shear strain (γ_r) for the pairs of specimens (denser and looser pairs) from each site, the comparison is as follows. At Site 6, average $\gamma_{r,denser}$ is 0.057 % and average $\gamma_{r,looser}$ is 0.074 %. The same relative comparison at Site 3 gives the average $\gamma_{r,denser}$ of 0.062 % and the average $\gamma_{r,looser}$ of 0.072 %. In general terms, $\gamma_{r,looser}$ is about 20 to 25 % larger than $\gamma_{r,denser}$. In terms of the average values of the curvature coefficient (a) for the pairs of specimens (denser and looser pairs) from each site, the comparison is as follows. At Site 6, average a_{denser} is 0.836 and average a_{looser} is 0.842. The same relative comparison at Site 3 gives the average a_{denser} of 0.847 and the average a_{looser} of 0.852. In general terms, this comparison shows that a is essentially the same for both densities.

Comparison of $G/G_{max} - \log\gamma$ relationships between the RC tests and Menq's predictions are presented in Table 5.12. Values of reference strain (γ_r) and curvature coefficient (a) for sandy soil have been predicted by Menq (2003) for use in the modified hyperbolic model suggested by Darendeli (2001). Menq's equations have γ_r to be a function of C_u and σ_0' while a is a function of σ_0'. Compared to the RC tests, Menq's predictions give quite good results even though void ratio is not considered. However, void ratio (e) does have an effect on γ_r even through it is less than about 25 %.

Table 5.12: Comparison of γ_r and a between the RC Test Results and Menq's Predictions.

Specimen ID.	Test ID.	Estimated Relative Density, D_r[1], (%)	Initial Void ratio, e	Modified Hyperbolic Relationship[2]			
				from RC Tests		from Menq, 2003	
				γ_r (%)	a	$\gamma_{r,Menq}$[3] (%)	a_{Menq}[4]
S6 (2m)	YWKH03	75	0.62	0.050	0.834	0.064	0.833
	YWKH04	38	0.79	0.063	0.879	0.064	
S6 (3m)	YWKH01	78	0.64	0.064	0.838	0.069	
	YWKH02	38	0.80	0.085	0.805	0.069	
S3 (2.5m)	YWKH05	74	0.62	0.064	0.857	0.063	
	YWKH06	45	0.75	0.070	0.857	0.063	
S3 (3m)	YWKH07	71	0.60	0.060	0.837	0.058	
	YWKH08	37	0.75	0.074	0.847	0.058	

Notes:
1. $D_r = (e_{max} - e)/(e_{max} - e_{min}) \times 100\%$,
   e_{max} and e_{min} are estimates based on Youd, 1973, and Menq, 2003
2. $G/G_{max} = 1/(1 + (\gamma/\gamma_r)^a)$,
   where G_{max} = small-strain shear modulus
   γ_r = reference shear strain, and,
   a = curvature coefficient.
3. $\gamma_r = 0.12 \times {C_u}^{-0.6} \times \left(\frac{\sigma_0'}{P_a}\right)^{0.5 \times {C_u}^{-0.15}}$,
4. $a = 0.86 + 0.1 \times \log\left(\frac{\sigma_0'}{P_a}\right)$
   where C_u = uniformity coefficient, and,
   σ_0' = effective isotropic confining pressure.

5.3.2 Nonlinear Material Damping Ratio of Liquefiable Sand

Nonlinear material damping ratios (D) of the liquefiable sand from Christchurch were also measured during the high-amplitude resonant column (RC) testing. These tests were performed in conjunction with the nonlinear shear modulus measurement at isotropic confining pressure equal to 8 psi after the low-amplitude unloading tests using

the RC device were completed. All eight specimens were involved in these tests. The variations in material damping ratio (D) with shear strain (γ) of the eight sand specimens from Sites 3 and 6 are shown in Figure 5.26.

It can be seen in Figure 5.26 that the material damping ratios of all specimens (D) increase with shear strain (γ), just as shown in numerous previous studies. The first point observed in Figure 5.26 is that, unlike $G - \log\gamma$ relationships shown in Figure 5.20 that separated into two groups (denser versus looser), all material damping relationships fall in a narrow zone, with little spread shown in the $D - \log\gamma$ relationships. This narrow zone in the relationships shows that void ratio is not a strong factor in these similar sands. Also, D increases as much as 13 times over the range in γ in the high-amplitude RC tests while G only decreased by a factor of about 5 as shown in Figure 5.23. Compared with the changes in D caused by γ, the differences between D of denser specimens and D of looser specimens is relatively small. The second point is that the $D - \log\gamma$ relationships are also well represented by hyperbolic models. To observe and compare the $D - \log\gamma$ relationship of each specimen in the pair of specimens (looser and denser specimens) for each depth at Sites 3 and 6, Figures 5.27 and 5.28, respectively, have been prepared. The equation that can be used to represent each hyperbolic curve in the $D - \log\gamma$ relationship is:

$$\frac{D}{D_{min}} = 1 + \left(\frac{\gamma}{\gamma_{r,D}}\right)^{b} \tag{5.5}$$

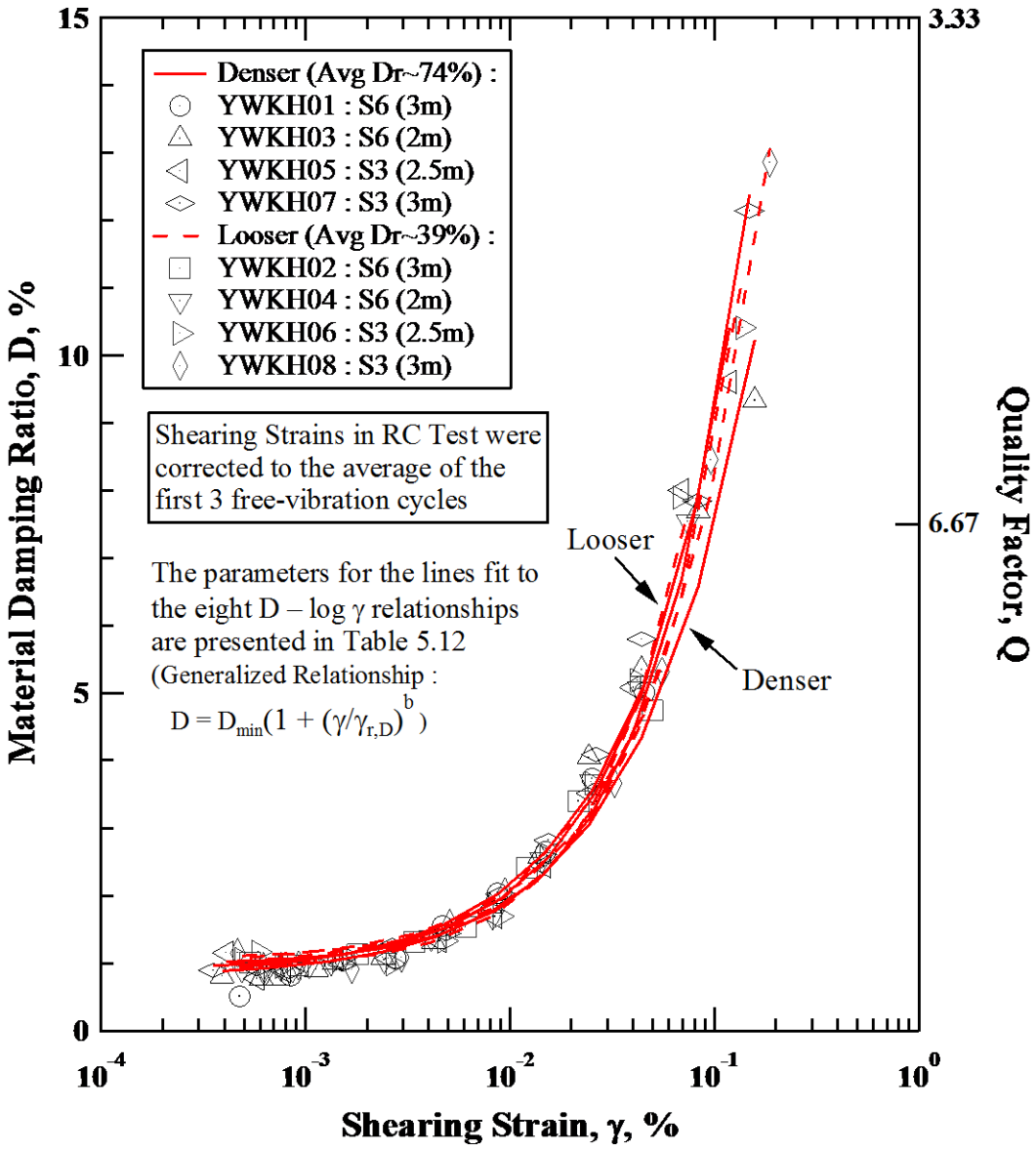

Figure 5.26 Variations in Material Damping Ratio with Shearing Strain at an Unloading Effective Isotropic Confining Pressure of 8 psi from Resonant Column Tests of Eight Sand Specimens from Sites 3 and 6.

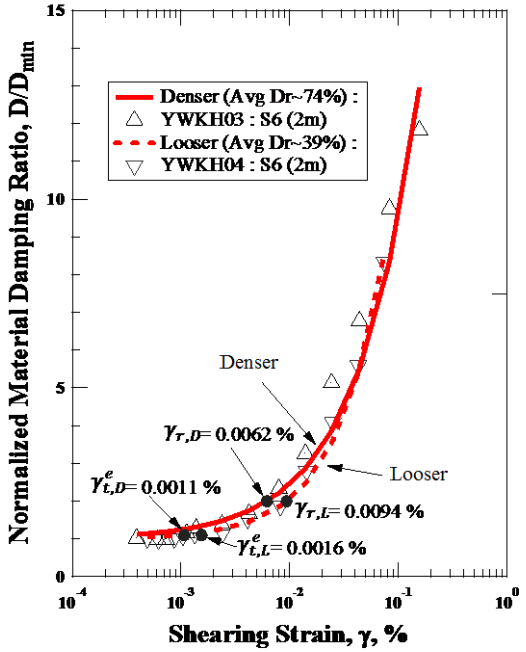

a. Soil from a depth of 2 m

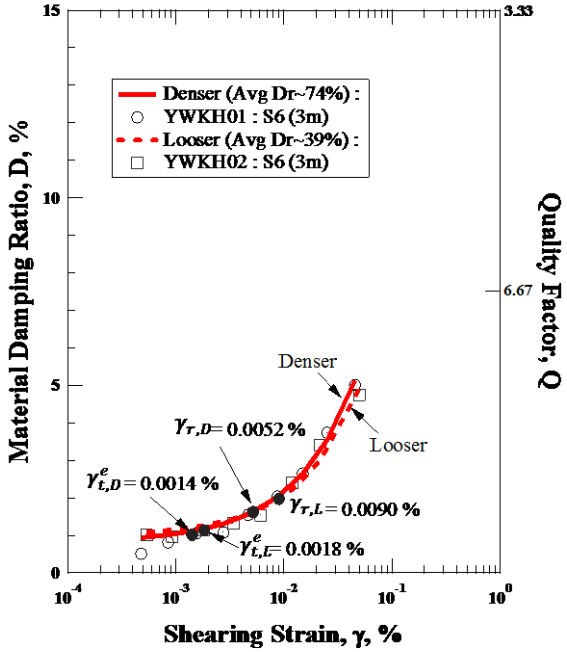

b. Soil from a depth of 3 m

Figure 5.27 Comparisons of the Variations in the $D - \text{Log}\,\gamma$ Relationships for Each Pair of Looser and Denser Specimens from Site 6.

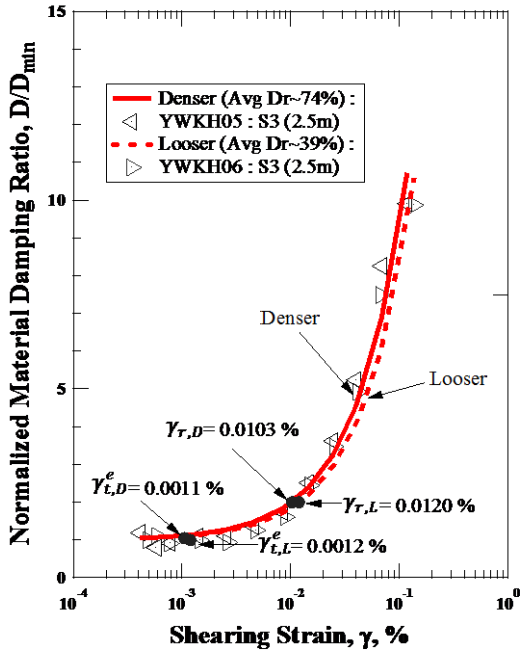

a. Soil from a depth of 2.5 m

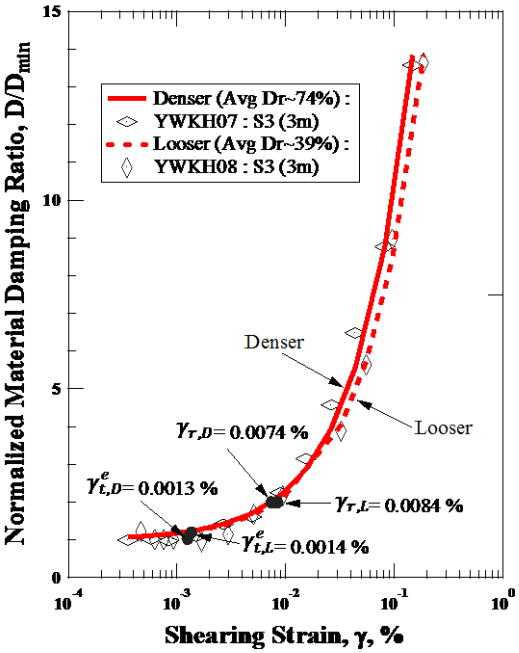

b. Soil from a depth of 3 m

Figure 5.28 Comparisons of the Variations in the $D - \text{Log}\,\gamma$ Relationships for Each Pair of Looser and Denser Specimens from Site 3.

in which D_{min} equals to the material damping ratio in small-strain range at unloading effective isotropic confining stress of 8 psi, $\gamma_{r,D}$ is equal to the reference shear strain at which the value of D/D_{min} is equal to 2, and b is a curvature coefficient. (It should be noted that $\gamma_{r,D}$ and b are not related to γ_r and a for the $G/G_{max} - \log\gamma$ relationships.) Each $D - \mathrm{Log}\,\gamma$ relationship shown in Figures 5.27 and 5.28 has been best-fit with Equation 5.5 using the least squares regression. The resulting best-fit values of the parameters ($\gamma_{r,D}$ and b) are presented in Table 5.12. The r^2 values for the best-fits to determine $\gamma_{r,D}$ and b range from 0.9574 to 0.9966 and average 0.9781.

Table 5.13: Parameters Fit to the $D - \mathrm{Log}\,\gamma$ Relationships from Resonant Column Tests of all Sand Specimens from Sites 3 and 6.

Specimen ID.	Test ID.	Estimated Relative Density, D_r[1], (%)	Initial Void ratio, e	Elastic threshold γ_t^{e2} (%)	Modified Hyperbolic Relationship Equation[3]	
					γ_r (%)	b
S6 (2m)	YWKH03	75	0.62	0.0011	0.0062	0.767
	YWKH04	38	0.79	0.0016	0.0094	0.976
S6 (3m)	YWKH01	78	0.64	0.0014	0.0052	0.770
	YWKH02	38	0.80	0.0018	0.0090	0.806
S3 (2.5m)	YWKH05	74	0.62	0.0011	0.0103	0.931
	YWKH06	45	0.75	0.0012	0.0120	0.926
S3 (3m)	YWKH07	71	0.60	0.0013	0.0074	0.851
	YWKH08	37	0.75	0.0014	0.0084	0.823

Notes:
1. $D_r = (e_{max} - e)/(e_{max} - e_{min}) \times 100\%$,
   e_{max} and e_{min} are estimates based on Youd, 1973, and Menq, 2003,
2. $\gamma_t^e =$ shear strain at which $G/G_{max} =$ 0.98,
3. $D/D_{min} = 1 + (\gamma/\gamma_r)^b$,
   where D_{min} = small-strain material damping ratio,
   γ_r = reference shear strain, and,
   b = curvature coefficient.

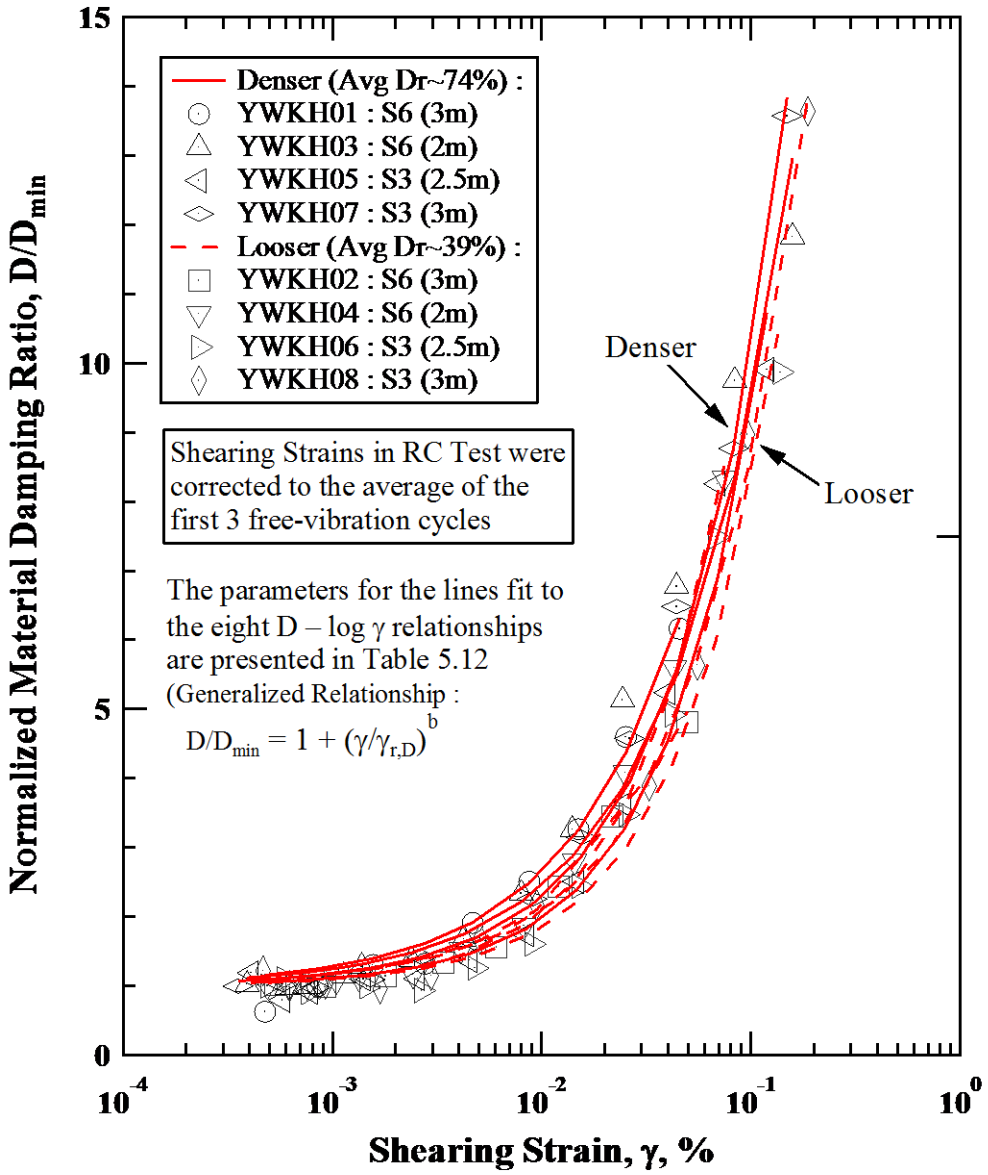

Figure 5.29 Variations in Normalized Material Damping Ratio (D/D_{min}) with Shearing Strain at an Unloading Effective Isotropic Confining Pressure of 8 psi from Resonant Column Tests of Eight Sand Specimens from Sites 3 and 6.

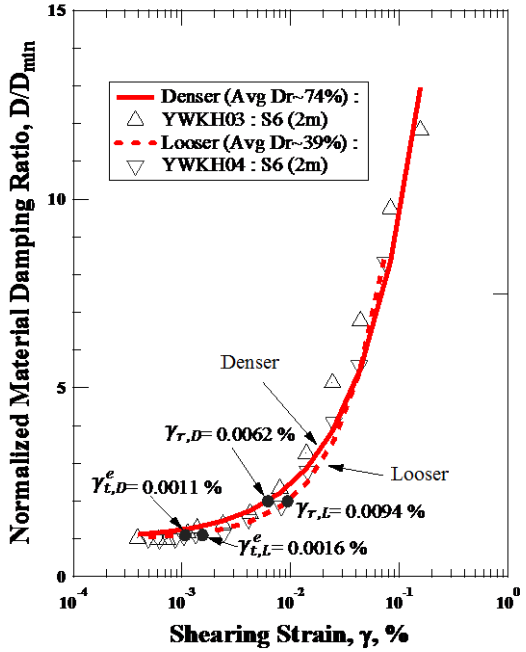

a. Soil from a depth of 2 m

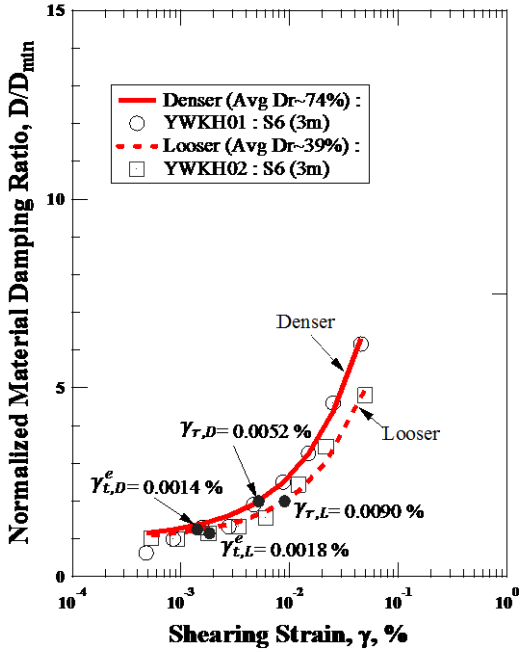

b. Soil from a depth of 3 m

Figure 5.30 Comparisons of the Variations in the $D/D_{min} - \mathrm{Log}\,\gamma$ Relationships for Each Pair of Looser and Denser Specimens from Site 6.

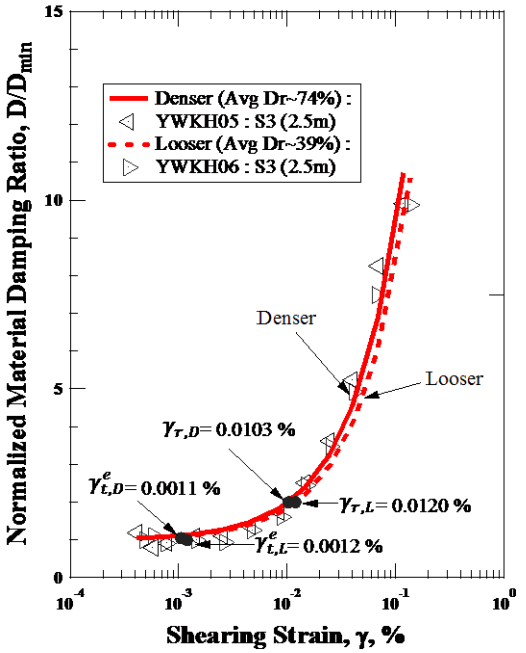

a. Soil from a depth of 2.5 m

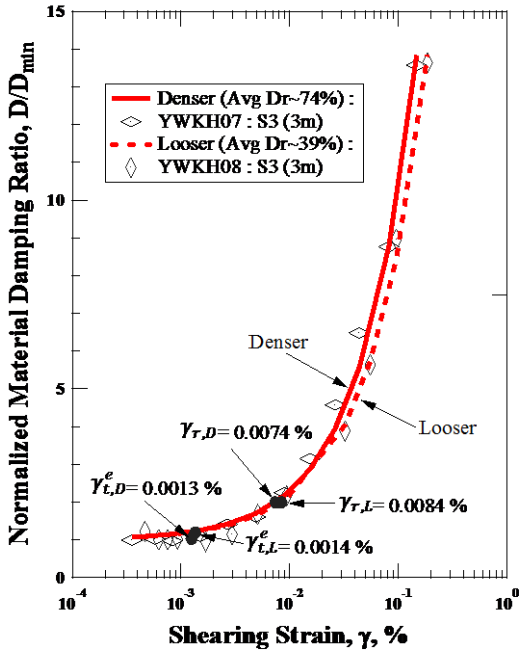

b. Soil from a depth of 3 m

Figure 5.31 Comparisons of the Variations in the $D/D_{min} - \mathrm{Log}\,\gamma$ Relationships for Each Pair of Looser and Denser Specimens from Site 3.

Denser specimens have smaller values of D_{min} than looser specimens for the same kind of sand, as discussed before. In order to eliminate the effect of D_{min} to the nonlinear material damping ratio behavior, the variations in normalized material damping ratio (D/D_{min}) with shear strain (γ) from RC testing of the eight sand specimens from Sites 3 and 6 are presented in Figure 5.29. To observe and compare the $D/D_{min} - \log \gamma$ relationship of each specimen in the pair of specimens (looser and denser specimens) for each depth at Sites 3 and 6, Figures 5.30 and 5.31, respectively, have been prepared.

In these figures, it can be seen that looser specimens and denser specimens have similar values of D/D_{min} when shear strain is in linear elastic range. As the shear strain goes up to moderately nonlinear and highly nonlinear range, denser specimens have higher values of D/D_{min} than looser specimens at each γ. In terms of the average values of reference shear strain $\gamma_{r,D}$ for the pairs of specimens (denser vs. looser) from each site, the comparison is as follows. At Site 6, average $\gamma_{r,D,denser}$ is 0.0057 % and average $\gamma_{r,D,looser}$ is 0.0092 %. The same relative comparison at Site 3 gives the average $\gamma_{r,D,denser}$ of 0.0088 % and the average $\gamma_{r,D,looser}$ of 0.0102 %. In terms of the average values of curvature coefficient b for the pairs of specimens (denser vs. looser) from each site, the comparison is as follows. At Site 6, average b_{denser} is 0.769 and average b_{looser} is 0.891. The same relative comparison at Site 3 gives the average b_{denser} of 0.891 and the average b_{looser} of 0.875. The comparison shows that $\gamma_{r,D}$ is affected by void ratio (e) since denser specimens always have smaller values of $\gamma_{r,D}$

than looser specimens for the same kind of sand. Void ratio may affect curvature coefficient b, but another factor is needed in normalizing curvature coefficient b.

5.4 SUMMARY

Low-amplitude and high-amplitude resonant column tests are performed to study the small-strain and nonlinear dynamic properties of liquefiable sand respectively. The impacts of factors like void ratios (e) and total unit weight γ_t on the dynamic properties of liquefiable sand are studied on eight specimens. Comparison of RC test results and Menq's prediction are also presented to show the consistency and inconsistency for recommendation of using Menq's equations for liquefiable sand.

Void ratio (e) has an influence on the low-amplitude shear wave velocity in the general way that denser soil fabrics form a stiffer soil skeleton. First, the denser specimens with smaller e alway have higher V_S values than the looser specimens with larger e at the same σ_0' level. Second, the denser specimens always have slightly smaller values of n_S, which represents the slopes of $\log V_S - \log \sigma_0'$ relationships, than looser specimens for the same kind of liquefiable sand. At last, the plots of void-ratio-adjusted shear wave velocities prove that $\sqrt{F(e)}$, ($F(e) = 1/0.3 + 0.7e^2$), is an important factor in evaluating A_S, (V_S at σ_0' of one atmosphere), but another factor is needed in normalizing n_S.

As with void ratio (e) having an effect on small-strain V_S through the stiffening effect of denser soil skeletons, void ratio also has an influence on the small-strain shear modulus. The effect is even more pronounced because the effect is further increased by the fact that total unit weight enters the calculation of shear modulus ($G = (\gamma_t/g)V_S^2$). First, denser specimens of the same material with lower values of e and higher values of γ_t always have larger G_{max} values than the looser specimens with higher values of e and lower values of γ_t at the same σ_0' level. Second, denser specimens always have smaller values of n_G, which represents the slopes of $\log G_{max} - \log \sigma_0'$ relationships, than looser specimens for the same kind of sand. At last, the plots of total-unit-weight-and-void-ratio-adjusted shear modulus prove that both $\sqrt{F(e)}$, ($F(e) = 1/0.3 + 0.7e^2$), and γ_t are important factors in evaluating A_G, (G_{max} at σ_0' of one atmosphere), but another factor is needed in normalizing n_G.

Void ratio also has an influence on the small-strain material damping ratio, even though the variation of small-strain material damping ratio is more complex than those of V_S and G_{max}. Denser specimens of the same material with lower values of e generally have smaller D_{min} values than the looser specimens with higher values of e at the same σ_0' level.

Menq's prediction can be somewhat unconservative for calculating G_{max} and D_{min}. Also Menq's equation does not consider changes in n_G and n_D caused by changes in e, which does show affects on n_G and n_D even though the influence is not large.

Hyperbolic models modified from Darendeli (2001) used in the study of nonlinear shear modulus behavior of liquefiable sand is as follows:

$$\frac{G}{G_{max}} = \frac{1}{1 + \left(\frac{\gamma}{\gamma_r}\right)^a} \tag{5.4}$$

in which G_{max} equals to the shear modulus in small-strain at unloading effective isotropic confining stress of 8 psi, γ_r is equal to the reference shear strain at which shear modulus equals to half of G_{max}, and a is a curvature coefficient. From the variations in normalized shear modulus (G/G_{max}) with shear strain (γ), it is found that γ_t^e, γ_r and a are both affected by void ratio (e) because denser specimens always have smaller values of γ_t^e, γ_r and a than looser specimens for the same kind of sand.

Compared to the RC tests, Menq's equations give not bad results for predicting nonlinear shear modulus behavior. However, void ratio (e) does have an effect on γ_r and a, even through it is minor.

Hyperbolic models modified from Darendeli (2001) used in the study of nonlinear material damping ratio behavior of liquefiable sand is as follows:

$$\frac{D}{D_{min}} = 1 + \left(\frac{\gamma}{\gamma_{r,D}}\right)^b \tag{5.5}$$

in which D_{min} equals to the material damping ratio in small-strain at unloading effective isotropic confining stress of 8 psi, $\gamma_{r,D}$ is equal to the reference shear strain at which the value of D is 100 % higher than that of D_{min}, and b is a curvature coefficient. From

the variations in normalized material damping ratio (D/D_{min}) with shear strain (γ), it is shown that $\gamma_{r,D}$ is affected by void ratio (e) since denser specimens always have smaller values of $\gamma_{r,D}$ than looser specimens for the same kind of sand. Void ratio may affect curvature coefficient b, but another factor is needed in normalizing b.

CHAPTER SIX

DYNAMIC PROPERTIES OF CALCAREOUS SAND FROM PUERTO RICO

6.1 INTRODUCTION

In this chapter, the dynamics properties of calcareous sand from Puerto Rico are discussed. Dynamics properties of the calcareous sand in the small-strain range are discussed in Section 6.2. Dynamics properties of the sand in the nonlinear strain range are discussed in Section 6.3. And, a brief summary of dynamic properties is given in Section 6.4.

6.2 SMALL-STRAIN DYNAMIC PROPERTIES OF CALCAREOUS SAND

The low-amplitude tests using the resonant column device were performed to determine the dynamic properties (V_S, G_{max} and D_{min}) of the calcareous sand in the small-strain range, $\gamma < 0.0003$ %. These tests were performed at the following six isotropic confining pressures: 2.25, 4.5, 9, 18, 36 and 72 psi. A total of five specimens of sand were tested. The variations of shear wave velocity, shear modulus and material damping ratio with isotropic confining pressure for the five sand specimens are discussed in Sections 6.2.1, 6.2.2 and 6.2.3, respectively.

6.2.1 Variation of Small-Strain Shear Wave Velocity with σ_0 and e

The variations in low-amplitude shear wave velocity with isotropic confining pressure from RC testing of the five sand specimens are shown in Figure 6.1. Since the specimens were in the drained state during testing, the confining pressure, σ_0, is estimated to equal the effective isotropic confining pressure, σ_0'; hence any negative capillary stresses are assumed to be small. From Figure 6.1, it can be seen that the low-amplitude shear wave velocities (V_S) of all specimens increase with effective isotropic confining pressures (σ_0'), just as shown in numerous previous studies. The first point readily observed in Figure 6.1 is that the denser specimens are stiffer (have larger V_S values at all σ_0's) than the looser specimens. The second point is that all the $\log V_S - \log \sigma_0'$ relationships are well represented by two lines (a bi-linear relationship), with the first line having a "flatter slope" in the bi-linear relationship. Each one of these points is discussed below.

In Figure 6.1, the bi-linear relationship for each one of the denser and looser specimens is easily seen. The bi-linear $\log V_S - \log \sigma_0'$ relationship indicates that all the denser and looser specimens were exhibiting a behavior similar to specimens that are behaving like overconsolidated (OC) specimens at lower pressures and then become normally consolidated at higher pressures. The equation that can be used to represent each linear segment in the $\log V_S - \log \sigma_0'$ relationship is:

$$V_S = A_S(\sigma_0'/P_a)^{n_S} \tag{6.1}$$

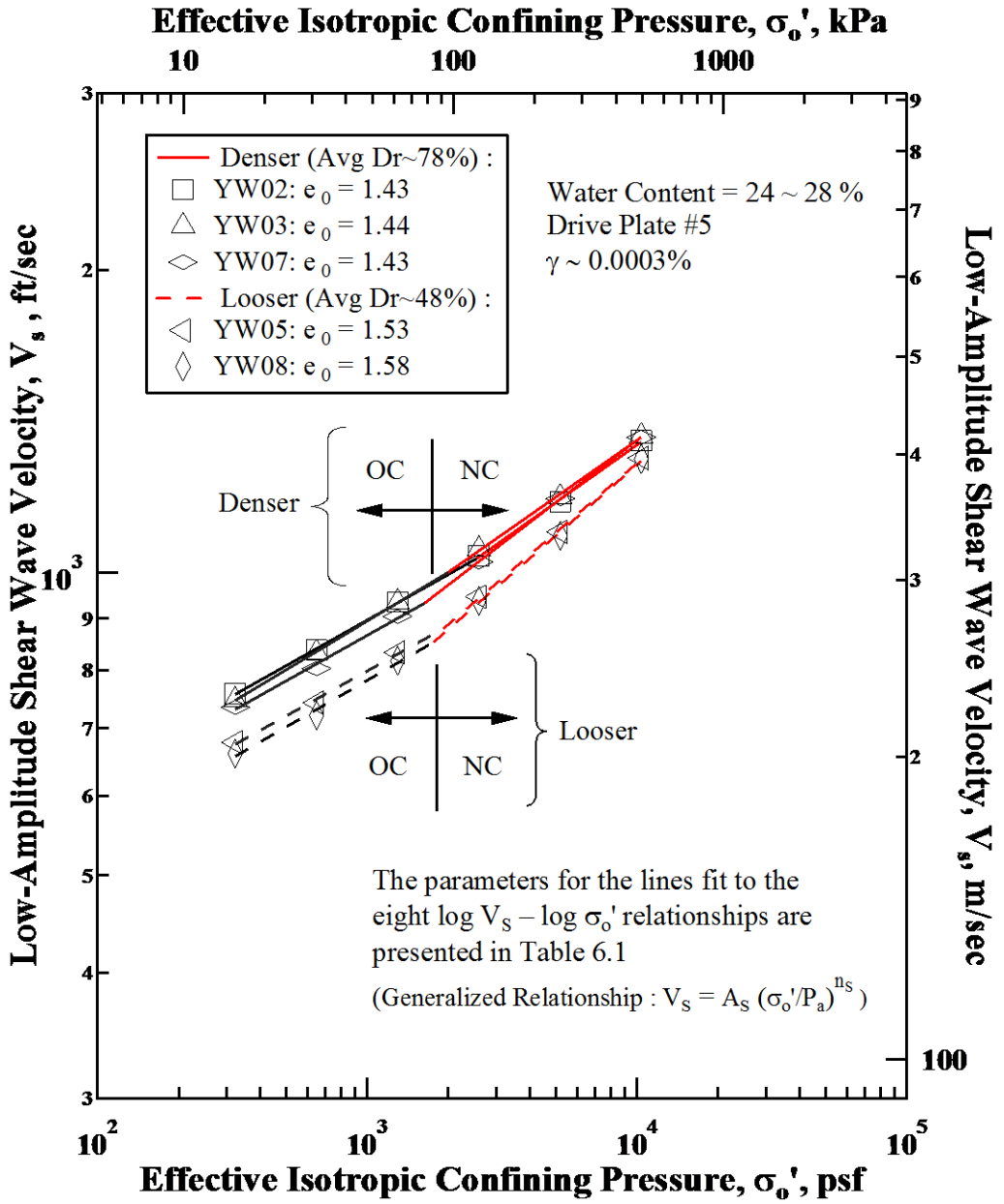

Figure 6.1 Variations in the Low-Amplitude Shear Wave Velocity with Effective Isotropic Confining Pressure from Resonant Column Tests of Five Calcareous Sand Specimens.

in which A_S equals the value of V_S at σ_0' equal to one atmosphere (hence, V_{S1}) and P_a is equal to one atmosphere with the same units as σ_0'. Each linear segment of the $\log V_S - \log \sigma_0'$ relationships shown in Figures 6.1 has been best-fit with Equation 6.1 using the least squares regression method. The resulting best-fit values of the parameters (A_S and n_S) are presented in Table 6.1. The r^2 values for the best-fits to determine A_S and n_S range from 0.9899 to 0.9999 and average 0.9971.

Table 6.1: Parameters Fit to Each Linear Section of the Five $\text{Log } V_S - \text{Log } \sigma_0'$ Relationships from Resonant Column Tests of Sand Specimens.

Test ID.	Estimated Relative Density, D_r[1], (%)	Initial Void Ratio, e	Consolidation State	V_S[2]	
				A_S (fps)	n_S
YW02	78	1.43	OC[3]	1005	0.151
			NC[4]	997	0.190
YW03	76	1.44	OC	1011	0.162
			NC	1012	0.187
YW05	54	1.53	OC	892	0.149
			NC	900	0.229
YW07	79	1.43	OC	969	0.150
			NC	984	0.206
YW08	42	1.58	OC	876	0.154
			NC	890	0.234

Notes:
1. $D_r = (e_{max} - e)/(e_{max} - e_{min}) \times 100\%$, e_{max} and e_{min} are provided by Baxter, 2013,
2. $V_s = A_s(\sigma_0'/P_a)^{ns}$, $P_a = one\ atmosphere$,
3. OC = overconsolidated state,
4. NC = normally consolidated state.

Void ratio (e) has an influence on the low-amplitude shear wave velocity in the general way that denser soil fabrics form a stiffer soil skeleton. The denser specimens with smaller e alway have higher V_S values than the looser specimens with larger e at

the same σ_0' level. For the sand specimens tested from Puerto Rico, the void ratio of a given specimen changed less 1.88 % during the time it was confined at each test pressure. The change in e with $\log \sigma_0'$ is shown for the five specimens in Figure 6.2. As the confining pressure increases, e of each specimen decreases a little because the soil skeleton densifies. In terms of the average values of V_S at σ_0' of one atmosphere for the denser and looser specimens, the comparison is as follows. The average value of $A_{S,denser}$ is 998 ft/sec and the average value of $A_{S,looser}$ is 895 ft/sec, a difference of about 10 %. This comparison is only for the NC portion of the relationship because the overconsolidated portion was caused by the compaction effect and does not relate to the in-situ condition unless the sand is overconsolidated. Also the values of the void ratios at σ_0' of one atmosphere are 1.43 and 1.56 for $A_{S,denser}$ and $A_{S,looser}$, respectively.

In Table 6.1, the value of n_S is also affected slightly by the value of e since denser specimens always have slightly smaller values of n_S than looser specimens. In terms of the average values of n_S for denser and looser specimens, the comparison is as follows. The average value of $n_{S,denser}$ is 0.194 and the average value of $n_{S,looser}$ is 0.232, a difference of about 16 %.. This comparison is only for the NC portion of the relationship because the overconsolidated portion was caused by the compaction effect and is assumed not to relate to the in-situ condition as noted above. The relative difference is reasonable because looser specimens are easier to densify than denser specimens. With the same increment of σ_0' , looser specimens have slightly larger changes in e and V_S than denser specimens.

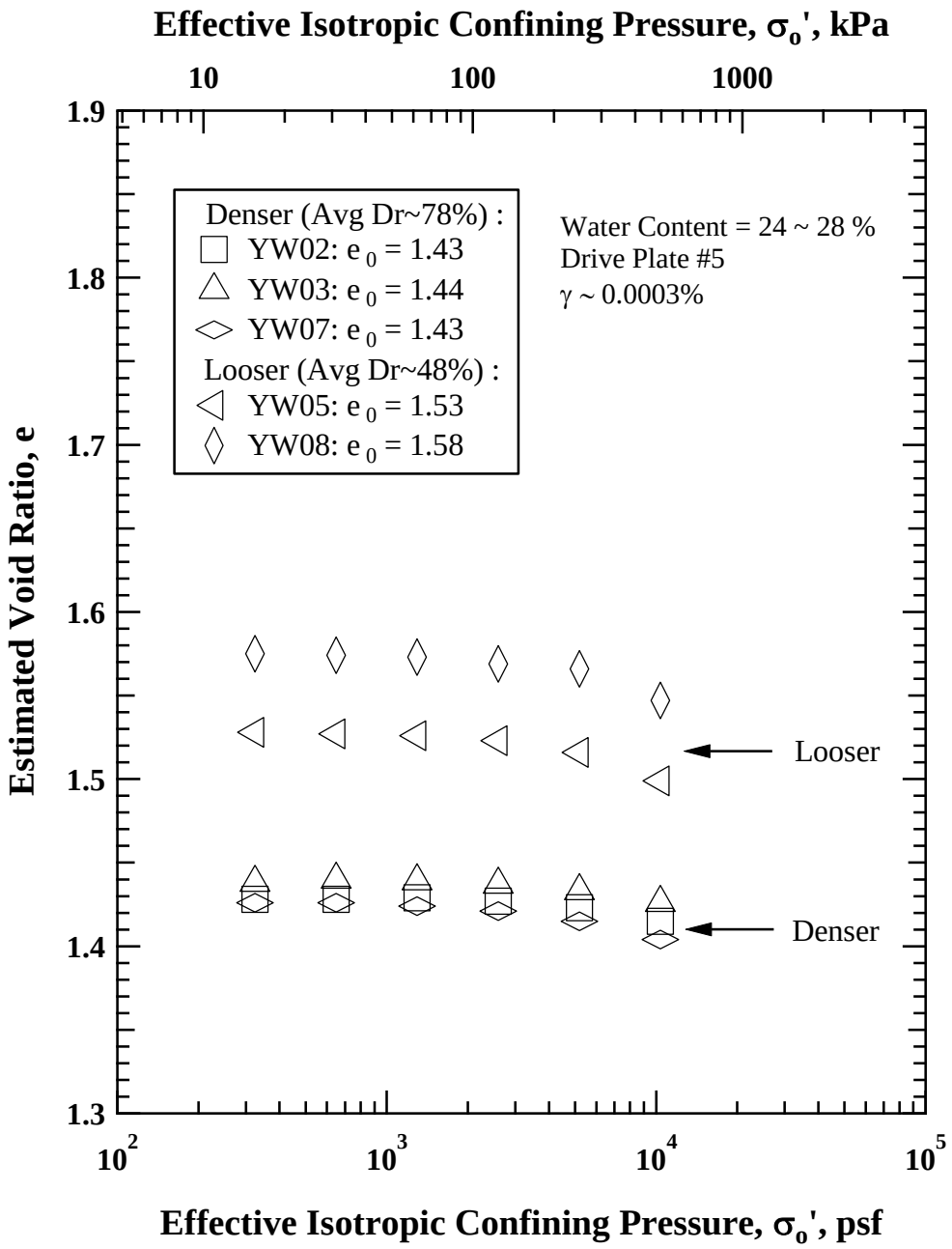

Figure 6.2 Variations in Void Ratio with Effective Isotropic Confining Pressure Determined during Resonant Column Testing of all Five Calcareous Sand Specimens.

Void-ratio-adjusted shear wave velocities, $V_S/\sqrt{F(e)}$ ($F(e)$ is calculated using Equation 2.8), for all specimens are plotted versus σ_0' on a log-log scale in Figure 6.3. Only the NC portion of the $\log V_S/\sqrt{F(e)} - \log \sigma_0'$ relationships are shown in Figures 6.3. The best-fit to the NC portion was done using Equation 6.1 and the least squares regression method. The resulting values of the parameters (A_{Se} and n_{Se}) are presented in Table 6.2. The r^2 values for the best-fits to determine A_{Se} and n_{Se} range from 0.9901 to 0.9998 and average 0.9973.

Table 6.2: Parameters Fit to the NC Portion of the Log $V_S/\sqrt{F(e)}$ − Log σ_0' Relationships from Resonant Column Tests of all Five Calcareous Sand Specimens.

Test ID.	Estimated Relative Density, D_r[1], (%)	Initial Void Ratio, e	$V_S/\sqrt{F(e)}$ [2]	
			A_{Se} (fps)	n_{Se}
YW02	78	1.43	1312	0.185
YW03	76	1.44	1339	0.183
YW05	54	1.53	1252	0.220
YW07	79	1.43	1291	0.199
YW08	42	1.58	1270	0.226

Notes:
1. $D_r = (e_{max} - e)/(e_{max} - e_{min}) \times 100\%$, e_{max} and e_{min} are provided by Baxter, 2013,
2. $V_S/\sqrt{F(e)} = A_{se}(\sigma_0'/P_a)^{n_{Se}}$, $P_a = one\ atmosphere.$

In terms of the average values of $V_S/\sqrt{F(e)}$ at σ_0' of one atmosphere for denser and looser specimens, the comparison is as follows. The average value of $A_{Se,denser}$ is 1314 ft/sec and the average value of $A_{Se,looser}$ is 1261 ft/sec, a difference of less than 4 %.. After the void ratio adjustment, the value of $A_{Se,denser}$ becomes closer to the value

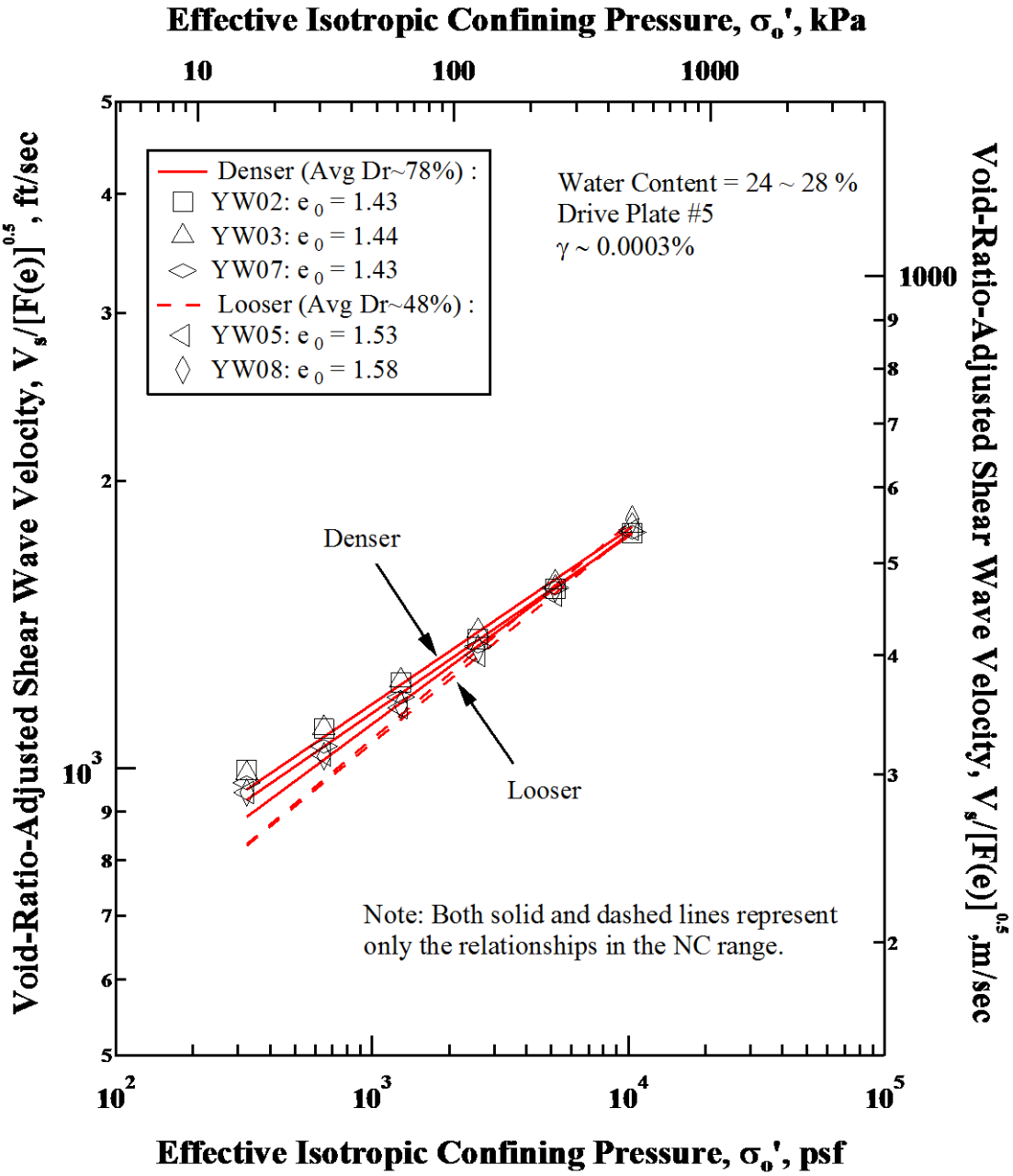

Figure 6.3 Variations in Void-Ratio-Adjusted Shear Wave Velocity ($V_S/\sqrt{F(e)}$) with Effective Isotropic Confining Pressure from Resonant Column Tests of the Five Calcareous Sand Specimens; Relationships Fit to the Normally Consolidated State.

of $A_{Se,looser}$, which makes the relationships plot close together as seen in Figures 6.3. In terms of the average values of n_{Se} for denser and looser specimens, the comparison is as follows. The average value of $n_{Se,denser}$ is 0.189 and the average $n_{Se,looser}$ is 0.223, a difference of about 15 %. The difference of n_{Se} values between denser and looser specimens does not change significantly from the comparison of n_S values discussed earlier. This comparison shows that $\sqrt{F(e)}$ is an important factor in evaluating A_S, but another factor is needed in normalizing n_S.

6.2.2 Small-Strain Shear Modulus of Calcareous Sand

The small-strain shear modulus can be calculated from the shear wave velocity and total unit weight of the specimen at the time of the measurement using the relationship between shear wave velocity and shear modulus in the wave propagation theory discussed in Chapter 2. The variations in small-strain shear modulus with effective isotropic confining pressure from RC testing of the five sand specimens are shown in Figure 6.4. Since the specimens were in the drained state during testing, the confining pressure, σ_0, is estimated to equal the effective isotropic confining pressure, σ_0'; hence any negative capillary stresses are assumed to be small.

It can be seen in Figure 6.4 that the small-strain shear moduli of all specimens (G_{max}) increase with effective isotropic confining pressures (σ_0'), just as shown in numerous previous studies. Similar to the $\log V_S - \log \sigma_0'$ relationships shown in Figure 6.1, the first point readily observed in Figure 6.4 is that the denser specimens are stiffer

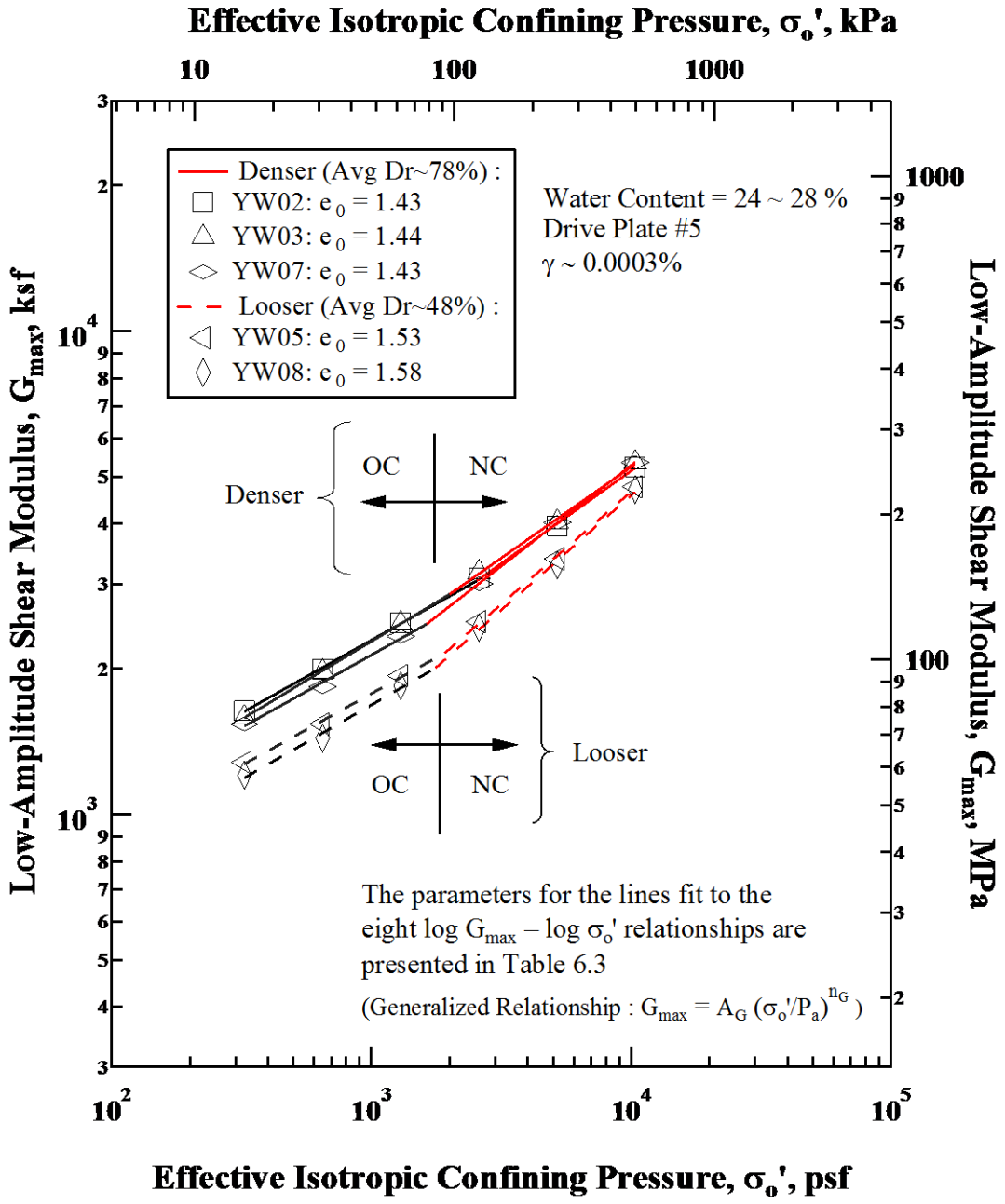

Figure 6.4 Variations in Small-Strain Shear Modulus with Effective Isotropic Confining Pressure from Resonant Column Tests of Five Calcareous Sand Specimens.

(have larger G_{max} values at all σ_0's) than the looser specimens. The second point is that all the $\log G_{max} - \log \sigma_0'$ relationships are well represented by two lines (a bi-linear relationship), with the first line having a "flatter slope" in the bi-linear relationship. This behavior is essentially the same as exhibited by the $\log V_S - \log \sigma_0'$ relationships, except that γ_t is needed in calculating G_{max}. The $\log G_{max} - \log \sigma_0'$ relationships are discussed in more detail below.

In Figure 6.4, the bi-linear relationship for all denser and looser specimens is readily seen. The bi-linear $\log G_{max} - \log \sigma_0'$ relationship indicates that the specimens were exhibiting a behavior similar to specimens that are behaving like overconsolidated (OC) specimens at low pressures and then become normally consolidated at higher pressures. The equation that can be used to represent each linear segment in the $\log G_{max} - \log \sigma_0'$ relationship is:

$$G_{max} = A_G(\sigma_0'/P_a)^{n_G} \tag{6.2}$$

in which A_G equals the value of G_{max} at σ_0' equal to one atmosphere (hence, G_{max1}) and P_a is equal to one atmosphere with the same units as σ_0'. Each linear segment of the $\log G_{max} - \log \sigma_0'$ relationships shown in Figures 6.4 has been best-fit with Equation 6.2 using the least squares regression method. The resulting best-fit values of the parameters (A_G and n_G) are presented in Table 6.3. The r^2 values for the best-fits to determine A_G and n_G range from 0.9900 to 0.9999 and average 0.9970.

As with void ratio (e) having an effect on small-strain V_S through the stiffening effect of denser soil skeletons, void ratio also has an influence on the small-strain shear

Table 6.3: Parameters Fit to Each Linear Section of the Five Log G_{max} − Log σ_0' Relationships from Resonant Column Tests of Sand Specimens.

Test ID.	Estimated Relative Density, D_r[1], (%)	Initial Void Ratio, e	Consolidation State	G_{max}[2]	
				A_G (ksf)	n_G
YW02	78	1.43	OC[3]	2879	0.302
			NC[4]	2836	0.383
YW03	76	1.44	OC	2906	0.323
			NC	2915	0.377
YW05	54	1.53	OC	2224	0.298
			NC	2261	0.465
YW07	79	1.43	OC	2679	0.301
			NC	2761	0.417
YW08	42	1.58	OC	2122	0.308
			NC	2188	0.475

Notes:
1. $D_r = (e_{max} - e)/(e_{max} - e_{min}) \times 100\%$, e_{max} and e_{min} are provided by Baxter, 2013,
2. $G_{max} = A_G(\sigma_0'/P_a)^{n_G}$, $P_a = one\ atmosphere$,
3. OC = overconsolidated state,
4. NC = normally consolidated state.

modulus. The effect is even more pronounced because the effect is further increased by the fact that total unit weight enters the calculation of shear modulus ($G = (\gamma_t/g)V_S^2$). Denser specimens of the same material with lower values of e and higher values of γ_t always have larger G_{max} values than the looser specimens with higher values of e and lower values of γ_t at the same σ_0' level. In terms of the average values of G_{max} at σ_0' of one atmosphere for the denser and looser specimens, the comparison is as follows. The average value of $A_{G,denser}$ is 2837 ksf and average value of $A_{G,looser}$ is 2225 ksf, a difference of about 22 %. This comparison is only for the NC portion of the relationship because the overconsolidated portion was caused by the compaction effect and is assumed not to relate to the in-situ condition.

In Table 6.3, n_G is also affected by e and γ_t since denser specimens have smaller values of n_G than looser specimens. In terms of the average values of n_G for the denser and looser specimens, the comparison is as follows. The average value of $n_{G,denser}$ is 0.392 and the average value of $n_{G,looser}$ is 0.470, a difference of about 17 %. This comparison is only for the NC portion of the relationship because the overconsolidated portion was caused by the compaction effect and is assumed not to relate to the in-situ condition. These relative values are reasonable because looser specimens are easier to be densified than denser specimens. With the same increment in σ_0' , looser specimens should have larger changes in e, γ_t and G_{max} than denser specimens.

Void-ratio-adjusted shear modulus, $G_{max}/F(e)$ ($F(e)$ is calculated using Equation 2.8), for all specimens were plotted versus σ_0' on a log-log scale in Figure 6.5. The NC portion of the $\log G_{max}/F(e) - \log \sigma_0'$ relationships shown in Figure 6.5 has been best-fit with Equation 6.2 using the least squares regression method. The resulting best-fit values of the parameters (A_{Ge} and n_{Ge}) are presented in Table 6.4. The r^2 values for the best-fits to determine A_{Ge} and n_{Ge} range from 0.9902 to 0.9999 and average 0.9972.

In terms of the average values of $G_{max}/F(e)$ at σ_0' of one atmosphere for the pairs of denser and looser specimens, the comparison is as follows. The average value of $A_{Ge,denser}$ is 4919 ksf and the average value of $A_{Ge,looser}$ is 4415 ksf, a difference of about 10 %. After the void ratio adjustment, $A_{Ge,denser}$ become closer to $A_{Ge,looser}$,

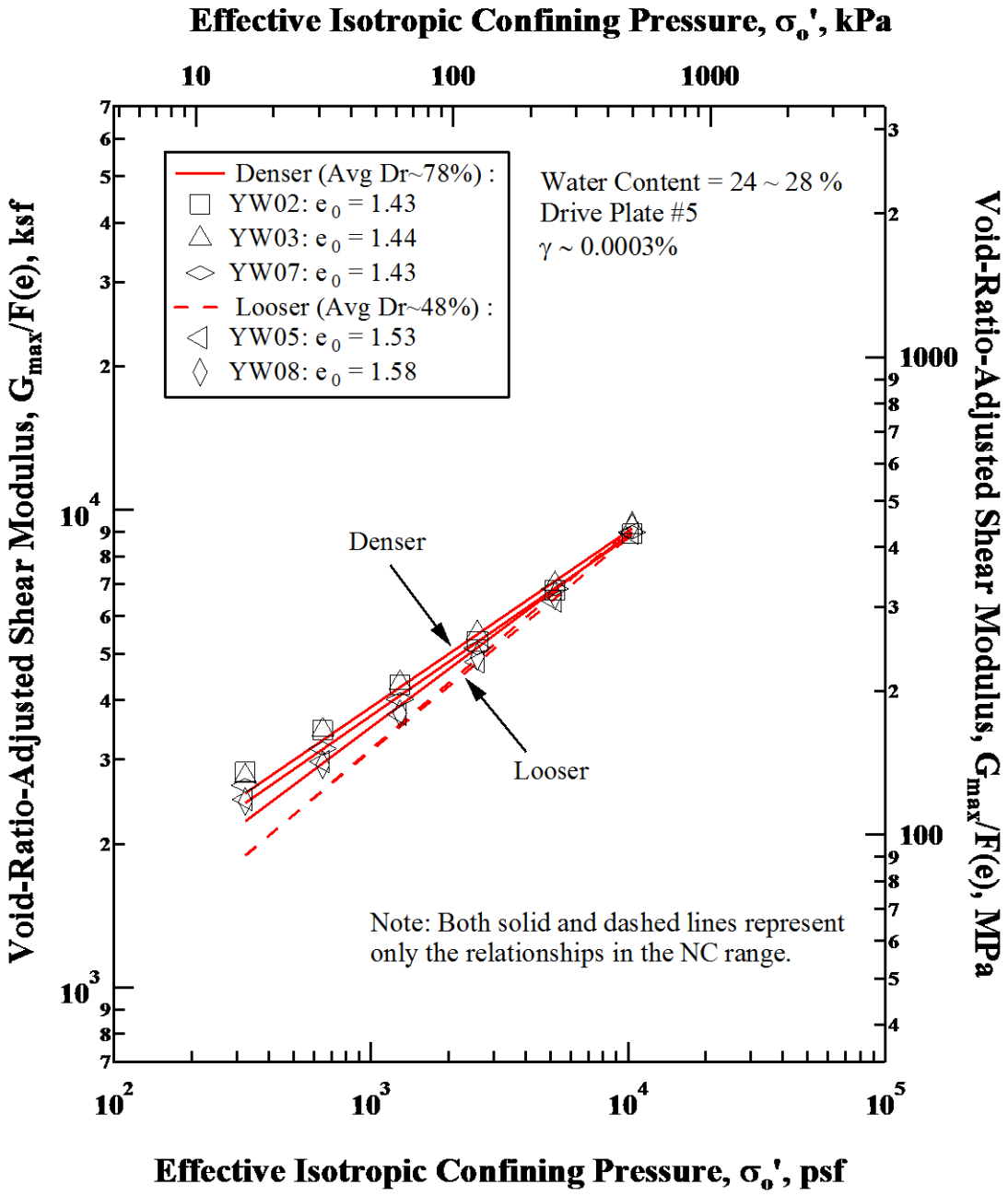

Figure 6.5 Variations in Void-Ratio-Adjusted Shear Modulus ($G_{max}/F(e)$) with Effective Isotropic Confining Pressure from Resonant Column Tests of all Five Calcareous Sand Specimens Tested in the Normally Consolidated State.

which makes the relationships plot closer together. In terms of the average values of n_{Ge} for the denser and looser specimens, the comparison is as follows. The average value of $n_{Ge,denser}$ is 0.381 and the average value of $n_{Ge,looser}$ is 0.452, a difference of about 17 %. The difference of n_{Ge} values between denser and looser specimens does not change significantly compared with the difference in the n_G comparison. This comparison shows that $F(e)$ is an important factor in evaluating A_G, but another factor seems to be needed in normalizing n_G.

To investigate the influence of total unit weight on small-strain shear modulus, a combined total unit weight and void ratio adjusted shear modulus, $G_{max}/[F(e) * \gamma_t/\gamma_w]$ ($F(e)$ was calculated using Equation 2.8, and γ_w equals the unit weight of water) is calculated. It should be noted that the unit weight factor is simply a normalized total unit weight defined as γ_t/γ_w. This "adjusted" G_{max} for each specimen is plotted versus σ_0'

Table 6.4: Parameters Fit to NC Portion of the $\text{Log}\, G_{max}/F(e) - \text{Log}\ \sigma_0'$ Relationships from Resonant Column Tests of all Five Calcareous Sand Specimens.

Test ID.	Estimated Relative Density, D_r[1], (%)	Initial Void Ratio, e	$G_{max}/F(e)$ [2]	
			A_{Ge} (ksf)	n_{Ge}
YW02	78	1.43	4910	0.373
YW03	76	1.44	5098	0.368
YW05	54	1.53	4374	0.446
YW07	79	1.43	4750	0.403
YW08	42	1.58	4456	0.457

Notes:
1. $D_r = (e_{max} - e)/(e_{max} - e_{min}) \times 100\%$, e_{max} and e_{min} are provided by Baxter, 2013,
2. $G_{max}/F(e) = A_{Ge}(\sigma_0'/P_a)^{n_G}$, $P_a = one\ atmosphere.$

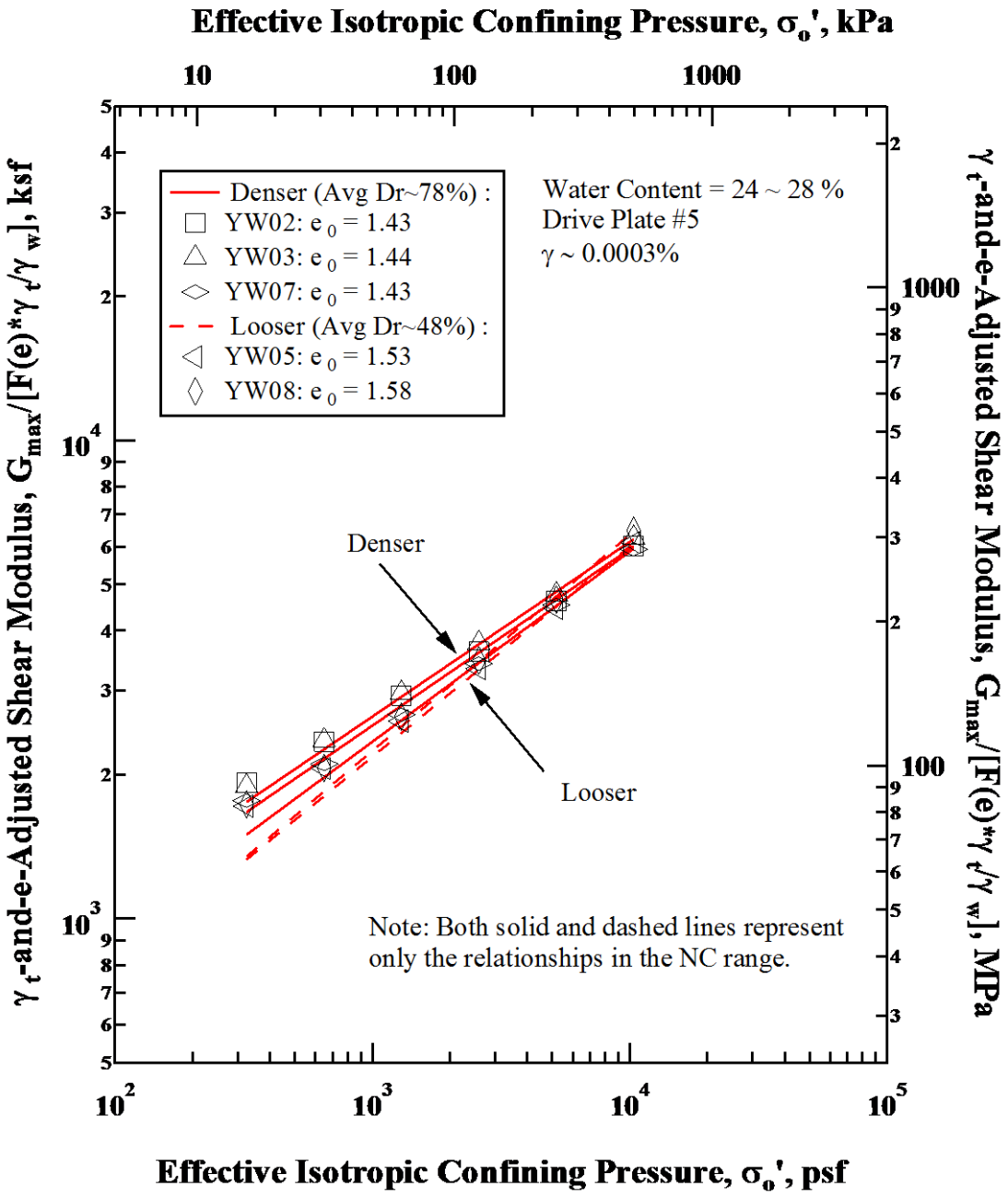

Figure 6.6 Variations in Total-Unit-Weight-and-Void-Ratio-Adjusted Shear Modulus ($G_{max}/[F(e) * \gamma_t/\gamma_w]$) with Effective Isotropic Confining Pressure from Resonant Column Tests of all Five Calcareous Sand Specimens Tested in the Normally Consolidated State.

Table 6.5: Parameters Fit to the NC Portion of the $\text{Log}\, G_{max}/[F(e) * \gamma_t/\gamma_w] - \text{Log}\ \sigma_0'$ Relationships from Resonant Column Tests of all Five Calcareous Sand Specimens.

Test ID.	Estimated Relative Density, D_r[1], (%)	Initial Total Unit Weight γ_t, (g/cm^3)	$G_{max}/[F(e) * \gamma_t/\gamma_w]$ [2]	
			$A_{Ge\gamma}$ (ksf)	$n_{Ge\gamma}$
YW02	78	1.47	3337	0.369
YW03	76	1.47	3478	0.365
YW05	54	1.44	3030	0.439
YW07	79	1.47	3156	0.398
YW08	42	1.42	3145	0.451

Notes:
1. $D_r = (e_{max} - e)/(e_{max} - e_{min}) \times 100\%$, e_{max} and e_{min} are provided by Baxter, 2013,
2. $G_{max}/[F(e) * \gamma_t/\gamma_w] = A_{Ge\gamma}(\sigma_0'/P_a)^{n_{Ge\gamma}}$, $P_a = one\ atmosphere,\ \gamma_w = water\ unit\ weight.$

on a log-log scale in Figure 6.6. The NC portions of the $\log G_{max}/[F(e) * \gamma_t/\gamma_w] - \log \sigma_0'$ relationships in Figures 6.6 have been best-fit with Equation 6.2 using the least squares regression method. The resulting best-fit values of the parameters ($A_{Ge\gamma}$ and $n_{Ge\gamma}$) are presented in Table 6.5. The r^2 values for the best-fits to determine $A_{Ge\gamma}$ and $n_{Ge\gamma}$ range from 0.9902 to 0.9999 and average 0.9974.

In terms of the average values of $G_{max}/[F(e) * \gamma_t/\gamma_w]$ at σ_0' of one atmosphere for the denser and looser specimens, the comparison is as follows. The average value of $A_{Ge\gamma,denser}$ is 3324 ksf and the average value of $A_{Ge\gamma,looser}$ is 3088 ksf, a difference of about 7 %. After the γ_t-and-e-adjustment, $A_{Ge\gamma,denser}$ becomes closer to $A_{Ge\gamma,looser}$, which make the relationships plot close together. In terms of the average values of $n_{Ge\gamma}$ for the similar specimens (denser vs. looser), the comparison is as follows. The average value of $n_{Ge\gamma,denser}$ is 0.377 and the average value of

$n_{Ge\gamma,looser}$ is 0.445, a difference of about 15 %. The difference in $n_{Ge\gamma}$ values between denser and looser specimens does not change significantly compared with the n_{Ge} values. This comparison seems to show that, like $F(e)$, the γ_t is also an important factor in evaluating A_G, but another factor is needed in normalizing n_G.

Comparison of the NC portion of the $\log G_{max} - \log \sigma_0'$ relationships between the RC tests measured results and the predicted results using Menq's (2003) equation are presented in Table 6.6. The values of A_G from Menq's prediction is much lower than the values of A_G from RC tests for the same specimen. For the denser specimens with $D_r \approx$ 78 %, Menq's equation gives much lower values of A_G than the RC test results, with the average value of $A_G = 2837\ ksf$ from RC tests and the average value of $A_G = 857$

Table 6.6: Comparison of $\text{Log}\, G_{max} - \text{Log}\, \sigma_0'$ Relationships in the NC portion between the RC Test Results and Menq's (2003) Prediction.

Test ID.	Estimated Relative Density, D_r[1], (%)	Initial Void Ratio, e	RC Test		Menq's Prediction[2]	
			A_G (ksf)	n_G	A_G (ksf)	n_G
YW02	78	1.43	2836	0.383	859	0.505
YW03	76	1.44	2915	0.377	853	
YW05	54	1.53	2261	0.465	801	
YW07	79	1.43	2761	0.417	859	
YW08	42	1.58	2188	0.475	774	

Notes:
1. $D_r = (e_{max} - e)/(e_{max} - e_{min}) \times 100\%$,
   e_{max} and e_{min} are provided by Baxter, 2013,
2. $G_{max} = C_{G3} \times {C_u}^{b1} \times e^x \times \left(\frac{\sigma_0'}{P_a}\right)^{n_G}$,
   where $C_{G3} = 67.1\ MPa\ (1400\ ksf)$,
   $b1 = -0.2$,
   $x = -1 - (D_{50}/20)^{0.75}$,
   $n_G = 0.48 \times {C_u}^{0.09}$
   C_u = uniformity coefficient, and,
   e = void ratio

ksf from Menq's equation. For the looser specimens with $D_r \approx 48$ %, Menq's equation also gives much lower values of A_G than the RC test results, with the average value of $A_G = 2225\ ksf$ from RC tests and the average value of $A_G = 788\ ksf$ from Menq's equation. This difference makes Menq's equation for small-strain shear modulus inapplicable to calcareous sand. The possible reasons may be the unusual sharp particles of calcareous sand, which can lead to unusually large void ratio. Also Menq's equation does not consider changes in n_G caused by changes in e, which does show affects on n_G even though the influence is not large. However, difference in n_G are small compared to the effect of A_G.

To compare the RC test results from this study with test data from previous studies, the average C_G and n_G values in Equation 2.6 are calculated from the RC test results. This comparison is shown in the Table 6.7. The calcareous sand from Puerto Rico has an unusually high average value of C_G about 20000 and a low n_G range from 0.39 to 0.47. This may result from the unusually high e of calcareous sand.

6.2.3 Small-strain Material Damping Ratio of Calcareous Sand

Small-strain material damping ratios (D_{min}) of calcareous sand were also measured during low-amplitude resonant column (RC) testing. The variations of D_{min} with effective isotropic confining stress (σ_0') from the five specimens are presented in Figure 6.7 in terms of $\log D_{min}$ versus $\log \sigma_0'$. Since the specimens were in the drained state during testing, the confining pressure, σ_0, is estimated to equal the effective

Table 6.7: Comparison of C_G and n_G Values[1, 2] of Calcareous Sand from Puerto Rico with Values from Sandy Soil from Previous Studies.

Source	$F(e)$	C_G	n_G	Soil description
Hardin and Richart (1963)	$\frac{(2.17-e)^2}{1+e}$	7000	0.5	Round grain Ottawa sand
	$\frac{(2.97-e)^2}{1+e}$	3300	0.5	Angular grained crushed quartz
Iwasski et al. (1978)	$\frac{(2.17-e)^2}{1+e}$	9000	0.38	Eleven kinds of clean sand
Kokusho (1980)	$\frac{(2.17-e)^2}{1+e}$	8400	0.5	Toyoura sand
Yu and Richart (1984)	$\frac{(2.17-e)^2}{1+e}$	7000	0.5	Three kinds of clean sand
This Thesis	$\frac{(2.17-e)^2}{1+e}$	7300	0.48	Dense liquefiable sand
		5700	0.52	Loose liquefiable sand
	$\frac{(2.97-e)^2}{1+e}$	23000	0.39	Dense calcareous sand
		16000	0.47	Loose calcareous sand

Notes:
1. $G_{max} = C_G \cdot F(e) \cdot (\sigma_0')^{n_G}$,
2. G_{max} and σ_0' are in kPa

isotropic confining pressure, σ_0'; hence any negative capillary stresses are assumed to be small.

It can be seen in Figure 6.7 that the small-strain material damping ratios of all specimens (D_{min}) decrease with effective isotropic confining pressures (σ_0'), just as shown in numerous previous studies. The first point readily observed in Figure 6.7 is that the trend for the variation of D_{min} is more complex than those of V_S and G_{max}. The second point is that denser specimens generally have larger D_{min} values at all σ_0's than the looser specimens. Given the variability of the measurement caused by the ambient background noise, the influence caused by the consolidation state is relatively minor.

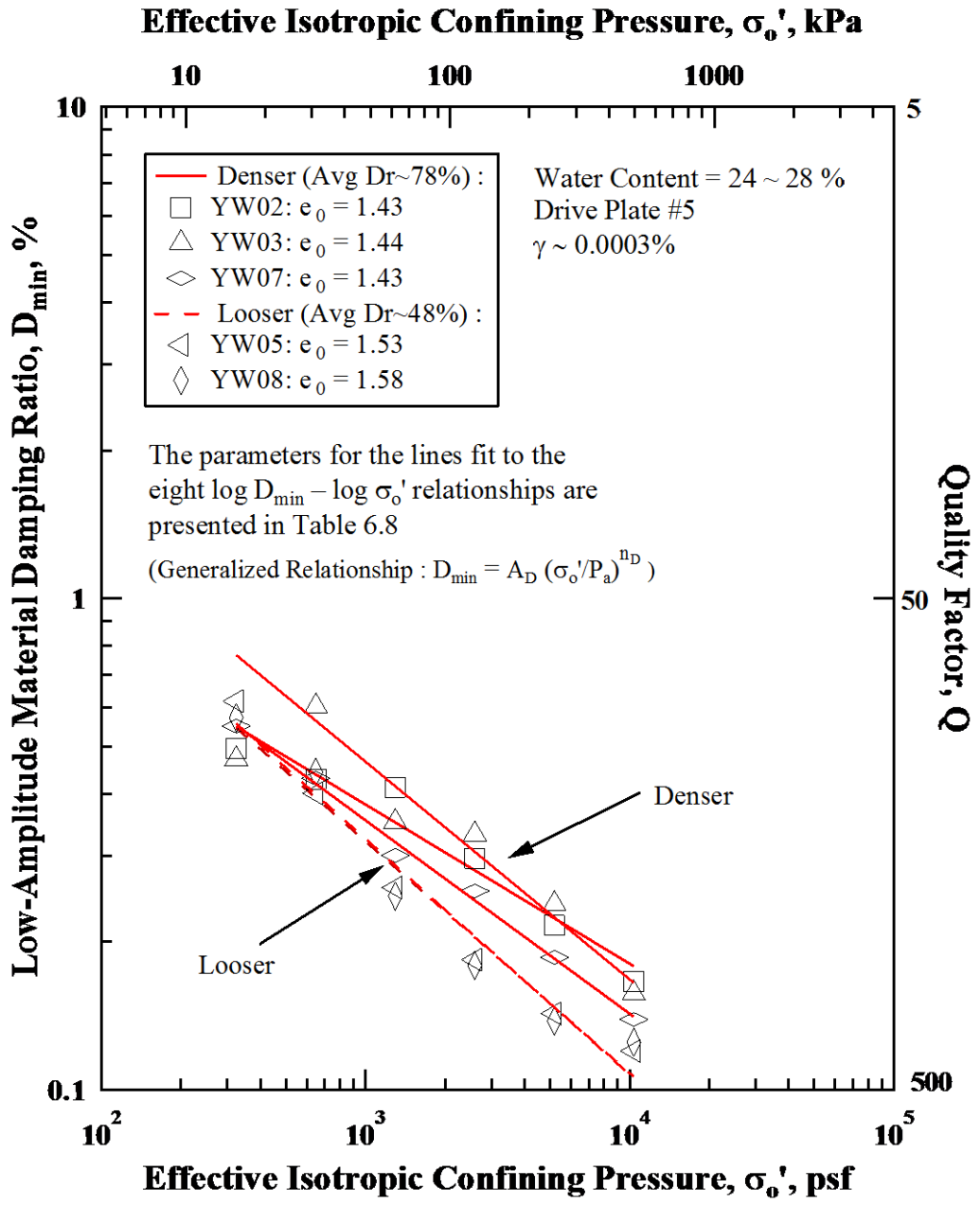

Figure 6.7 Variations in Low-Amplitude Material Damping Ratio with Effective Isotropic Confining Pressure from Resonant Column Tests of Five Calcareous Sand Specimens

Then each $\log D_{min} - \log \sigma_0'$ relationship is represented by a single line (a single linear relationship) for convenience.

In Figure 6.7, the linear relationship shown by each specimen contains more scatter (variability) than found in the V_S and G_{max} measurements. The equation that can be used to represent each linear segment in the $\log D_{min} - \log \sigma_0'$ relationship is:

$$D_{min} = A_D(\sigma_0'/P_a)^{n_D} \tag{6.3}$$

in which A_D equals the value of D_{min} at σ_0' equal to one atmosphere (hence, D_{min1}) and P_a is equal to one atmosphere with the same units as σ_0'. Each linear segment of the $\log D_{min} - \log \sigma_0'$ relationships shown in Figures 6.7 has been best-fit with Equation 6.3 using the least squares regression method. The resulting best-fit values of the parameters (A_D and n_D) are presented in Table 6.8. The r^2 values for the best-fits to determine A_D

Table 6.8: Parameters Fit to Each Linear Segment of the Log D_{min} − Log σ_0' Relationships from Resonant Column Tests of Five Calcareous Sand Specimens.

Test ID.	Estimated Relative Density, D_r[1], (%)	Initial Void Ratio, e	D_{min} [2]	
			A_D (%)	n_D
YW02	78	1.43	0.299	-0.324
YW03	76	1.44	0.334	-0.443
YW05	54	1.53	0.226	-0.480
YW07	79	1.43	0.263	-0.394
YW08	42	1.58	0.225	-0.472

Notes:
1. $D_r = (e_{max} - e)/(e_{max} - e_{min}) \times 100\%$, e_{max} and e_{min} are provided by Baxter, 2013,
2. $D_{min} = A_D(\sigma_0'/P_a)^{n_D}$, $P_a = one\ atmosphere.$

and n_D range from 0.9142 to 0.9945 and average 0.9647, among which r^2 value of Specimen YW02 ($e = 1.43$) is 0.9142. In test YW03, D_{min} at the lowest confining pressure of 2.25 psi was affected by background noise and was determined to be unusually low, thus, this value was discarded.

From previous studies, void ratio has an influence on the small-strain material damping ratio through the stiffening effect of denser soil skeletons, which means denser specimens of the same material with lower values of e generally have smaller D_{min} values than the looser specimens with higher values of e at the same σ_0' level. From Figure 6.7, void ratio seems to affect D_{min} but in an abnormal way; that is, D_{min} values of loose specimens are generally lower than those of dense specimens at given σ_0'. This is caused by the effect of assumed equipment-generated damping. Since the metal specimens have very low D_{min}, the measured D_{min} from metal specimens is assumed to be equipment-generated damping. The following equation is used to calculate equipment-generated damping:

$$D_{equipment-generated} = q/f_n \tag{6.4}$$

where q = calibration factor updated annually,

f_n = resonant frequency, Hz.

Dense specimens have higher f_n than the loose ones, which means the calculated $D_{equipment-generated}$ in dense specimens is smaller than that in loose specimen. The

difference is neglect when the measured D_{min} is high. But when the measured D_{min} is very low like this case, dense specimens may get higher D_{min} by subtracting a small $D_{equipment-generated}$ from the measured D_{min}. That makes the D_{min} data unusable for analyzing the influence of e.

6.3 NON-LINEAR DYNAMIC PROPERTIES OF CALCAREOUS SAND

6.3.1 Nonlinear Shear Moduli of Calcareous Sand

The high-amplitude resonant column (RC) tests were performed to obtain the dynamic properties of the calcareous sand specimens in the nonlinear shear strain range. These tests were performed at three effective isotropic confining pressure (σ_0') levels: 4.5, 18 and 72 psi. The nonlinear testing was performed after the low-amplitude loading test at each confining pressure using the RC device. The variations in shear modulus (G) with shear strain (γ) of the five calcareous sand specimens are shown in Figure 6.8.

It can be seen in Figure 6.8 that the shear moduli of all specimens decrease with increasing shear strain (γ), just as shown in numerous previous studies. The first point observed in Figure 6.8 is that the denser specimens are stiffer (have larger G_{max} values at all shearing strains) than the looser specimens at each confining pressure level. The second point is that the $G - \mathrm{Log}\,\gamma$ relationships are well represented by hyperbolic models. The Darendeli's (2001) equation that can be used to represent each hyperbolic curve in the $G - \mathrm{Log}\,\gamma$ relationship:

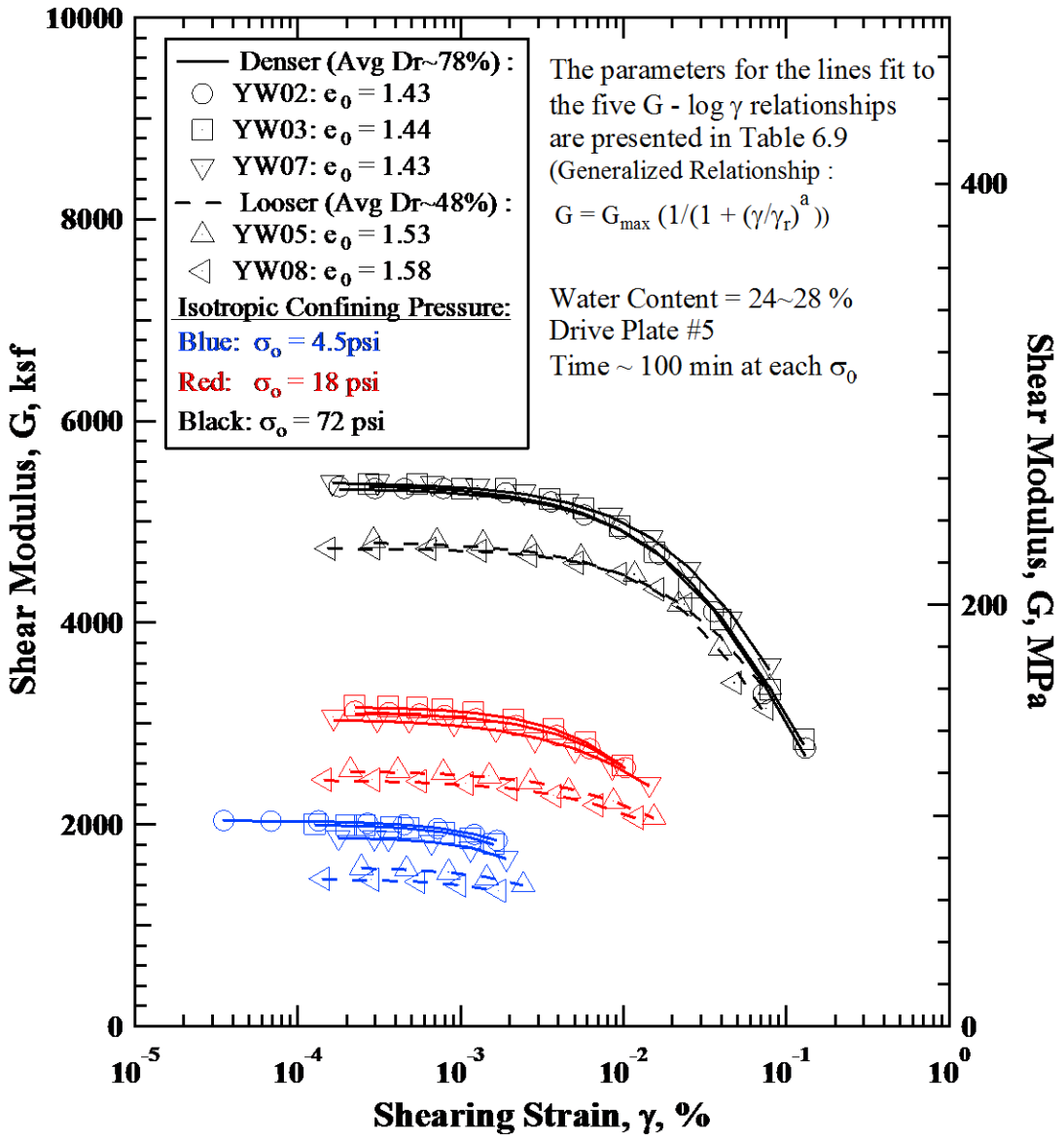

Figure 6.8 Variation in Shear Modulus with Shearing Strain at three loading Effective Isotropic Confining Pressures of 4.5, 18 and 72 psi from Resonant Column Tests of five Calcareous Sand Specimens.

$$\frac{G}{G_{max}} = \frac{1}{1 + \left(\frac{\gamma}{\gamma_r}\right)^a} \tag{6.4}$$

in which G_{max} equals the shear modulus in the small-strain range at each of the three loading effective isotropic confining stress of 4.5, 18 and 72 psi, γ_r is equal to the reference shear strain at which shear modulus equals to half of G_{max}, and a is a curvature coefficient. Each $G - \text{Log}\,\gamma$ relationship shown in Figures 6.8 has been best-

Table 6.9: Parameters Fit to the $G - \text{Log}\,\gamma$ Relationships from Resonant Column Tests of all Calcareous Sand Specimens.

Test ID.	Estimated Relative Density, D_r[1], (%)	Initial Void Ratio, e	Isotropic Confining Pressure σ_0', (psi)	Elastic threshold γ_t^{e2}, (%)	Modified Hyperbolic Relationship Equation[3]	
					γ_r (%)	a
YW02	78	1.43	4.5	0.00044	0.010	1.233
			18	0.00125	0.041	1.096
			72	0.00310	0.132	0.941
YW03	76	1.44	4.5	0.00050	0.007	1.467
			18	0.00125	0.036	1.143
			72	0.00290	0.140	0.895
YW05	54	1.53	4.5	0.00065	0.012	1.315
			18	0.00135	0.077	0.913
			72	0.00370	0.188	0.900
YW07	79	1.43	4.5	0.00060	0.007	1.578
			18	0.00112	0.058	0.911
			72	0.00270	0.160	0.913
YW08	42	1.58	4.5	0.00059	0.010	1.398
			18	0.00123	0.076	0.913
			72	0.00350	0.132	1.094

Notes:
1. $D_r = (e_{max} - e)/(e_{max} - e_{min}) \times 100\%$,
   e_{max} and e_{min} are provided by Baxter, 2013,
2. $\gamma_t^e =$ shear strain at which $G/G_{max} =$ 0.98,
3. $G/G_{max} = 1/(1 + (\gamma/\gamma_r)^a)$,
   where G_{max} = small-strain shear modulus
   γ_r = reference shear strain, and,
   a = curvature coefficient.

fit with Equation 6.4 using the least-squares regression method. The resulting best-fit values of the parameters (γ_r and a) are presented in Table 6.9. The r^2 values for the best-fits to determine γ_r and a range from 0.9847 to 0.9978 and average 0.9920.

In $G - \log \gamma$ plots, denser specimens always have a higher shear modulus at given shear strains than the looser specimens at each confining pressure level, and this difference is mainly caused by the higher G_{max} of the denser specimens, which has been discussed in previous chapters. In order to eliminate the effect of G_{max} on the nonlinear shear modulus behavior, the variations in normalized shear modulus (G/G_{max}) with shear strain (γ) from RC testing of the five calcareous sand specimens are presented in Figure 6.9.

In Figure 6.9, the first point observed is that the effective isotropic confining pressure σ_0' has an influence on the nonlinear shear modulus behavior. In terms of the average values of elastic threshold γ_t^e, reference shear strain γ_r and curvature coefficient a for all five sand specimens at each isotropic effective confining pressure level, the comparison is as follows. At σ_0' of 4.5 psi, the average value of γ_t^e is 0.00056, the average value of γ_r is 0.009 and the average value of a is 1.398. At σ_0' of 18 psi, the average value of γ_t^e is 0.00124, the average value of γ_r is 0.058 and the average value of a is 0.995. At σ_0' of 72 psi, the average value of γ_t^e is 0.00318, the average value of γ_r is 0.150 and the average value of a is 0.949. The comparison shows that γ_t^e, γ_r and a are all affected by σ_0' since specimens at higher confining

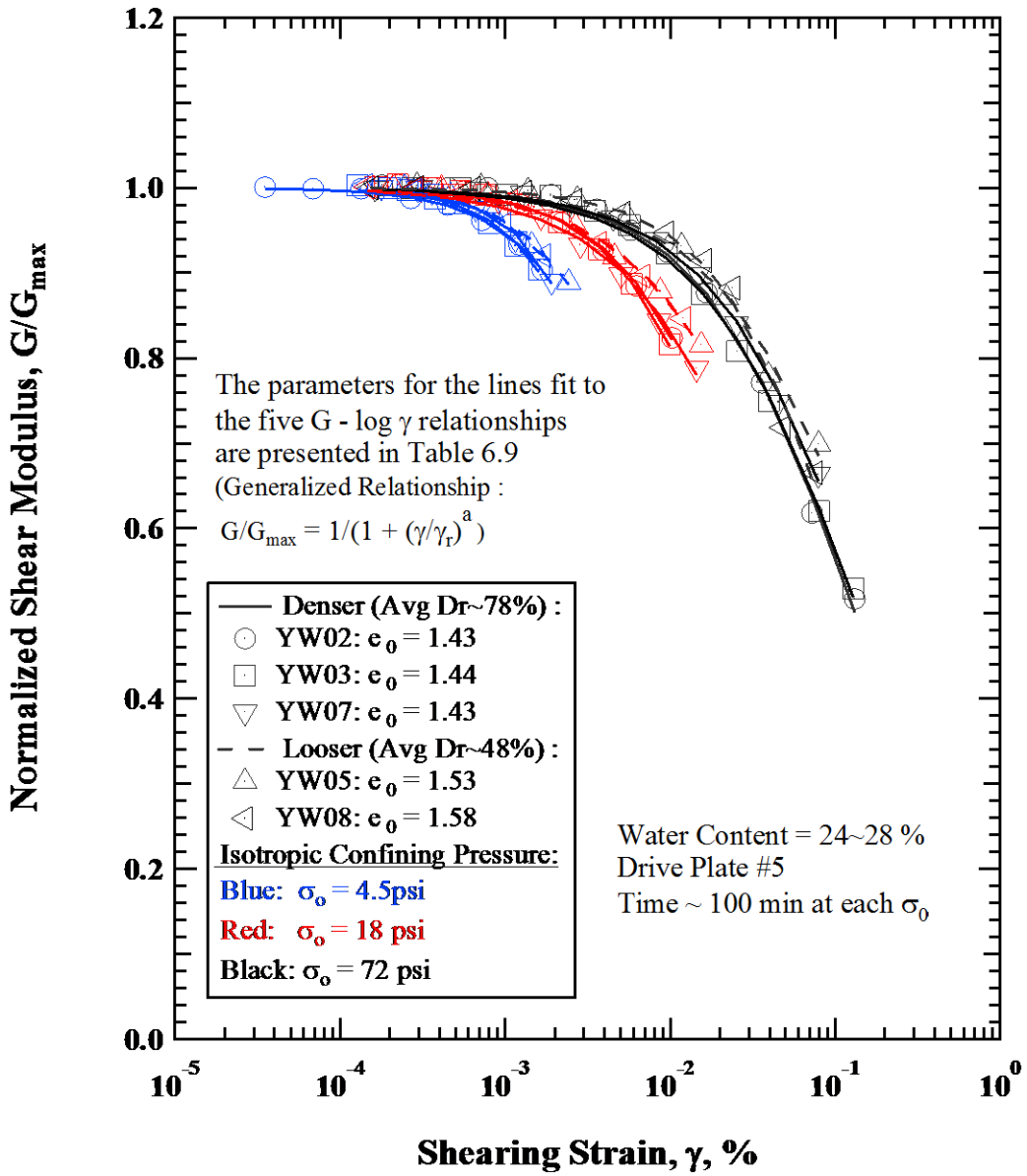

Figure 6.9 Variation in Normalized Shear Modulus with Shearing Strain at three loading Effective Isotropic Confining Pressures of 4.5, 18 and 72 psi from Resonant Column Tests of five Calcareous Sand Specimens.

pressure levels always have larger values of γ_t^e and γ_r and smaller values of a than specimens at lower confining pressure.

The second point observed in Figure 6.9 is that the void ratio e also has an influence on the nonlinear shear modulus behavior. In terms of the average values of elastic threshold γ_t^e for the pairs of specimens (denser vs. looser) at each effective isotropic confining pressure, the comparison is as follows. At σ_0' of 4.5 psi, the average value of $\gamma_{t,denser}^e$ is 0.00051 and the average value of $\gamma_{t,looser}^e$ is 0.00062. At σ_0' of 18 psi, the average value of $\gamma_{t,denser}^e$ is 0.00121 and the average value of $\gamma_{t,looser}^e$ is 0.00129. At σ_0' of 72 psi, the average value of $\gamma_{t,denser}^e$ is 0.0029 and the average value of $\gamma_{t,looser}^e$ is 0.0036. The looser specimens always have higher values of elastic threshold than the denser specimens at each effective isotropic confining.

In terms of the average values of reference shear strain γ_r for the pairs of specimens (denser vs. looser) at each effective isotropic confining pressure, the comparison is as follows. At σ_0' of 4.5 psi, the average value of $\gamma_{r,denser}$ is 0.008 and the average value of $\gamma_{r,looser}$ is 0.011. At σ_0' of 18 psi, the average value of $\gamma_{r,denser}$ is 0.045 and the average value of $\gamma_{r,looser}$ is 0.077. At σ_0' of 72 psi, the average value of $\gamma_{r,denser}$ is 0.144 and the average value of $\gamma_{r,looser}$ is 0.160. The looser specimens always have higher values of reference shear strain than the denser specimens at each effective isotropic confining.

In terms of the average values of curvature coefficient a for the pairs of specimens (denser vs. looser) at each effective isotropic confining pressure, the

comparison is as follows. At σ_0' of 4.5 psi, the average value of a_{denser} is 1.426 and the average value of a_{looser} is 1.357. At σ_0' of 18 psi, the average value of a_{denser} is

Table 6.10: Comparison of γ_r and a of between RC Test Results and Menq's Prediction.

Test ID.	Estimated Relative Density, D_r[1], (%)	Initial Void ratio, e	Isotropic Confining Pressure σ_0', (psi)	Modified Hyperbolic Relationship Equation[2]			
				from RC Tests		from Menq, 2003	
				γ_r (%)	a	$\gamma_{r,Menq}$[3] (%)	a_{Menq}[4]
YW02	78	1.43	4.5	0.010	1.233	0.050	0.809
			18	0.041	1.096	0.094	0.869
			72	0.132	0.941	0.178	0.929
YW03	76	1.44	4.5	0.007	1.467	0.050	0.809
			18	0.036	1.143	0.094	0.869
			72	0.140	0.895	0.178	0.929
YW05	54	1.53	4.5	0.012	1.315	0.050	0.809
			18	0.077	0.913	0.094	0.869
			72	0.188	0.900	0.178	0.929
YW07	79	1.43	4.5	0.007	1.578	0.050	0.809
			18	0.058	0.911	0.094	0.869
			72	0.160	0.913	0.178	0.929
YW08	42	1.58	4.5	0.010	1.398	0.050	0.809
			18	0.076	0.913	0.094	0.869
			72	0.132	1.094	0.178	0.929

Notes:
1. $D_r = (e_{max} - e)/(e_{max} - e_{min}) \times 100\%$,
   e_{max} and e_{min} are provided by Baxter, 2013,
2. $G/G_{max} = 1/(1 + (\gamma/\gamma_r)^a)$,
   where G_{max} = small-strain shear modulus
   γ_r = reference shear strain, and,
   a = curvature coefficient.
3. $\gamma_r = 0.12 \times {C_u}^{-0.6} \times \left(\frac{\sigma_0'}{P_a}\right)^{0.5 \times {C_u}^{-0.15}}$,
4. $a = 0.86 + 0.1 \times \log\left(\frac{\sigma_0'}{P_a}\right)$
   where C_u = uniformity coefficient, and,
   σ_0' = effective isotropic confining pressure.

1.050 and the average value of a_{looser} is 0.913. At σ_0' of 72 psi, the average value of a_{denser} is 0.916 and the average value of a_{looser} is 0.997. The looser specimens have lower values of curvature coefficient a than the denser specimens at each effective isotropic confining, except for the case at σ_0' of 72 psi.

Comparison of $G/G_{max} - \log\gamma$ relationships between the RC tests and Menq's prediction are presented in Table 6.10. According to the reference strain γ_r and curvature coefficient a for sandy soil suggested by Menq (2003) in the modified hyperbolic model suggested by Darendeli (2001), γ_r is a function of C_u and σ_0' while a is a function of σ_0'. However, differences are found between the parameters from RC tests and Menq's prediction. The values of γ_r from Menq's prediction are almost constantly higher than the values of γ_r from RC tests, with the average absolute difference of γ_r equal to about 0.035 %. The values of a from Menq (2003) increases with increasing σ_0', while the values of a from RC tests decreases with increasing σ_0' in most cases.

6.3.2 Nonlinear Material Damping Ratio of Calcareous Sand

Nonlinear material damping ratios (D) of calcareous sand from Puerto Rico are also measured during the high-amplitude resonant column (RC) tests. These tests were performed at three effective isotropic confining pressure (σ_0') levels: 4.5, 18 and 72 psi. The nonlinear testing was performed after the low-amplitude loading test at each

confining pressure using the RC device. The variations in material damping ratio (D) with shear strain (γ) from RC testing of the five calcareous sand specimens are shown in Figure 6.10.

It can be seen in Figure 6.10 that the material damping ratios of all specimens (D) increase with shear strain (γ), just as shown in numerous previous studies. The first point observed in Figure 6.10 is that specimens at lower confining pressures always have higher value of material damping ratios than specimens at higher confining pressures at each γ. The second point is that, unlike $G - \log\gamma$ plots shown in Figure 6.8, the denser specimens and looser specimens are close together at each σ_0'. This is because D increases as much as 30 times over γ in the high-amplitude RC tests while G only decrease by 0.5. Compared with the changes in D caused by γ, the differences between D of denser specimens and D of looser specimens is relatively small. The third point is that the $D - \mathrm{Log}\,\gamma$ relationships are also well represented by hyperbolic models. The equation that can be used to represent each hyperbolic curve in the $D - \mathrm{Log}\,\gamma$ relationship is:

$$\frac{D}{D_{min}} = 1 + \left(\frac{\gamma}{\gamma_{r,D}}\right)^{b} \tag{6.5}$$

in which D_{min} equals to the material damping ratio in the small-strain range at each of the three loading effective isotropic confining stress of 4.5, 18 and 72 psi, $\gamma_{r,D}$ is equal to the reference shear strain at which the value of D is 100 % higher than that of D_{min}, and b is a curvature coefficient. Each $D - \mathrm{Log}\,\gamma$ relationship shown in Figures 6.10

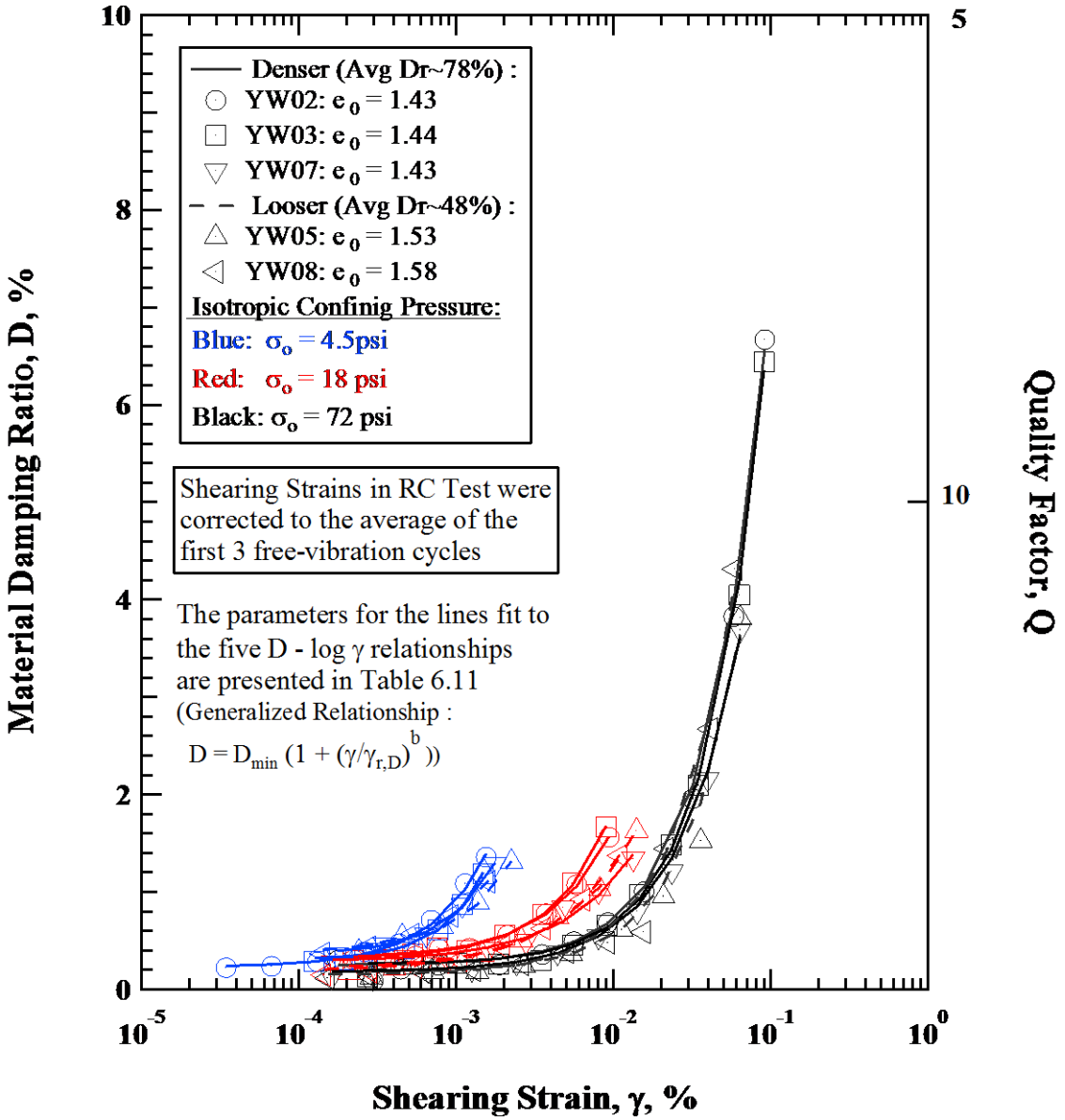

Figure 6.10 Variation in Material Damping Ratio with Shearing Strain at three loading Effective Isotropic Confining Pressures of 4.5, 18 and 72 psi from Resonant Column Tests of five Calcareous Sand Specimens.

has been best-fit with Equation 6.5 using the least squares regression. The resulting best-fit values of the parameters ($\gamma_{r,D}$ and b) are presented in Table 6.11. The r^2 values for the best-fits to determine $\gamma_{r,D}$ and b range from 0.9700 to 0.9982 and average 0.9917.

Table 6.11: Parameters Fit to the $D - \mathrm{Log}\,\gamma$ Relationships from Resonant Column Tests of all Calcareous Sand Specimens.

Test ID.	Estimated Relative Density, D_r[1], (%)	Initial Void Ratio, e	Isotropic Confining Pressure σ_0', (psi)	Elastic threshold γ_t^{e2}, (%)	Modified Hyperbolic Relationship Equation[3]	
					γ_r (%)	b
YW02	78	1.43	4.5	0.00044	0.0004	1.221
			18	0.00125	0.0028	1.113
			72	0.00310	0.0058	1.173
YW03	76	1.44	4.5	0.00050	0.0008	1.635
			18	0.00125	0.0027	1.204
			72	0.00290	0.0068	1.216
YW05	54	1.53	4.5	0.00065	0.0012	1.301
			18	0.00135	0.0020	0.973
			72	0.00370	0.0054	1.200
YW07	79	1.43	4.5	0.00060	0.0009	1.389
			18	0.00112	0.0032	0.950
			72	0.00270	0.0042	1.082
YW08	42	1.58	4.5	0.00059	0.0009	1.233
			18	0.00123	0.0015	0.937
			72	0.00350	0.0035	1.161

Notes:
1. $D_r = (e_{max} - e)/(e_{max} - e_{min}) \times 100\%$,
   e_{max} and e_{min} are provided by Baxter, 2013
2. $\gamma_t^e =$ shear strain at which $G/G_{max} =$ 0.98,
3. $D/D_{min} = 1 + (\gamma/\gamma_r)^b$,
   where D_{min} = small-strain material damping ratio,
   γ_r = reference shear strain, and,
   b = curvature coefficient.

In Figure 6.10, the first point observed is that the effective isotropic confining pressure σ_0' has an influence on the nonlinear material damping ratio behavior. In terms of the average values of reference shear strain γ_r and curvature coefficient b for all five sand specimens at each isotropic effective confining pressure level, the comparison is as follows. At σ_0' of 4.5 psi, the average value of γ_r is 0.0008 and the average value of b is 1.356. At σ_0' of 18 psi, the average value of γ_r is 0.0024 and the average value of b is 1.035. At σ_0' of 72 psi, the average value of γ_r is 0.0051 and the average value of b is 1.166. γ_r is affected by σ_0' since specimens at higher confining pressure levels always have larger values of γ_r than specimens at lower confining pressure. However, the specimens at σ_0' of 18 psi have the largest values of b and the specimens at σ_0' of 4.5 psi have the smallest values of b. The comparison shows that σ_0' is an important factor in evaluating γ_r, but another factor seems to be needed in normalizing b.

As discussed in the chapter of small strain material damping ratio (D_{min}), due to the influence of $D_{equipment-generated}$, D_{min} data is unusable for analysis. Unlike σ_0' which has a big influence on the nonlinear damping ratio behavior, void ratio (e) has a relatively small influence on the nonlinear damping ratio behavior. The abnormal D_{min} data makes the nonlinear material damping ratio data inapplicable for analyzing the influence of e.

6.4 SUMMARY

Low-amplitude and high-amplitude resonant column tests are performed to study the small-strain and nonlinear dynamic properties of calcareous sand respectively. The impacts of factors like void ratios (e), total unit weight γ_t and effective confining pressure (σ_0') on the dynamic properties of calcareous sand are studied on five specimens. Comparison of RC test results and Menq's prediction are also presented to show the consistency and inconsistency for recommendation of using Menq's equations for calcareous sand.

Void ratio (e) has an influence on the low-amplitude shear wave velocity in the general way that denser soil fabrics form a stiffer soil skeleton. First, the denser specimens with smaller e always have higher V_S values than the looser specimens with larger e at the same σ_0' level. Second, the denser specimens always have slightly smaller values of n_S, which represents the slopes of $\log V_S - \log \sigma_0'$ relationships, than looser specimens for the calcareous sand. At last, the plots of void-ratio-adjusted shear wave velocities prove that $\sqrt{F(e)}$, ($F(e) = 1/0.3 + 0.7e^2$), is an important factor in evaluating A_S, (V_S at σ_0' of one atmosphere), but another factor is needed in normalizing n_S.

As with void ratio (e) having an effect on small-strain V_S through the stiffening effect of denser soil skeletons, void ratio also has an influence on the small-strain shear modulus. The effect is even more pronounced because the effect is further increased by the fact that total unit weight enters the calculation of shear modulus ($G = (\gamma_t/g)V_S^2$).

First, denser specimens of the same material with lower values of e and higher values of γ_t always have larger G_{max} values than the looser specimens with higher values of e and lower values of γ_t at the same σ_0' level. Second, denser specimens always have smaller values of n_G, which represents the slopes of $\log G_{max} - \log \sigma_0'$ relationships, than looser specimens for the same kind of sand. At last, the plots of total-unit-weight-and-void-ratio-adjusted shear modulus prove that both $\sqrt{F(e)}$, ($F(e) = 1/0.3 + 0.7e^2$), and γ_t are important factors in evaluating A_G, (G_{max} at σ_0' of one atmosphere), but another factor is needed in normalizing n_G.

Menq's equation for small-strain shear modulus is inapplicable for calcareous sand. The possible reasons may be the unusual sharp particles of calcareous sand, which can lead to unusually large void ratio. Also Menq's equation does not consider changes in n_G caused by changes in e, which does show affects on n_G even though the influence is not large.

Hyperbolic models modified from Darendeli (2001) used in the study of nonlinear shear modulus of calcareous sand is as follows:

$$\frac{G}{G_{max}} = \frac{1}{1 + \left(\frac{\gamma}{\gamma_r}\right)^a} \tag{6.4}$$

in which G_{max} equals to the shear modulus in small-strain at each of the three loading effective isotropic confining stresses of 4.5, 18 and 72 psi, γ_r is equal to the reference shear strain at which shear modulus equals to half of G_{max}, and a is a curvature

coefficient. From the variations in normalized shear modulus (G/G_{max}) with shear strain (γ), it is found that γ_t^e, γ_r and a are all affected by σ_0' since specimens at higher confining pressure levels always have larger values of γ_t^e and γ_r and smaller values of a than specimens at lower confining pressures. It is also found that γ_t^e, γ_r and a are both affected by void ratio (e) because denser specimens always have smaller values of γ_t^e, γ_r and a than looser specimens.

Differences are found between the RC tests results and Menq's prediction for nonlinear shear modulus behavior. The values of γ_r from Menq's prediction are almost constantly higher than the values of γ_r from RC tests, with the average absolute difference of γ_r equal to about 0.035 %. The values of a from Menq (2003) increases with increasing σ_0', while the values of a from RC tests decreases with increasing σ_0' in most cases.

Hyperbolic models modified from Darendeli (2001) used in the study of nonlinear shear modulus of calcareous sand is as follows:

$$\frac{D}{D_{min}} = 1 + \left(\frac{\gamma}{\gamma_{r,D}}\right)^b \tag{6.5}$$

in which D_{min} equals to the material damping ratio in small-strain at each of the three loading effective isotropic confining stresses of 4.5, 18 and 72 psi, $\gamma_{r,D}$ is equal to the reference shear strain at which the value of D is 100 % higher than that of D_{min}, and b is a curvature coefficient. From the variations in material damping ratio (D) with shear strain (γ), it is shown that $\gamma_{r,D}$ is affected by σ_0' since specimens at higher confining

pressure levels always have larger values of $\gamma_{r,D}$ than specimens at lower confining pressures.

CHAPTER SEVEN

CONCLUSION

7.1 SUMMARY

In this study, the dynamic properties of liquefiable sand from Christchurch, New Zealand and calcareous sand from Puerto Rico are investigated using torsional resonant column tests performed in the Soil and Rock Dynamics Laboratory at University of Texas at Austin. Four pairs of specimens were reconstituted using the liquefiable sand from Christchurch. Each pair of specimens was composed of one looser ($D_r \sim 40$ %) and one denser specimen ($D_r \sim 80$ %) from the same depth and site. The four pairs of specimens came from two depths at two different sites. For the calcareous sand from Puerto Rico, five specimens with three different relative densities were reconstituted. Slightly different test programs were applied to the liquefiable sand specimens and the calcareous sand specimens. Both low-amplitude and high-amplitude resonant column tests were performed on all the specimens.

The effects of isotropic effective confining pressure (σ_0'), shear strain amplitude (γ), void ratio (e) and total unit weight (γ_t) on the small-strain and nonlinear dynamic properties of the liquefiable sand and the calcareous sand are discussed. Empirical models from previous studies are examined and fit to the test results and recommendations are given for the application of the empirical models to specific kinds of soils.

7.2 CONCLUSIONS

7.2.1 Dynamic Properties of Liquefiable Sand from Christchurch, New Zealand

Low-amplitude and high-amplitude resonant column tests were performed to study the small-strain and nonlinear dynamic properties of the liquefiable sand, respectively. Eight reconstituted specimens of the liquefiable sand were used to study the impact of factors such as void ratios (e) and total unit weight γ_t on the dynamic properties. Comparison of RC test results and Menq's (2003) prediction are also presented to show the consistency and inconsistency in using Menq's equations for liquefiable sand.

Void ratio (e) has an influence on the low-amplitude shear wave velocity in the general way that a denser soil particle arrangement forms a stiffer soil skeleton. First, the denser specimens always have higher V_S values than the looser specimens at the same σ_0' level. Second, denser specimens always have slightly smaller values of n_S, which represent the slopes of $\log V_S - \log \sigma_0'$ relationships. Very interestingly, plots of void-ratio-adjusted shear wave velocities, $V_S/\sqrt{F(e)}$, where $F(e) = 1/(0.3 + 0.7e^2)$, is an important factor in evaluating A_S, (V_S at σ_0' of one atmosphere). However, no factor was found to normalize n_S.

As void ratio (e) was found to have an effect on small-strain V_S through the stiffening effect of denser soil skeletons, void ratio also has an influence on the small-strain shear modulus. The effect is even more pronounced because the effect is further increased by the fact that total unit weight enters the calculation of shear modulus ($G =$

$(\gamma_t/g)V_S^2$). First, denser specimens of the same material with lower values of e and higher values of γ_t always have larger G_{max} values than the looser specimens at the same σ_0' level. Second, denser specimens always have smaller values of n_G than looser specimens, where n_G represents the slopes of $\log G_{max} - \log \sigma_0'$ relationships. Plots of total-unit-weight-and-void-ratio-adjusted shear modulus were used to show that both $\sqrt{F(e)}$, (where $F(e) = 1/(0.3 + 0.7e^2)$), and γ_t are important factors in evaluating A_G (G_{max} at σ_0' of one atmosphere), but another factor that was not determined is needed in normalizing n_G.

Void ratio also has an influence on the small-strain material damping ratio, even though the variation of small-strain material damping ratio is more complex than those of V_S and G_{max}. Denser specimens of the same material with lower values of e generally have smaller D_{min} values than the looser specimens with higher values of e at the same σ_0' level.

Menq's prediction is somewhat unconservative in calculating G_{max} and D_{min}. Also, Menq's equation does not consider changes in n_G and n_D caused by changes in e, which does occur in the n_G and n_D values even though the influence is not large.

The hyperbolic model modified from Darendeli (2001) was used in the study of nonlinear shear modulus behavior of liquefiable sand. This model is:

$$\frac{G}{G_{max}} = \frac{1}{1 + \left(\frac{\gamma}{\gamma_r}\right)^a} \tag{5.4}$$

in which G_{max} equals the shear modulus in the small-strain at an unloading effective isotropic confining stress of 8 psi, γ_r is equal to the reference shear strain at which the shear modulus equals half of G_{max}, and a is a curvature coefficient. From the variation in normalized shear modulus (G/G_{max}) with shear strain (γ) of the eight specimens, it is found that γ_t^e, γ_r and a are both affected by void ratio (e) because denser specimens always have smaller values of γ_t^e, γ_r and a than looser specimens.

Compared to the RC tests, Menq's equations gave reasonable results for predicting the nonlinear shear modulus behavior. However, void ratio (e) does have an effect on γ_r and a, even through it is minor, and Menq's (2003) equations do not predict this effect.

Hyperbolic models modified from Darendeli (2001) were used in this study of nonlinear material damping ratio behavior of liquefiable sand. The modified hyperbolic model is:

$$\frac{D}{D_{min}} = 1 + \left(\frac{\gamma}{\gamma_{r,D}}\right)^b \tag{5.5}$$

in which D_{min} equals the material damping ratio at small strains at an unloading effective isotropic confining stress of 8 psi, $\gamma_{r,D}$ is equal to the reference shear strain at which the value of D is 100 % higher than that of D_{min}, and b is a curvature coefficient. From the variation in normalized material damping ratio (D/D_{min}) with shear strain (γ), it is shown that $\gamma_{r,D}$ is affected by void ratio (e) since denser specimens always have smaller values of $\gamma_{r,D}$ than looser specimens. Void ratio also affect the

curvature coefficient, b. However, another factor, that was not determined, is needed in normalizing b.

7.2.2 Dynamic Properties of Calcareous Sand from Puerto Rico

Low-amplitude and high-amplitude resonant column tests were also performed to study the small-strain and nonlinear dynamic properties of calcareous sand from Puerto Rico. The impacts of factors like void ratio (e), total unit weight γ_t and effective confining pressure (σ_0') on the dynamic properties of calcareous sand were studied using five reconstituted specimens. Comparisons of RC test results and Menq's (2003) predictions are also presented to show the consistency and inconsistency found using Menq's (2003) equations applied to the calcareous sand.

Void ratio (e) has an influence on the low-amplitude shear wave velocity in the general way that denser granular arrangements form a stiffer soil skeleton. First, the denser specimens with smaller void ratios always have higher V_S values than the looser specimens. Second, the denser specimens always have slightly smaller values of n_S, which represent the slopes of $\log V_S - \log \sigma_0'$ relationships. The plots of void-ratio-adjusted shear wave velocities prove that $\sqrt{F(e)}$, (where $F(e) = 1/(0.3 + 0.7e^2)$), is an important factor in evaluating A_S, (V_S at σ_0' of one atmosphere), but, just as found with the Christchurch liquefiable sands, another yet-to-be-determined factor is needed in normalizing n_S.

As with void ratio (e) having an effect on small-strain V_S, void ratio also has an influence on the small-strain shear modulus. The effect is even more pronounced because the effect is further increased by the fact that total unit weight enters the calculation of shear modulus ($G = (\gamma_t/g)V_S^2$). First, denser specimens of the same material with lower values of e and higher values of γ_t always have larger G_{max} values at the same σ_0' level. Second, denser specimens always have smaller values of n_G, which represent the slopes of $\log G_{max} - \log \sigma_0'$ relationships. Finally, plots of total-unit-weight-and-void-ratio-adjusted shear modulus were used to show that both $\sqrt{F(e)}$, (where $F(e) = 1/(0.3 + 0.7e^2)$), and γ_t are important factors in evaluating A_G (G_{max} at σ_0' of one atmosphere), but another factor that was not determined is needed in normalizing n_G.

Menq's equation for small-strain shear modulus is not applicable to calcareous sand. The possible reasons may be the unusual sharp, angular particles of the calcareous sand, which can lead to unusually large void ratios. Also, Menq's equation does not consider changes in n_G caused by changes in e, which does have an effect on n_G even though the influence is not large.

The hyperbolic model modified from Darendeli (2001) was used in the study of nonlinear shear modulus of calcareous sand. This nonlinear model is given by Equation 5.4. In this case, the value of G_{max} equals the shear modulus in the small-strain range at each of the three effective isotropic confining stresses of 4.5, 18 and 72 psi, γ_r is equal to the reference shear strain at which shear modulus equals half of G_{max}, and a is a curvature coefficient. From the variation in normalized shear modulus (G/G_{max}) with

shear strain (γ), it is found that γ_t^e, γ_r and a are all affected by σ_0' since specimens at higher confining pressure levels always have larger values of γ_t^e and γ_r and smaller values of a than specimens at lower confining pressures. It is also found that γ_t^e, γ_r and a are both affected by void ratio (e) because denser specimens always have smaller values of γ_t^e, γ_r and a than looser specimens.

Differences were found between the RC tests results and Menq's prediction for nonlinear shear modulus behavior. The values of γ_r from Menq's prediction are almost constantly higher than the values of γ_r from RC tests, with the average absolute difference of γ_r equal to about 0.035 %. The values of a from Menq (2003) increases with increasing σ_0', while the values of a from RC tests decreases with increasing σ_0' in most cases.

The hyperbolic model from Darendeli (2001) was modified in this study of nonlinear material damping ratio of calcareous sand as follows:

$$\frac{D}{D_{min}} = 1 + \left(\frac{\gamma}{\gamma_{r,D}}\right)^b \tag{6.5}$$

in which D_{min} equals the material damping ratio in the small-strain range at each of the three loading effective isotropic confining stresses of 4.5, 18 and 72 psi, $\gamma_{r,D}$ is equal to the reference shear strain at which the value of D is 100 % higher than that of D_{min}, and b is a curvature coefficient. From the variations in material damping ratio (D) with shear strain (γ), it is shown that $\gamma_{r,D}$ is affected by σ_0' since specimens at higher confining

pressure levels always have larger values of $\gamma_{r,D}$ than specimens at lower confining pressures.

7.2.3 Comparisons of Dynamic Properties between Liquefiable Sand and Calcareous Sand

To better visualize the comparison of the small-strain dynamic properties of liquefiable sand with those of calcareous sand, $\log G_{max} - \log \sigma_0'$ and $\log D_{min} - \log \sigma_0'$ relationships in the NC portion for both sands in the dense state are represented in Figure 7.1. The parameters fit to $\log G_{max} - \log \sigma_0'$ and $\log D_{min} - \log \sigma_0'$ relationship for both sands in dense state are presented in Table 7.1.

The first point observed in Figure 7.1 is that dense calcareous sand specimens constantly have higher values of G_{max} (Figure 7.1a) and lower values of D_{min} (Figure 7.1b) than dense liquefiable sand specimens at each confining pressure. In terms of the average values of G_{max} at σ_0' of one atmosphere for the dense liquefiable sand specimens and the dense calcareous sand specimens, the comparison is as follows. The average value of $A_{G,liquefiable}$ is 2045 ksf and average value of $A_{G,calcareous}$ is 2837 ksf. In terms of the average values of D_{min} at σ_0' of one atmosphere for dense liquefiable and dense calcareous sand specimens, the comparison is as follows. The average value of $A_{D,liquefiable}$ is 0.72 % and average value of $A_{D,calcareous}$ is 0.29 %.

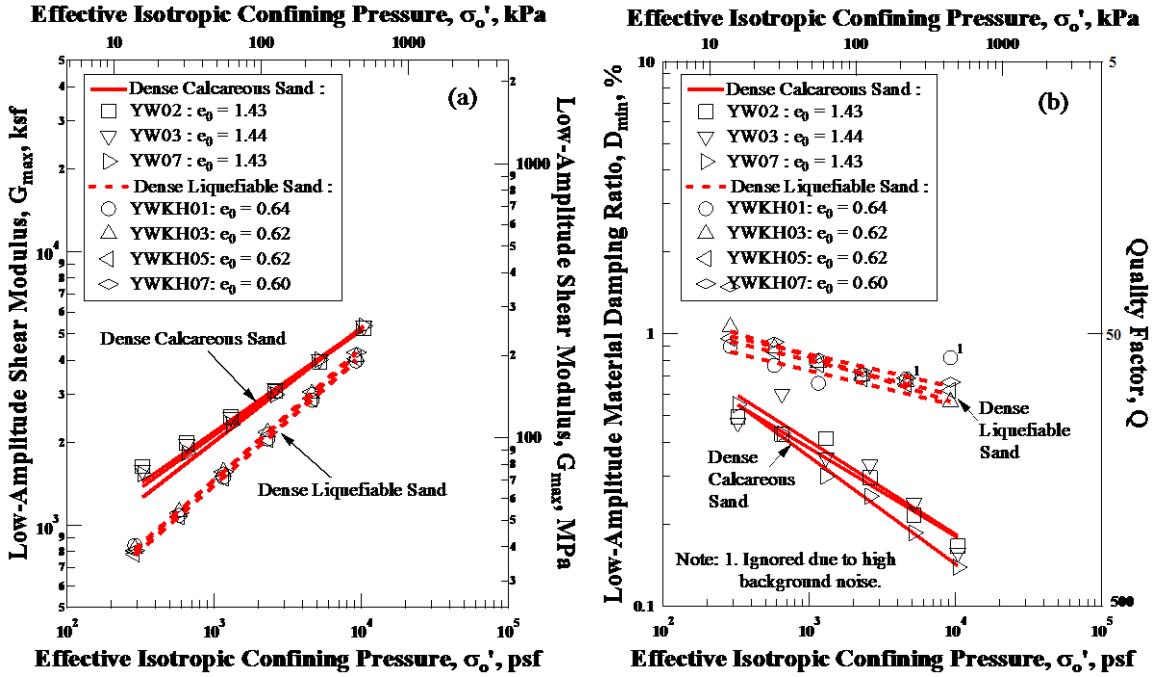

Figure 7.1 Comparisons of $\text{Log}\, G_{max} - \text{Log}\, \sigma_0'$ and $\text{Log}\, D_{min} - \text{Log}\, \sigma_0'$ Relationships in the NC portion between Dense Liquefiable Sand and Dense Calcareous Sand.

Table 7.1: Parameters Fit to $\text{Log}\ G_{max} - \text{Log}\ \sigma_0'$ and $\text{Log}\ D_{min} - \text{Log}\ \sigma_0'$ Relationships from Resonant Column Tests of Dense liquefiable Sand Specimens and Dense Calcareous Sand Specimens.

Specimen	Test ID.	Initial Void Ratio, e	G_{max} [1]		D_{min} [2]	
			A_G (ksf)	n_G	A_D (%)	n_D
Dense Liquefiable Sand Specimens	YWKH01	0.64	1990	0.470	0.666	-0.127
	YWKH03	0.62	2090	0.468	0.727	-0.171
	YWKH05	0.62	2000	0.475	0.724	-0.129
	YWKH07	0.60	2100	0.483	0.767	-0.122
Dense Calcareous Sand Specimens	YW02	1.43	2836	0.383	0.299	-0.324
	YW03	1.44	2915	0.377	0.312	-0.342
	YW07	1.43	2761	0.417	0.263	-0.394

Notes:
1. $G_{max} = A_G(\sigma_0'/P_a)^{n_G}$, $P_a = one\ atmosphere$,
2. $D_{min} = A_D(\sigma_0'/P_a)^{n_D}$, $P_a = one\ atmosphere$.

The second point observed in the $\log G_{max} - \log \sigma_0'$ relationships in Figure 7.1a is that dense calcareous sand specimens have slightly flatter slopes than dense liquefiable sand specimens. This difference means that the shear modulus of dense calcareous sand is somewhat less sensitive to the isotropic effective stress σ_0' compared with dense liquefiable sand. In terms of the average values of n_G for dense liquefiable sand specimens and dense calcareous sand specimens, the comparison is as follows. The average value of $n_{G,liquefiable}$ is 0.474 and average value of $n_{G,calcareous}$ is 0.392.

One key point observed in Figure 7.1b is that the $\log D_{min} - \log \sigma_0'$ relationship of dense calcareous sand specimens exhibit steeper slopes than dense liquefiable sand specimens. This difference means that the material damping ratio of dense calcareous sand is more sensitive to the isotropic effective confining pressure σ_0' compared with dense liquefiable sand. In terms of the average values of n_D for dense liquefiable sand specimens and dense calcareous sand specimens, the comparison is as follows. The average value of $n_{D,liquefiable}$ is -0.141 and average value of $n_{D,calcareous}$ is -0.387.

The second point observed in Figure 7.1b is that the values of D_{min} of the dense calcareous sand are significantly lower than the D_{min} values of the dense liquefiable sand.

To compare the nonlinear dynamic properties of liquefiable sand with those of calcareous sand, the $G - \log \gamma$ and $G/G_{max} - \log \gamma$ relationships for both sands in the dense state are presented in Figure 7.2. The nonlinear $D - \log \gamma$ and $D/D_{min} - \log \gamma$ relationships for both sands in the dense state are presented in Figure 7.3. In both Figures

7.2 and 7.3, the curves for dense calcareous sand specimens are developed from nonlinear RC testing results at three confining pressure levels (4.5, 18 and 72 psi) and these results have been interpolated to an isotropic effective confining pressure of 8 psi so that the results are at the same σ_0' of 8 psi at which the nonlinear RC tests of the dense liquefiable sand specimens were performed. The parameters fit to the $G/G_{max} - \log \gamma$ and $D/D_{min} - \log \gamma$ relationships for both the liquefiable and calcareous sands in the

Table 7.2: Parameters Fit to $G/G_{max} - \text{Log } \gamma$ and $D/D_{min} - \text{Log } \gamma$ Relationships from Resonant Column Tests of Dense liquefiable Sand Specimens and Dense Calcareous Sand Specimens.

Specimen	Test ID.	Initial Void Ratio, e	Elastic Threshold γ_t^{e1} (%)	Modified Hyperbolic Relationship[2]		Modified Hyperbolic Relationship[3]	
				γ_r (%)	a	$\gamma_{r,D}$ (%)	b
Dense Liquefiable Sand Specimens	YWKH01	0.64	0.00140	0.064	0.838	0.0052	0.770
	YWKH03	0.62	0.00110	0.050	0.834	0.0062	0.767
	YWKH05	0.62	0.00110	0.064	0.857	0.0103	0.931
	YWKH07	0.60	0.00130	0.060	0.837	0.0074	0.851
Dense Calcareous Sand Specimens	YW02	1.43	0.00065	0.028	0.941	0.0012	1.245
	YW03	1.44	0.00069	0.033	0.895	0.0013	1.246
	YW07	1.43	0.00074	0.043	0.913	0.0018	1.177

Notes:
1. $\gamma_t^e =$ shear strain at which $G/G_{max} =$ 0.98,
2. Modified hyperbolic relationship:
   $G/G_{max} = 1/(1 + (\gamma/\gamma_r)^a)$,
   where G_{max} = small-strain shear modulus
   γ_r = reference shear strain at which $G/G_{max} =$ 0.5, and,
   a = curvature coefficient,
3. Modified hyperbolic relationship:
   $D/D_{min} = 1 + \left(\gamma/\gamma_{r,D}\right)^b$,
   where D_{min} = small-strain material damping ratio,
   $\gamma_{r,D}$ = reference shear strain at which $D/D_{min} =$ 2.0, and,
   b = curvature coefficient.

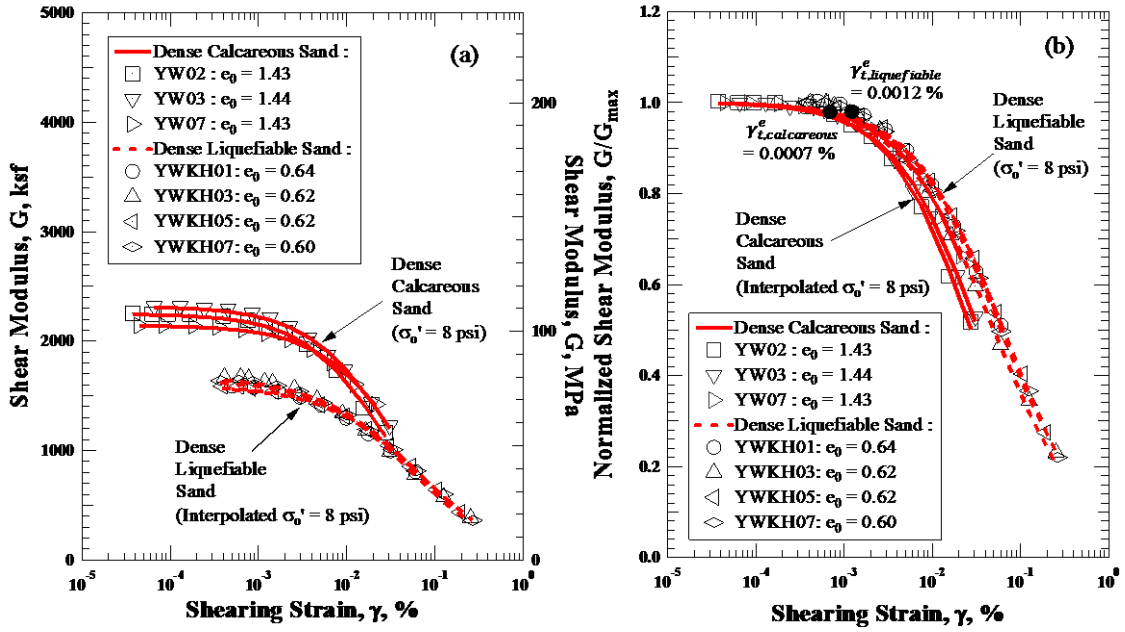

Figure 7.2 Comparisons of $G - \log\gamma$ and $G/G_{max} - \log\gamma$ Relationships between Dense Liquefiable Sand and Dense Calcareous Sand.

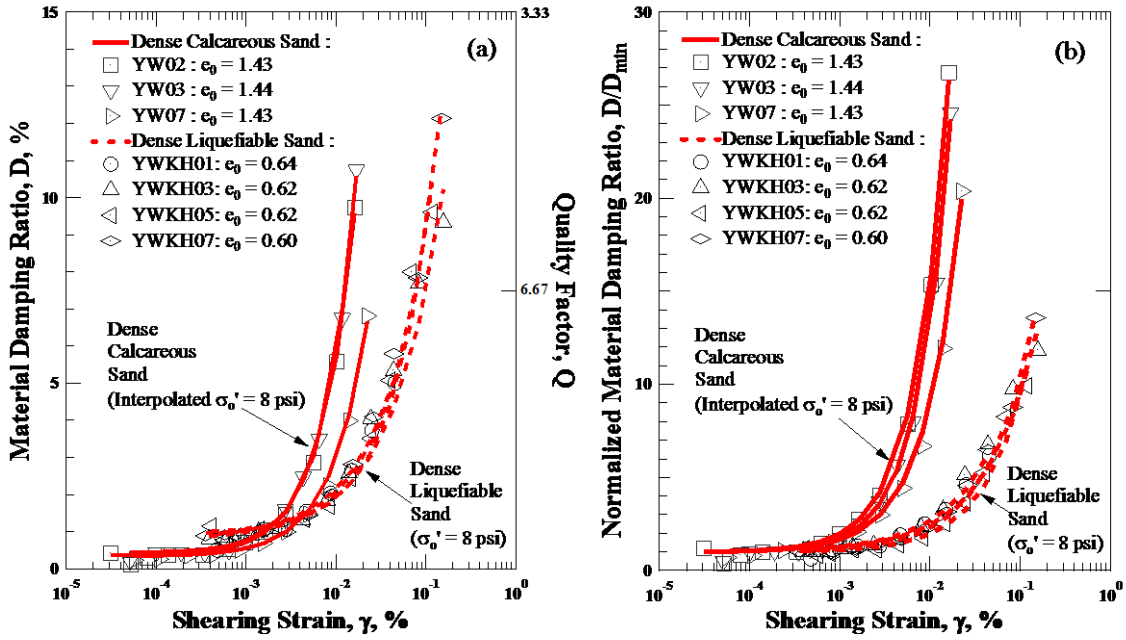

Figure 7.3 Comparisons of $D - \log\gamma$ and $D/D_{min} - \log\gamma$ Relationships between Dense Liquefiable Sand and Dense Calcareous Sand.

dense state are presented in Table 7.2.

In the $G - \log \gamma$ plots in Figure 7.2a, dense calcareous sand specimens always have a higher shear modulus at a given shear strain than the dense liquefiable sand specimens. In the $G/G_{max} - \log \gamma$ plots in Figure 7.2b, the dense liquefiable sand specimens and dense calcareous sand specimens have same values of G/G_{max} $(= 1.0)$ at the start when the shear strain is in linear, small-strain range. When the normalized shear modulus initially begins to exhibit nonlinearity, this strain is taken as the elastic threshold strain (γ_t^e). The average threshold shear strains for dense liquefiable sand specimens and dense calcareous sand specimens show the following comparison. The average value of $\gamma_{t,liquefiable}^e$ is about 0.0012 % and the average value of $\gamma_{t,calcareous}^e$ is about 0.0007 %. The dense liquefiable sand specimens have higher values of elastic threshold than the dense calcareous sand specimens, which means dense liquefiable sand specimens have higher values of G/G_{max} than dense calcareous sand specimens at the same γ in the nonlinear elastic range. As the shear strain increases from the linear to the moderately nonlinear and then to the highly nonlinear range, dense liquefiable sand specimens have somewhat higher values of G/G_{max} than dense calcareous sand specimens at each γ. In terms of the average values of reference shear strain (γ_r) for dense liquefiable sand specimens and dense calcareous sand specimens, the comparison is as follows. The average values of $\gamma_{r,liquefiable}$ is 0.060 % and the average values of $\gamma_{r,calcareous}$ is 0.035 %. In terms of the average values of the curvature coefficient (a) for dense liquefiable sand specimens and dense calcareous sand specimens, the

comparison is as follows. The average values of $a_{liquefiable}$ is 0.84 and the average values of $a_{calcareous}$ is 0.92.

In $D - \log \gamma$ plots of Figure 7.3, dense calcareous sand specimens have a lower material damping ratio than dense liquefiable sand specimens in the small shear strain range. As the shear strain increases beyond about 0.002 ~ 0.003 %, dense calcareous sand specimens begin to have a higher material damping ratio than dense liquefiable sand specimens. In $D/D_{min} - \log \gamma$ plots of Figure 7.3, it can be seen that, of course, dense liquefiable and dense calcareous sand specimens have same values of D/D_{min} $(= 1.0)$ when the shear strain is in the linear small-strain range. As the shear strain increases from the linear to moderately nonlinear range and then to the highly nonlinear range, dense calcareous sand specimens have much higher values of D/D_{min} than dense liquefiable sand specimens at each γ. In terms of the average values of reference shear strain ($\gamma_{r,D}$) for dense liquefiable sand specimens and dense calcareous sand specimens, the comparison is as follows. The average values of $\gamma_{r,D,liquefiable}$ is 0.0073 % and the average values of $\gamma_{r,D,calcareous}$ is 0.0014 %. In terms of the average values of the curvature coefficient (b) for dense liquefiable sand specimens and dense calcareous sand specimens, the comparison is as follows. The average values of $b_{liquefiable}$ is 0.830 and the average values of $b_{calcareous}$ is 1.223.

REFERENCES

ASTM D 2587-11 (2006). Standard Practice for Classification of Soils for Engineering Purposes (Unified Soil Classification System). doi:10.1520/D2487-11.

ASTM D 6913-04 (2009). Standard Test Methods for Particle-Size Distribution (Gradation) of Soils Using Sieve. doi:10.1520/D6913-04R09E01.2.

Darendeli, B. M. (2001). "Development of a new family of normalized modulus reduction and material damping curves." Ph. D. Dissertation, The University of Texas at Austin., 362 p.

Dobry, R. and Vucetic, M. (1987). "Dynamic Properties and Seismic Response of Soft Clay Deposits," International Symposium on Geotech. Eng. Of Soft Soils., Vol. 2, Mexico City, pp. 51-87.

Elmamlouk, H., Salem, M., & Agaiby, S. S. (1999). "Liquefaction Susceptibility of Loose Calcareous Sand of Northern Coast in Egypt." Proceedings of the 18th International Conference on Soil Mechanics and Geotechnical Engineering, Paris 2013, pp. 1463–1466.

Hall, J.R., Jr. and Richart F.E., Jr. (1963). "Effects of Vibration Amplitude on Wave Velocities in Granular Materials," Proceedings, Second Pan-American Conference on Soil Mechanics and Foundations Engineering, Vol. 1, pp. 145-162.

Hardin, B. O. and Black, W. L. (1968). "Vibration Modulus of Normally Consolidated Clay." J. of Soil Mech. and Found. Div., ASCE, Vol. 94 No. SM2, pp 353-369.

Hardin, B. O. and Drnevich, V. P. (1972). "Shear Modulus and Damping in Soils: Measurement and Parameter Effects." J. of Soil Mech. and Found. Div. ASCE, Vol. 98 No. SM6, pp. 603-624.

Hardin, B. O. (1978). "The nature of stress-strain behavior of soils." Proceedings, Geotech. Eng. Div. Specialty Conf. on Earthquake Eng. and Soil Dynamics, Vol. 1 ASCE, Pasadena, pp. 3-90.

Hazen, A. (1920). Transactions of the American Society of Civil Engineers 83: 1717–1745.

Hwang, S. K. (1997). “Investigation of the Dynamic Properties of Natural Soils,” Ph.D. Dissertation, University of Texas at Austin, 394 pp.

Isenhower, W.M. (1979). “Torsional Simple Shear / Resonant Column Properties of San Francisco Bay Mud,” M.S. Thesis, University of Texas at Austin, 307 pp.

Kim, D.S. (1991). “Deformational Characteristics of Soils at Small to Intermediate Strains from Cyclic Tests.” Ph.D. Dissertation, The University of Texas at Austin, 341 p.

Krama, S.L. (1996). Geotechnical Earthquake Engineering, Prentice Hall, Upper Saddler River, N.J., pp. 19, 551.

Ladd, R. S. (1978). “Preparing Test Specimens Using Undercompaction.”Geotechincal Testing Journal. GTJODJ, Vol. 1, No. 1, pp. 16-23.

Laird, J. P. (1994). “Linear and Nonlinear Dynamic Properties of Soil at High Confining Pressures,” M.S. Thesis, University of Texas at Austin, 291 p.

Lodde, P.F. (1982). “Shear Moduli and Material Damping of San Francisco Bay Mud,” M.S. Thesis, University of Texas at Austin.

Madhusudhan, B. N., Kumar, J. (2013). “Damping of Sands for Varying Saturation.” Journal of Geotechnical and Geoenvironmental Engineering, ASCE, September 2013, doi:10.1061/(ASCE)GT.1943-5606.0000895.

Menq, F.-Y. (2003). “Dynamic Properties of Sandy and Gravelly Soils.” Ph.D. Dissertation. University of Texas at Austin. 364 p.

Ni, S.-H. (1987). “Dynamic Properties of Sand Under True Triaxial Stress States from Resonant Column/Torsional Shear Tests.” Ph.D. Dissertation, The University of Texas at Austin, 421 pp.

Richart, J. E., Jr., Hall, J. R., Jr. and Woods R. O. (1970). “Vibrations of Soils and Foundations.” Prentice-Hall Inc. Englewood Cliff, New Jersey, 414 p.

Seed, H. B., Wong, R. T., Idriss, I. M. and Tokimatsu, K. (1986). “Moduli and Damping factors for Dynamic Analyses of Cohesionless Soil.” J. of Getech. Engr., ASCE, Vol. 112, No. GT11, pp. 1016- 103.

Shin, B. (2014). “Effects of Oversized Particles on the Dynamic Properties of Sand Specimens Evaluated by Resonant Column Testing.” M.S. Thesis, University of Texas at Austin. 109 p.

Stokoe, K. H., II, Darendeli, M. B., Andrus, R. D. and Brown, L. T. (1999). "Dynamic soil properties: laboratory, field and correction studies." Seco e Pinto, (ed.), Proceedings, Second Int. Conf. On Earthquake Geotechnical Engineering, Lisbon. 21-25 June 1999, (3): pp. 811-845, Rotterdam, Balkema.ASTM D 6913-04 (2009). Standard Test Methods for Particle-Size Distribution (Gradation) of Soils Using Sieve. doi:10.1520/D6913-04R09E01.2.

Tanaka, Y., Kudo, K., Nishi, K., and Okamoto, T. (1994). "Shear modulus and damping ratio of gravelly soils measured by several methods." Pre-Failure Deformation of Geomaterials, Vol I. Mitachi & Miura, Eds. pp 47-53.ASTM D 6913-04 (2009). Standard Test Methods for Particle-Size Distribution (Gradation) of Soils Using Sieve. doi:10.1520/D6913-04R09E01.2.

Umberg, D. (2012). "Dynamic Properties of Soils with Non-Plastic Fines." M.S. Thesis, University of Texas at Austin. 422 p.

Youd, T. L. (1973). "Factors controlling maximum and minimum densities of sands." ASTM STP 523, p. 98-112.

VITA

Yaning Wang was born in Shandong, China. After graduating from Boxing No.2 High School in 2008, he attended the Tongji University at Shanghai where he studied Civil Engineering. He graduated from Tongji University with a B.E. degree in July 2012 and entered the graduate school at the University of Texas at Austin in August 2012.

Email address: yaningwang11@gmail.com

This thesis was typed by the author.